

**Synergistic Effect of X-ray Crystallography and Solution NMR
on Structural Characterization of Organolithium Complexes**

By

Jie Guang

B. Sc., Peking University, 2010

B. Ec., Peking University, 2010

A Dissertation Submitted in Partial Fulfillment of the
Requirements for the Degree of Doctor of Philosophy
in the Department of Chemistry at Brown University

Providence, Rhode Island

May, 2015

© Copyright 2015 by Jie Guang

This Dissertation by Jie Guang is accepted in its present form
by the Department of Chemistry as satisfying the
dissertation requirement for the degree of Doctor of Philosophy

Date _____
Paul G. Williard, Advisor

Recommended to the Graduate Council

Date _____
Christopher T. Seto, Reader

Date _____
Amit Basu, Reader

Approved by the Graduate Council

Date _____
Peter M. Weber, Dean of the Graduate School

Curriculum Vitae

Jie Guang was born in the city of Wuhan, China, on May 9th, 1987. She attended No. 1 Middle School Attached to Central China Normal University at Wuhan and was graduated in 2005. In the fall of the same year, she entered Peking University at Beijing. She completed her three-years undergraduate research in the lab of Professor Zhenfeng Xi and was graduated in 2010 with a Bachelor of Science degree in chemistry and a Bachelor of Economic degree. She enrolled in the doctoral chemistry program at Brown University in the fall of 2010, where she was accepted into Professor Williard's group and started the research on main-group organometallic compounds in January 2011.

Publications

Ph. D. Program:

1. Su, C.; **Guang, J.**; Williard, P. G. "Structures of Lithium N-Monosubstituted Anilides: Trisolvated Monomer to Tetrasolvated Dimer", *J. Org. Chem.* **2014**, *79*, 1032-1039.
2. Su, C.; **Guang, J.**; Li, W.; Wu, K.; Hopson, R.; Williard, P. G. "Chiral Lithium Diamides Derived from Linked N-isopropyl Valinol or Alaninol", *J. Am. Chem. Soc.* **2014**, *136*, 11735-11747.
3. **Guang, J.**; Liu, Q.; Hopson, R.; Williard, P. G. "Lithium Pinacolone Enolate Solvated by Hexamethylphosphoramide (HMPA)", *submitted*.
4. **Guang, J.**; Hopson, R.; Williard, P. G. "Diffusion Coefficient-Formula Weight (D-FW) Analysis of ²H Diffusion-Ordered NMR Spectroscopy (DOSY)", *submitted*.
5. **Guang, J.**; Liu, Q.; Monroe, T. B.; Williard, P. G. "Lithium Pinacolone Enolate Hexamer", *in preparation*.

6. **Guang, J.**; Fujiu, M.; Hopson, R.; Mikami, K.; Williard, P. G. “Perfluoroalkyl Grignard Reagents: NMR Study of 1-Heptafluoropropylmagnesium Halide in Ethereal Solution”, *in preparation*.

B. Sc. Program:

1. Li, D.; **Guang, J.**; Zhang, W.-X.; Wang, Y.; Xi, Z. “Zn(OTf)₂ – catalyzed Addition of Amines to Carbodiimides: Efficient Synthesis of Guanidines and Unpredicted Formation of Zn-N Amido Species”, *Org. Biomol. Chem.* **2010**, *8*, 1816-1820.

2. Li, D.; Wang, Y.; Zhang, W.-X.; **Guang, J.**; Xi, Z. “One-Pot Synthesis and Unpredicted Hydrogen Bonds of the Guanidinium Triflates from Readily Available Amines, Carbodiimides, and Zn(OTf)₂”, *Organometallics* **2011**, *30*, 5278-5283.

3. Geng, W.; Wang, C.; **Guang, J.**; Hao, W.; Zhang, W.-X.; Xi, Z. “1, 2, 3, 4-Tetrasubstituted Cyclopentadienes and Their Applications for Metallocenes: Efficient Synthesis through Zirconocene- and CuCl- Mediated Intermolecular Coupling of Two Alkynes and One Diiodomethane”, *Chem.- Eur. J.* **2013**, *19*, 8657-8664.

To My Dear Parents

Acknowledgements

I highly appreciate my advisor Professor Paul G. Williard. His deep and precise understanding and sharp opinions of chemistry, especially organolithium and synthetic chemistry, always inspired me to understand and explain better in my research. Every time we chatted or discussed, I always found understanding, patience, support and encouragement from Professor Williard.

I would like to express my gratitude to Dr. Russell Hopson. He taught my NMR course and trained me how to use NMR machines. More importantly, he let me feel comfortable and confident to apply NMR techniques in the research, which will also benefit my future academic career.

I would like to thank Professor Christopher Seto and Professor Amit Basu served as my committees for all the RPD, ORP and thesis. I have also obtained a lot of precious help and advices from faculty members and students from Williard Group, Cane Group, Basu Group, Zimmt Group, Seto Group, Bernskoetter Group and Wang Group. They not only help me in chemistry, but also make my life more reactive and happier.

I am greatly appreciated my parents for their unconditional love. All my achievement is attributed to them.

Table of Contents

Chapter 1 General Introduction.....	1
1.1 Organolithium Chemistry: Aggregates and Mixed Aggregates.....	1
1.2 Methods for Structural Characterization	2
1.2.1 Solid-State Structures.....	2
1.2.2 Solution-State Structures.....	3
1.3 Synergistic Effect of X-ray Crystallography and Solution NMR	5
1.4 References.....	7
Chapter 2 Diffusion Coefficient-Formula Weight (D-FW) Analysis of ² H Diffusion- Ordered NMR Spectroscopy (DOSY).....	11
2.1 Abstract.....	11
2.2 Introduction	11
2.3 Results and Discussion	12
2.3.1 Experimental Temperature	12
2.3.2 Internal References	14
2.3.3 Application on Organometallic Complex.....	17
2.3.4 Application on amide via Hydrogen-Deuterium Exchange Labeling.....	19
2.4 Conclusion	21
2.5 Experimental Section.....	21
2.6 References.....	24
Chapter 3 Lithium Pinacolone Enolate Solvated by Hexamethylphosphoramide (HMPA)	27
3.1 Abstract.....	27
3.2 Introduction	27
3.3 Results and Discussion	30

3.3.1 Characterization of HMPA-solvated Lithium Pinacolone Enolate in the Solid State.....	30
3.3.2 Characterization of HMPA-solvated Lithium Pinacolone Enolate Complexes in Solution.....	33
3.4 Conclusion.....	45
3.5 Experimental Section.....	46
3.6 References.....	47
Chapter 4 Lithium Pinacolone Enolate Hexamer	51
4.1 Abstract.....	51
4.2 Introduction	51
4.3 Results and Discussion	52
4.3.1 Polymorphic Crystal Structure of Unsolvated Lithium Pinacolone Enolate Hexamer	52
4.3.2 Solution-state Structure of Unsolvated Lithium Pinacolone Enolate.....	57
4.4 Conclusion.....	67
4.5 Experimental Section.....	68
4.6 References.....	70
Chapter 5 Chiral Lithium Diamides Derived from Linked <i>N</i>-Isopropyl Valinol or Alaninol	71
5.1 Abstract.....	71
5.2 Introduction	71
5.3 Background	73
5.4 Results and Discussion	74
5.4.1 Solution-state Characterization of Lithiated Diamino Ethers 9.....	74
5.4.2 Solution-state Characterization of Lithiated Diamino Ethers 10	83
5.5 Conclusion.....	85

5.6 Experimental Section	86
5.7 References.....	87
Chapter 6 Perfluoroalkyl Grignard Reagents: NMR Study of 1- Heptafluoropropylmagnesium Halide in Solution.....	89
6.1 Abstract.....	89
6.2 Introduction	89
6.3 Results and Discussion	90
6.3.2 Perfluoropropyl Magnesium Chloride (^F PrMgCl) in Diethyl Ether Solution ...	92
6.3.2 Perfluoropropyl Magnesium Chloride (^F PrMgCl) in THF Solution	95
6.3.3 Schlenk Equilibrium.....	97
6.4 Conclusion	100
6.5 Experimental Section	100
6.6 References.....	101
Appendix A. CCDC numbers for all crystal structures	102
Appendix B. Supporting Information for Chapter 2.....	103
Appendix C. Supporting Information for Chapter 3.....	122
Appendix D. Supporting Information for Chapter 4.....	129

List of Figures

Figure 1.1. Common aggregation states of organolithium complexes that have been characterized in the solid state or in solution.....	2
Figure 2.1. Dependence of T_1 on temperature	14
Figure 2.2. ^2H DOSY NMR in general THF for the test of internal references	16
Figure 2.3. D-FW analysis of ^2H DOSY data for the test of internal references....	17
Figure 2.4. ^2H DOSY NMR of LDA- <i>d</i> in general toluene with 1 eq of THF- <i>d</i> ₈ and 9 eq of general THF	18
Figure 2.5. ^1H DOSY NMR of 0.4 M acetanilide in acetone- <i>d</i> ₆ with 10 μl D ₂ O (2.5 eq)	20
Figure 2.6. ^2H DOSY NMR of 0.4 M acetanilide in general acetone with 10 μl H ₂ O (2.5 eq)	20
Figure 3.1. Crystal structure of (PinOLi) ₄ • HMPA ₃ - hydrogen atoms and methyl groups of HMPA are omitted for clarity.....	31
Figure 3.2. Simplified skeleton of (PinOLi) ₄ • HMPA ₃ tetrameric structure.....	33
Figure 3.3. ^1H NMR (delay time 60 s) and ^{13}C NMR of LiOPin/HMPA T ₃ Complex in toluene- <i>d</i> ₈ at -20 °C	35
Figure 3.4. HMPA titration experiment of lithium pinacolone enolate in cyclohexane- <i>d</i> ₁₂ at room temperature. 70~80 ppm region (=CH ₂ carbon of enolate) of ^{13}C NMR.. ..	37
Figure 3.5. HMPA titration experiment of lithium pinacolone enolate in Toluene- <i>d</i> ₈ at -20 °C. 70~80 ppm region (=CH ₂ carbon of enolate) of ^{13}C NMR.....	38
Figure 3.6. HMPA titration experiment of lithium pinacolone enolate in toluene- <i>d</i> ₈ at -20 °C	38

Figure 3.7. Crystal structure of [(LiOPin) ₅ • LDA • Li ₂ O • HMPA ₂] (hydrogen atoms omitted)	39
Figure 3.8. Crystal structure of [(LiOPin) ₄ • (LiOH) ₂ • HMPA ₄] (pseudo-T₄), each enolate is solvated by one HMPA (hydrogen atoms omitted)	41
Figure 3.9. Crystal structure of (LiOcP • HMPA) ₄ , hydrogen atoms are omitted ..	42
Figure 3.10. ¹ H DOSY of LiOPin/HMPA T₃ Complex in Toluene- <i>d</i> ₈ at -20 °C ...	44
Figure 4.1. H₁/H₂ overlay: structural differences between two LiOPin hexamers.	55
Figure 4.2. Short distances between lithium atoms and terminal methylene carbons indicate the existence of cation- π interactions	55
Figure 4.3. Hexameric structure of H₁ and H₂ , observed from top. Hydrogen atoms have been omitted for clarity	56
Figure 4.4. ¹³ C NMR of LiOPin hexamer crystal dissolving in toluene- <i>d</i> ₈ at -20 °C.	57
Figure 4.5. ¹ H NMR of LiOPin hexamer crystal dissolving in toluene- <i>d</i> ₈ at -20 °C..	58
Figure 4.6. ¹ H DOSY spectra of LiOPin hexamer crystal dissolved in Tol- <i>d</i> ₈ at -20 °C	60
Figure 4.7. D-FW analysis of ¹ H DOSY data of LiOPin hexamer crystal dissolved in Tol- <i>d</i> ₈ at -20 °C	60
Figure 4.8. Overlay of ¹³ C NMR and DEPT135 spectra	62
Figure 4.9. ¹³ C NMR of LiOPin hexamer crystal dissolving in Tol- <i>d</i> ₈ at -20 °C with sw 260ppm and o1p 100 ppm	63

Figure 4.10. Up-field region (10 ~50 ppm) of ^{13}C NMR of LiOPin hexamer crystal dissolving in Tol- d_8 at -20 °C	63
Figure 4.11. ^1H NMR of LiOPin hexamer crystal dissolving in Tol- d_8 at -20 °C ..	64
Figure 4.12. $\{^1\text{H}, ^1\text{H}\}$ NOESY spectra of LiOPin and lithium pinacolone aldolate in Tol- d_8 at -20 °C.....	66
Figure 4.13. ^1H DOSY spectra of LiOPin hexamer crystal dissolved in cyclohexane- d_{12} at 23 °C.....	67
Figure 5.1. ^6Li NMR of dilithiated- 9 in Tol- d_8 /THF- d_8 (4:1). L* is chiral ligand 9	75
Figure 5.2. ^6Li NMR (a) and ^6Li DOSY (b) of dilithiated- 9 in THF- d_8 at -30 °C... ..	77
Figure 5.3. ^{13}C NMR of chiral ligand 9 and dilithiated- 9	77
Figure 5.4. Multiplicity edited ^1H - ^{13}C HSQC spectrum of dilithiated- 9 in THF- d_8 at -30 °C.....	78
Figure 5.5. ^1H - ^1H COSY spectrum of dilithiated- 9 in THF- d_8 at -30 °C.....	79
Figure 5.6. ^6Li EXSY NMR of dilithiated- 9 in THF- d_8 at -30 °C (a) and -10 °C (b) ..	80
Figure 5.7. ^1H DOSY (with internal references) of dilithiated- 9 in THF- d_8 at -70 °C ..	81
Figure 5.8. D-FW analysis of ^1H DOSY data	82
Figure 5.9. Multiplicity Edited ^1H - ^{13}C HSQC spectrum of dilithiated- 10 in THF- d_8 at -50 °C	84
Figure 5.10. ^6Li NMR of dilithiated- 10 in THF- d_8 at -50 °C and diffusion coefficient values of each ^6Li peaks.....	84
Figure 5.11. ^1H DOSY (with internal references) of dilithiated- 10 in THF- d_8 at -70 °C	85
Figure 5.12. D-FW analysis of ^1H DOSY data	85

Figure 6.1. Preparation of ${}^{\text{F}}\text{PrMgCl}$, with ${}^{19}\text{F}$ chemical shift values of reactant and major byproducts	91
Figure 6.2. ${}^{19}\text{F}$ NMR, 0.4 M ether solution of ${}^{\text{F}}\text{PrMgCl}$ at $-78\text{ }^{\circ}\text{C}$	92
Figure 6.3. ${}^{19}\text{F}$ NMR (downfield), 0.4 M ether solution of ${}^{\text{F}}\text{PrMgCl}$ at $-78\text{ }^{\circ}\text{C}$	93
Figure 6.4. ${}^{19}\text{F}$ NMR (upfield), 0.4 M ether solution of ${}^{\text{F}}\text{PrMgCl}$ at $-78\text{ }^{\circ}\text{C}$	93
Figure 6.5. $\{{}^{19}\text{F}, {}^{19}\text{F}\}$ COSY NMR, 0.4 M ether solution of ${}^{\text{F}}\text{PrMgCl}$ at $-78\text{ }^{\circ}\text{C}$...	94
Figure 6.6. 0.2 M ether solution of ${}^{\text{F}}\text{PrMgCl}$ at $-78\text{ }^{\circ}\text{C}$	95
Figure 6.7. 0.4 M THF solution of ${}^{\text{F}}\text{PrMgCl}$ at $-78\text{ }^{\circ}\text{C}$	96
Figure 6.8. $\{{}^{19}\text{F}, {}^{19}\text{F}\}$ COSY NMR, 0.4 M THF solution of ${}^{\text{F}}\text{PrMgCl}$ at $-78\text{ }^{\circ}\text{C}$	97
Figure 6.9. ${}^{19}\text{F}$ PGSE data and results of 0.4 M ether solution of ${}^{\text{F}}\text{PrMgCl}$ at $-78\text{ }^{\circ}\text{C}$	97
Figure 6.10. $\{{}^{19}\text{F}, {}^{19}\text{F}\}$ NOESY of 0.4 M ether solution of ${}^{\text{F}}\text{PrMgCl}$ at $-78\text{ }^{\circ}\text{C}$	99

List of Tables

Table 2.1. D-FW analysis of ^2H DOSY data for the test of internal references	16
Table 4.1. Selected Crystallographic Data of Two Hexameric LiOPin	54
Table 4.2. D-FW analysis of ^1H DOSY data of LiOPin hexamer crystal dissolved in Tol- d_8 at $-20\text{ }^\circ\text{C}$	61
Table 5.1. D-FW analysis of ^1H DOSY data of dilithiated- 9	
.....	82

List of Schemes

Scheme 2.1. Results of ^2H DOSY of LDA- <i>d</i> in general toluene with 1 ~ 20 eq of THF/THF- d_8 at room temperature.....	19
Scheme 3.1 Dissolving LiOPin/HMPA T_3 Crystal in Hydrocarbon Solvents	45
Scheme 4.1. Lithium pinacolone enolate hexamer deaggregate to tetramer in toluene and form mixed aggregate with lithium aldolate	68
Scheme 5.1. The Trimeric Complexes 2 and the Homodimer 3	72
Scheme 5.2. The equivalently solvated dimer 5 and non-equivalently solvated dimer 6	73
Scheme 5.3. Synthesis of chiral diamino ethers 7, 8, 9 and 10	74
Scheme 5.4. Crystallization of dilithiated chiral diamino ethers 7, 8, 9 and 10 in ethereal solvents.....	74
Scheme 5.5. Solution state of dilithiated- 9 in THF	83
Scheme 6.1. Schlenk equilibrium observed in ethereal solutions	99

Chapter 1 General Introduction

1.1 Organolithium Chemistry: Aggregates and Mixed Aggregates

Since the first organolithium reagents (alkyl lithium compounds) were prepared by Schlenk in 1917,¹ Organolithium intermediates have been employed in various reactions, such as alkylation, nucleophilic addition, condensation, epoxide opening, rearrangement and transmetalation.² Those intermediates are either commercially available or can be easily prepared via lithium halogen exchange, metalation or transmetalation with other cheap and commercially available organolithium reagents, which makes organolithium reagents and intermediates even popular than and widely applied to modern organic synthesis in research laboratories, pharmaceutical³ and fine chemical industries.

Organolithium compounds can form oligomers (even polymers), mixed aggregates, close or separated ion pairs (CIP/SIP). Each aggregate can afford various solvation states. Aggregation and solvation patterns of organolithium complexes are complicated, as they depend on concentration, solvents, temperature, substituents, etc.⁴ They are also important, because they can significantly influence reactivity and selectivity of the reactions involving these organolithium intermediates.⁵ Therefore, structural characterization is the foundation for understanding the mechanism of any reaction containing organolithium reagents.

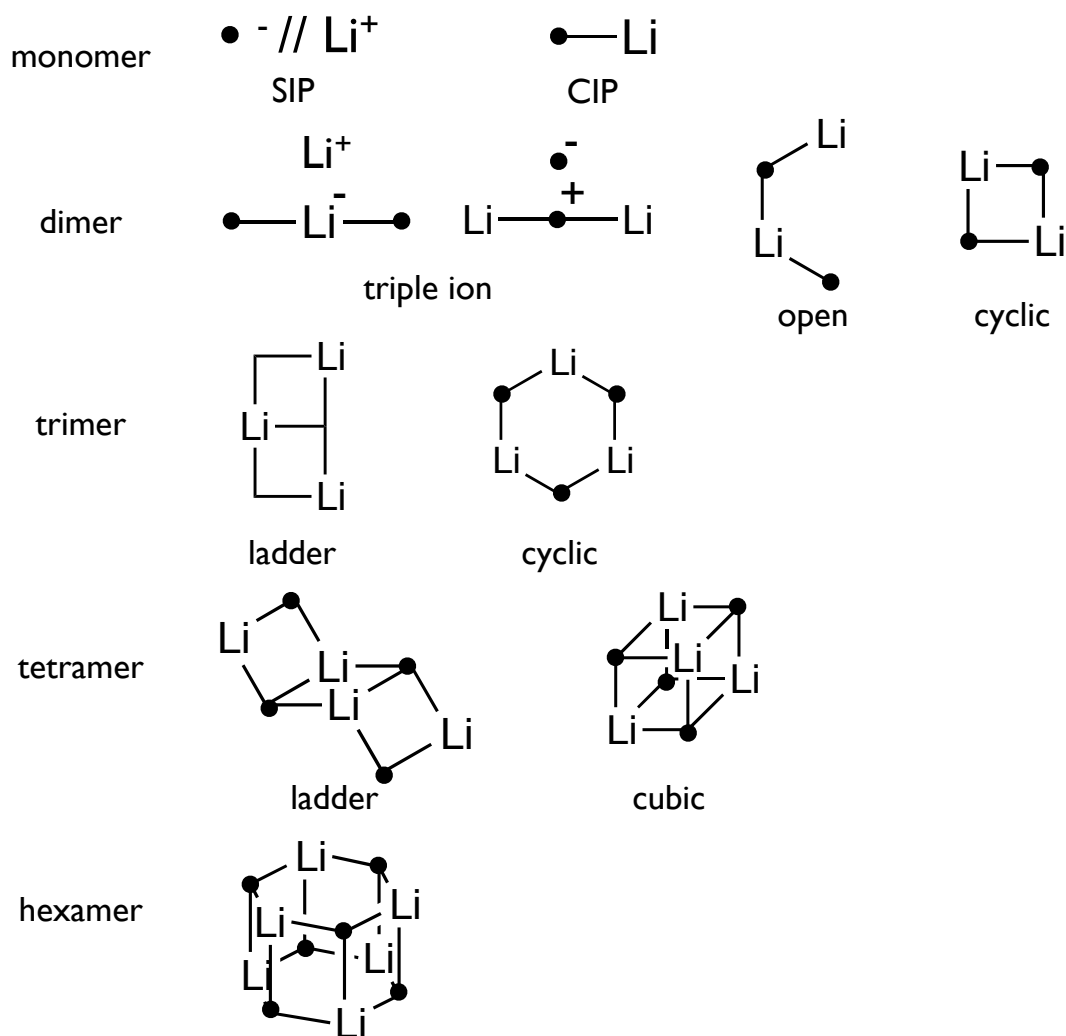


Figure 1.1. Common aggregation states of organolithium complexes that have been characterized in the solid state or in solution.

1.2 Methods for Structural Characterization

1.2.1 Solid-State Structures

Since organolithium reagents are usually applied in the solutions of synthetic reactions, the real research interest is solution-state structural determination. However, X-ray crystallography analysis is still a widely used and irreplaceable technique for characterization of organolithium complexes, as it provides precise and unambiguous

structural information.⁶ These solid-state structures are crucial models or guidelines, which lead to reasonable interpretation of possible organolithium intermediates.

The limitations of X-ray diffraction (XRD) analysis are also obvious. First, solid-state structures provide only indirect evidences for solution aggregations.⁷ Second, crystallization of organolithium compounds is not an easy task due to their sensitivity to as air, moisture or even temperature. Third, existing forms of organolithium intermediates are influenced by a variety of factors, including temperature, solvents, concentrations additives and some unavoidable impurities (such as lithium hydroxide, lithium oxide, lithium halide salts, butoxide lithium, etc). Hence it is very possible that several organolithium complexes co-exist in the same environment. Thus observing part of the complexes via XRD will present a misleading or partial picture of the whole system.

1.2.2 Solution-State Structures

Colligative Methods. Colligative measurements (cryoscopy, vapor phase osmometry, differential pressure barometry, or ebullioscopy) can suggest aggregation states. These techniques have been extensively applied to organolithium compounds.⁸ However these methods are suffering several drawbacks. First, the result is a single number for aggregation degree. Non-integer values are interpreted to reflect a possible equilibrium between two aggregates, which can lead to some spurious interpretation. Second, the experimental results are highly sensitive to impurities. Last but not least, colligative methods are limited to the physical properties of the solvents, such as boiling and freezing points.

UV-vis Spectroscopy Methods. Streitwieser and co-workers have developed a method to measure aggregation equilibrium constants based on the change in UV-vis

spectra with concentration.⁹ However, this method is restricted to lithium enolates with aromatic groups due to the concentration and UV wavelength requirements.

NMR-Based Methods. A variety of methods have been built up to explore the aggregation and solvation states of organolithium reagents based on nuclear magnetic resonance (NMR) spectroscopy.

Jackman and co-workers combined ^{13}C spin-lattice relaxation time (T_1) measurement, colligative measurements and ^7Li quadrupolar splitting constants (QSC) to study the aggregation states of lithium amides, phenyllithium, phenolates and hindered aromatic lithium enolates.¹⁰

For those reagents that contain Li-C or Li-N bonds, isotopic labeling methods are often used to interpret aggregation states and even solvation states¹¹ based on splitting patterns and coupling constants between $^6\text{Li}/^7\text{Li}$ and $^{13}\text{C}/^{15}\text{N}$ from multi-nuclei 1D NMR spectra. Some special 2D NMR techniques¹² have been developed to distinguish similar aggregates, such as cyclic dimers and cyclic trimers.

Several groups (Reich, Noyori, Jacobsen, etc) have utilized additive titration methods to study various solvation states for a specific aggregate, such as monomer or cubic tetramer.¹³ Reich and co-workers also used this technique with low-temperature NMR to observe the formation of various aggregates including SIP and triple ions while using HMPA as the co-solvent, on the basis of signal ratio and their splitting patterns.¹⁴

When J-coupling information is not available, such as lithium enolate or phenolate systems, Collum and co-workers utilized an effective method called continuous variation or Job plot to map the mixed species of two related lithium compounds (A and B). If each mixed aggregates of A and B have a clear and non-overlapping signal

in NMR spectra, than aggregation states are determined by comparing the ratio of signals with various combinations of A and B.¹⁵

Referenced diffusion-ordered NMR spectroscopy (DOSY) with diffusion coefficient-formula weight (D-FW) analysis method was developed and involved in aggregation and mixed aggregation studies of lithium enolates, lithium amide bases and alkyl lithium reagents by Williard and co-workers.¹⁶ This method provides molecular weights of organolithium intermediates in solution which are quite helpful information for understanding aggregation and solvation states. More details of these methods and applications can be found in Chapter 2 and its citations.

1.3 Synergistic Effect of X-ray Crystallography and Solution NMR

X-ray crystallography analysis is a direct method for structural detection, while NMR is an indirect method. However, based on various NMR techniques mentioned before, solution NMR can supply more plentiful information and present a wider scope of solution-state structures for organolithium reagents than XRD. Therefore, the combination of both will afford more reliable and clearer structural characterization of organolithium compounds in solution.

Organolithium compounds not only form various aggregates and mixed aggregates, but also generated mixed aggregates with unwanted impurities, such as lithium hydroxide, lithium oxide, alkyl oxide lithium, etc. Therefore, the NMR spectra of *in-situ* prepared samples sometimes are quite complicated to explain. On the contrary, NMR samples prepared by directly dissolving crystals usually exhibit much cleaner spectra which supply us some unambiguous assignments for peaks in the complex spectra of *in-situ* prepared NMR samples. But *in-situ* prepared solutions are closer to the real reaction systems involving organolithium intermediates than the samples

from pure crystals. In order to interpret the whole complex spectra of *in-situ* prepared solutions, various NMR tools are applied to figure out the relationship between unassigned aggregates and complexes having been determined by X-ray crystallography.

Variable temperature (VT) NMR experiments are used to improve signal resolution and to optimize the NMR temperature for a specific system. For example, see Chapter 4 where this technique is utilized to separate peaks of different intermediates in one solution.

$\{^1\text{H}, ^{13}\text{C}\}$ HSQC/HMBC and $\{^1\text{H}, ^1\text{H}\}/\{^{19}\text{F}, ^{19}\text{F}\}$ COSY are helpful tools to correlate peaks belonging to one compound in a mixture (see examples in Chapter 3, 4, 5 and 6). $\{^1\text{H}, ^1\text{H}\}$ NOESY, $\{^1\text{H}, ^6\text{Li}\}$ HMBC and DOSY are applied to confirm the existence of mixed aggregates. $\{^6\text{Li}, ^6\text{Li}\}$ EXSY provide information about exchangeable organolithium species. PGSE experiments on multi-nuclei (^1H , ^6Li , ^{13}C or ^{19}F) are exploited for comparing the molecular sizes of various intermediates. (See examples in Chapter 3 ~ 6). An HMPA titration experiment was invoked to map different solvation states (Chapter 3). In all the cases, we involve the referenced DOSY method to measure the MW's of species in solution. This combination offers us information for both aggregation and solvation states.

On the basis of all the techniques mentioned above, we can assign and explain most parts of the NMR spectra of *in-situ* prepared solution. Then we modify conditions, like temperature, solvent, concentration, additive and ratio of different components, and monitor the changes by NMR. This protocol is effective to optimize the conditions for preparing crystals of various coexisting complexes (Chapter 3 ~5). The X-ray crystallography data helps us confirm previous interpretation of NMR spectra.

Finally we achieve fully assignment and comprehensive explanation for a complicated system via synergism of XRD and solution NMR.

1.4 References

-
- ¹ Schlenk, W.; Holtz, J. *Ber. Dtsch. Chem. Ges.* **1917**, *50*, 262-274.
- ² (a) Mahrwald, R.; *Modern Aldol Reactions, Vol. 1: Enolates, Organocatalysis, Biocatalysis and Natural Product Synthesis*; Wiley-VCH: Weinheim, **2004**. (b) Stowell, J. C.; *Carbanions in Organic Synthesis*; Wiley: New York, **1979**. (c) Trost, B. M.; Fleming, I. *Comprehensive Organic Synthesis*; Pergamon: Oxford, **1991**. (d) Elschenbroich, C.; Salzer, A. *Organometallics: A Concise Introduction*; Wiley-VCH, **1992**. (e) Wakefield, B. J. *The Chemistry of Organolithium Compounds*; Pergamon: New York, **1974**. (f) Clayden, J. *Organolithiums: Selectivity for Synthesis*; Pergamon: New York, **2002**. (g) Rappoport, Z.; Marek, I.; Eds, *The Chemistry of Organolithium Compounds*; John Wiley & Sons: Chichester, U.K., **2006**. (h) Gawley, R. E.; Ed. *Stereochemical Aspects of Organolithium Compounds*; Topics in Stereochemistry, Vol. 26; John Wiley & Sons: New York, **2010**.
- ³ Wu, G.; Huang, M. *Chem. Rev.* **2006**, *106*, 2596-2616.
- ⁴ (a) Gawley, R. E.; Ed. *Stereochemical Aspects of Organolithium Compounds*; Topics in Stereochemistry, Vol. 26; John Wiley & Sons: New York, **2010**. (b) Elschenbroich, C., *Organometallics*; Wiley-VCH: Weinheim, **2006**. (c) Reich, H. J. *Chem. Rev.* **2013**, *113*, 7130-7178. (d) Harrison-Marchand, A.; Mongin, F. *Chem. Rev.* **2013**, *113*, 7470-7456. (e) Mongin, F.; Harrison-Marchand, A. *Chem. Rev.* **2013**, *113*, 7563-7727. (f) Su, C.; Guang, J.; Williard, P. G. *J. Org. Chem.* **2014**, *79*, 1031-1039. (g) Lewis, H. L.; Brown, T. L. *J. Am. Chem. Soc.* **1970**, *92*, 4664-4670. (h) Kimura, B. Y.; Brown, T. L. *J. Orgmet. Chem.* **1971**, *26*, 57-67. (i) Novak, D. P.; Brown, T. L. *J. Am. Chem. Soc.* **1972**, *94*, 3793-3798. (j) Jackman, L. M.; DeBrosse, C. W. *J. Am. Chem. Soc.* **1983**, *105*, 4177- 4184. (k) Barr, D.; Clegg, W.; Mulvey, R. E.; Snaith, R. *J. Chem. Soc., Chem. Commun.* **1984**, 285-287. (l) Romesberg, F. E.; Gilchrist, J. H.; Harrison, A. T.; Fuller, D. J.; Collum, D. B. *J. Am. Chem. Soc.* **1991**, *113*, 5751-5757. (m) Collum, D. B. *Acc. Chem. Res.* **1992**, *25*, 448-454. (n) Corset, J.; Froment, F.; Lautie, M. F.; Ratovelomanana, N.; Seyden-Penne, J.; Strzalko, T.; Roux- Schmit, M. C. *J. Am. Chem. Soc.* **1993**, *115*, 1684-1694. (o) Abbotto, A.; Streitwieser, A. *J. Am. Chem. Soc.* **1995**, *117*, 6358-6359. (p) Reich, H. J.; Kulicke, K. J. *J. Am. Chem. Soc.* **1995**, *117*, 6621-6622. (q) Reich, H. J.; Kulicke, K. J. *J. Am. Chem. Soc.* **1996**, *118*, 273-274. (r) Remenar, J. F.; Lucht, B. L.; Collum, D. B. *J. Am. Chem. Soc.* **1997**, *119*, 5567-5572. (s) Rutherford, J. L.; Collum, D. B. *J. Am. Chem. Soc.* **2001**, *123*, 199-202. (t) Rutherford, J. L.; Hoffmann, D. Collum, D. B. *J. Am. Chem. Soc.* **2002**, *124*, 264-271. (u) Liou, L. R.; McNeil, A. J.; Ramirez, A.; Toombes, G. E. S.; Gruver, J. M.; Collum, D. B. *J. Am. Chem. Soc.* **2008**, *130*, 4859-4868. (v) Hoepker, A. C.; Gupta, L.; Ma, Y.; Fagggin, M. F.; Collum, D. B. *J. Am. Chem. Soc.* **2011**, *132*, 7135-7151. (w) Tomasevich, L. L.; Collum, D. B. *J. Org. Chem.* **2013**, *78*, 7498-7507.

⁵ (a) West, P.; Waack, R.; Purmort, J. I. *J. Am. Chem. Soc.* **1970**, *92*, 840-845. (b) McGarrity, J. F.; Ogle, C. A.; Brich, Z.; Loosli, H. *J. Am. Chem. Soc.* **1985**, *107*, 1810-1815. (c) Bates, T. F.; Clarke, M. T.; Thomas, R. D. *J. Am. Chem. Soc.* **1988**, *110*, 5109-5112. (d) Sato, D.; Kawasaki, H.; Shimada, I.; Arata, Y.; Okamura, K.; Date, T.; Koga, K. *J. Am. Chem. Soc.* **1992**, *114*, 761-763. (e) Brown, C. A.; Yamaichi, A. *J. Chem. Soc., Chem. Commun.* **1979**, 100-101. (f) Lucht, B. L.; Bernstein, M. P.; Remenar, J. F.; Collum, D. B. *J. Am. Chem. Soc.* **1996**, *118*, 10707-10718. (g) Reich, H. J.; Green, D. P.; Medina, M. A.; Goldenberg, W. S.; Gudmundsson, B. O.; Dykstra, R. R.; Phillips, N. H. *J. Am. Chem. Soc.* **1998**, *120*, 7201-7210. (h) Arvidsson, P. I.; Hilmersson, G.; Ahlberg, P. *J. Am. Chem. Soc.* **1999**, *121*, 1883-1887. (i) Arvidsson, P. I.; Hilmersson, G.; Davidsson, O. *Chem. -Eur. J.* **1999**, *5*, 2348-2355. (j) Rutherford, J. L.; Hoffmann, D.; Collum, D. B. *J. Am. Chem. Soc.* **2002**, *124*, 264-271. (k) Sott, R.; Granander, J.; Hilmersson, G. *Chem. -Eur. J.* **2002**, *8*, 2081-2087. (l) Jones, A. C.; Sanders, A. W.; Bevan, M. J.; Reich, H. J. *J. Am. Chem. Soc.* **2007**, *129*, 3492-3493. (m) Pate, F.; Duguet, N.; Oulyadi, H.; Harrison-Marchand, A.; Fressigne, C.; Valnot, J.; Lasne, M.; Maddaluno, J. *J. Org. Chem.* **2007**, *72*, 6982-6991. (n) Liu, J.; Li, D.; Sun, C.; Williard, P. G.; *J. Org. Chem.* **2008**, *73*, 4045-4052. (o) Lecachey, B.; Duguet, N.; Oulyadi, H.; Fressigne, C.; Harrison-Marchand, A.; Yamamoto, Y.; Tomioka, K.; Maddaluno, J. *Org. Lett.* **2009**, *11*, 1907-1910. (p) Kolonko, K. J.; Wherritt, D. J.; Reich, H. J. *J. Am. Chem. Soc.* **2011**, *133*, 16774-16777. (q) Hunt, D. A. *Org. Prep. Proced. Int.* **1989**, *21*, 705-749. (r) Ando, K.; Takemasa, Y.; Tomioka, K.; Koga, K. *Tetrahedron* **1993**, *49*, 1579-1588. (s) Gawley, R. E.; Zhang, Q.; McPhail, A. T. *Tetrahedron: Asymmetry* **2000**, *11*, 2093-2106. (t) Ireland, R. E.; Mueller, R. H.; Willard, A. K. *J. Am. Chem. Soc.* **1976**, *98*, 2868-2877; (u) Corey, E. J.; Gross, A. W. *Tet. Lett.* **1984**, *25*, 495-498.

⁶ (a) Seebach, D. *Angew. Chem. Int. Ed. Engl.* **1998**, *27*, 1624-1654. (b) Gessner, V. H.; Daschlein, C.; Strohmam, C. *Chem. Eur.-J.* **2009**, *15*, 3320-3334. (c) Reich, H. J. *Chem. Rev.* **2013**, *113*, 7130-7178.

⁷ (a) Collum, D. B.; Kahne, D.; Gut, S. A.; Depue, R. T.; Mohamadi, F.; Wanat, R. A.; Clardy, J.; Duyne, G. V. *J. Am. Chem. Soc.* **1984**, *106*, 4865-4869. (b) Xu, F.; Reamer, R. A.; Tillyer, R.; Cummins, J. M.; Grabowski, E. J. J.; Reider, P. J.; Collum, D. B.; Huffman, J. C. *J. Am. Chem. Soc.* **2000**, *122*, 11212-11218. (c) Kaufman, M. J.; Streitwieser, A., Jr. *J. Am. Chem. Soc.* **1987**, *109*, 6092-6097.

⁸ (a) Arnett, E. M.; Moe, K. D. *J. Am. Chem. Soc.* **1991**, *113*, 7288-7293. (b) Arnett, E. M.; Fisher, F. J.; Nichols, M. A.; Ribeiro, A. A. *J. Am. Chem. Soc.* **1990**, *112*, 801-808. (c) Seebach, D.; Bauer, von W. *Helv. Chim. Acta* **1984**, *67*, 1972-1988. (d) Shobatake, K.; Nakamoto, K. *Inorg. Chim. Acta* **1980**, *4*, 485-487. (e) den Besten, R.; Harder, S.; Brandsma, L. *J. Organomet. Chem.* **1990**, *385*, 153-159. (f) Halaska, V.; Lochmann, L. *Collect. Czech. Chem. Commun.* **1973**, *38*, 1780-1782. (g) Armstrong, D. R.; Davies, J. E.; Davies, R. P.; Raithby, P. R.; Snaith, R.; Wheatley, A. E. H. *New J. Chem.* **1999**, *23*, 35-41. (h) Lochmann, L.; Lim, D. *J. Organomet. Chem.* **1973**, *50*, 9-16. (i) Zune, C.; Jerome, R. *Prog. Polym. Sci.* **1999**, *24*, 631-664. (j) West, P.; Waack, R. *J. Am. Chem. Soc.* **1967**, *89*, 4395-4399. (k) Kallman, N.; Collum, D. B. *J. Am. Chem. Soc.* **1987**, *109*, 7466-7472. (l) DePue, J. S.; Collum, D. B. *J. Am. Chem. Soc.* **1988**, *110*, 5518-5524. (m) West, P.; Waack, R.; Purmort, J. I. *J. Am. Chem. Soc.* **1970**, *92*, 840-845.

⁹ (a) Streitwieser, A. *J. Mol. Model.* **2006**, *12*, 673-680. (b) Streitwieser, A.; Wang, D.

Z. J. Am. Chem. Soc. **1999**, *121*, 6213-6219. (c) Leung, S. S.-W.; Streitwieser, A. *J. Org. Chem.* **1999**, *64*, 3390-3391. (d) Wang, D. Z.; Kim, Y.-J.; Streitwieser, A. *J. Am. Chem. Soc.* **2000**, *122*, 10754-10760. (e) Kim, Y.-J.; Streitwieser, A. *Org. Lett.* **2002**, *4*, 573-575. (f) Streitwieser, A.; Leung, S. S.-W.; Kim, Y.-J. *Org. Lett.* **1999**, *1*, 145-147. (g) Abbotto, A.; Leung, S. S.-W.; Streitwieser, A.; Kilway, K. V. *J. Am. Chem. Soc.* **1998**, *120*, 10807-10813. (h) Leung, S. S.-W.; Streitwieser, A. *J. Am. Chem. Soc.* **1998**, *120*, 10557-10558. (i) Abu-Hasanayn, F.; Streitwieser, A. *J. Org. Chem.* **1998**, *63*, 2954-2960. (j) Abu-Hasanayn, F.; Streitwieser, A. *J. Org. Chem.* **1996**, *118*, 8136-8137. (k) Gareyev, R.; Ciula, J. C.; Streitwieser, A. *J. Org. Chem.* **1996**, *61*, 4589-4593. (l) Abu-Hasanayn, F.; Stratakis, M.; Streitwieser, A. *J. Org. Chem.* **1995**, *60*, 4688-4689. (m) Dixon, R. E.; Williams, P. G.; Saljoughian, M.; Long, M. A.; Streitwieser, A. *Magn. Reson. Chem.* **1991**, *29*, 509-512.

¹⁰ (a) Jackman, L. M.; Chen, X. *J. Am. Chem. Soc.* **1997**, *119*, 8681-8684. (b) Jackman, L. M.; Petrei, M. M.; Smith, B. D. *J. Am. Chem. Soc.* **1991**, *113*, 3451-3458. (c) Jackman, L. M.; Scarmoutzos, L. M.; DeBrosse, C. W. *J. Am. Chem. Soc.* **1987**, *109*, 5355-5361. (d) Jackman, L. M.; DeBrosse, C. W. *J. Am. Chem. Soc.* **1983**, *105*, 4177-4184. (e) Also, see: Quan, W.; Grutzner, J. B. *J. Org. Chem.* **1986**, *51*, 4220-4224. (f) Jackman, L. M.; Rakiewicz, E. F. *J. Am. Chem. Soc.* **1991**, *113*, 1202-1210. (g) Jackman, L. M.; Smith, B. D. *J. Am. Chem. Soc.* **1988**, *110*, 3829-3835. (h) Jackman, L. M.; Scarmoutzos, L. M. *J. Am. Chem. Soc.* **1984**, *106*, 4627-4629.

¹¹ Knorr, R.; Menke, T.; Ferchland, K.; Mehlstaubl, J.; Stephenson, D. S. *J. Am. Chem. Soc.* **2008**, *130*, 14179-14188.

¹² (a) Bauer, W. *J. Am. Chem. Soc.* **1996**, *118*, 5450-5455. (b) Romesberg, F. E.; Bernstein, M. P.; Gilchrist, J. H.; Harrison, A. T.; Fuller, D. J.; Collum, D. B. *J. Am. Chem. Soc.* **1993**, *115*, 3475-3483. (c) Gilchrist, J. H.; Collum, D. B. *J. Am. Chem. Soc.* **1992**, *114*, 794-795.

¹³ (a) Suzuki, M.; Koyama, H.; Noyori, R. *Bull. Chem. Soc. Jpn.* **2004**, *77*, 259-268. (b) Suzuki, M.; Koyama, H.; Noyori, R. *Tetrahedron* **2004**, *60*, 1571-1579. (c) Biddle, M. M.; Reich, H. J. *J. Org. Chem.* **2006**, *71*, 4031-4039. (d) Pospisil, P. J.; Wilson, S. R.; Jacobsen, E. N. *J. Am. Chem. Soc.* **1992**, *114*, 7585-7587. (e) Reich, H. J. *J. Org. Chem.* **2012**, *77*, 5471-5491. (f) Kolonko, K. J.; Biddle, M. M.; Guzei, L. A.; Reich, H. J. *J. Am. Chem. Soc.* **2009**, *131*, 11525-11534; (g) Kolonko, K. J.; Guzei, L. A.; Reich, H. J. *J. Org. Chem.* **2010**, *75*, 6163-6172.

¹⁴ (a) Reich, H. J.; Green, D. P.; Phillips, N. H. *J. Am. Chem. Soc.* **1989**, *111*, 3444-3445; (b) Carlier, P. R.; Lo, C. W.-S. *J. Am. Chem. Soc.* **2000**, *122*, 12819-12823.

¹⁵ Collum's Job polt: a) Liou, L. R.; McNeil, A. J.; Toombes, G. E. S.; Collum, D. B. *J. Am. Chem. Soc.* **2008**, *130*, 17334-17341. (b) Liou, L. R.; McNeil, A. J.; Ramirez, A.; Toombes, G. E. S.; Gruver, J. M.; Collum, D. B. *J. Am. Chem. Soc.* **2008**, *130*, 4859-4868. (c) Gruver, J. M.; Liou, L. R.; McNeil, A. J.; Ramirez, A.; Collum, D. B. *J. Org. Chem.* **2008**, *73*, 7743-7747. (d) De Vries, T. S.; Goswami, A.; Liou, L. R.; Gruver, J. M.; Jayne, E.; Collum, D. B. *J. Am. Chem. Soc.* **2009**, *131*, 13142-13154. (e) Renny, J. S.; Tomasevich, L. L.; Tallmadge, E. H.; Collum, D. B. *Angew. Chem. Int. Ed.* **2013**, *52*, 11998-12013. (f) Tomasevich, L. L.; Collum, D. B. *J. Org. Chem.* **2013**, *78*, 7498-7507. (g) Tomasevich, L. L.; Collum, D. B. *J. Am. Chem. Soc.* **2014**, *136*, 9710-9718.

¹⁶) Kagan, G.; Li, W.; Russell, H.; Williard, P. G. *Org. Chem.* **2010**, *12*, 50-53. (b) Li, W.; Kagan, G.; Yang, H.; Cai, C.; Hopson, R.; Dai, W.; Sweigart, D. A.; Williard, P. G. *Organometallics* **2010**, *29*, 1309-1311. (c) Li, W.; Kagan, G.; Yang, H.; Cai, C.; Hopson, R.; Sweigart, D. A.; Williard, P. G. *Org. Lett.* **2010**, *12*, 2698-2701. (d) Li, D.; Keresztes, I.; Hopson, R.; Williard, P. G. *Acc. Chem. Res.* **2009**, *42*, 270-280. (e) Li, D.; Kagan, G.; Hopson, R.; Williard, P. G. *J. Am. Chem. Soc.* **2009**, *131*, 5627-5634. (f) Keresztes, I.; Williard, P. G. *J. Am. Chem. Soc.* **2000**, *122*, 10228-10229. (g) Su, C.; Guang, J.; Li, W.; Wu, K.; Hopson, R.; Williard, P. G. *J. Am. Chem. Soc.* **2014**, *136*, 11735-11747. (h) Su, C.; Hopson, R.; Williard, P. G. *J. Am. Chem. Soc.* **2014**, *136*, 3246-7863. (i) Su, C.; Hopson, R.; Williard, P. G. *J. Am. Chem. Soc.* **2013**, *135*, 12400-12406. (j) Su, C.; Hopson, R.; Williard, P. G. *Eur. J. Inorg. Chem.* **2013**, *24*, 4136-4141. (k) Su, C.; Hopson, R.; Williard, P. G. *J. Org. Chem.* **2013**, *78*, 7288-7292. (l) Su, C.; Hopson, R.; Williard, P. G. *J. Am. Chem. Soc.* **2013**, *135*, 14367-14379. (m) Kagan, G.; Li, W.; Li, D.; Hopson, R.; Williard, P. G. *J. Am. Chem. Soc.* **2011**, *133*, 6596-6602. (n) Kagan, G.; Li, W.; Sun, C.; Hopson, R.; Williard, P. G. *J. Org. Chem.* **2011**, *76*, 65-70.

Chapter 2 Diffusion Coefficient-Formula Weight (D-FW) Analysis of ^2H Diffusion-Ordered NMR Spectroscopy (DOSY)

2.1 Abstract

Referenced ^2H DOSY with D-FW analysis method is developed with great linear relationship ($R^2 > 0.99$) between $\log D$ and $\log FW$. Solution-state structure of THF solvated LDA is studied in hydrocarbon solvent via this novel method and an equilibrium between mono-solvated and di-solvated dimer complexes is observed at room temperature. Finally, a non-deuterated compound with exchangeable proton can be applied in ^2H DOSY experiment through the convenient proton-deuterium exchange process and achieve consistent result as in ^1H DOSY method.

2.2 Introduction

Pulsed gradient spin-echo (PGSE) diffusion NMR spectroscopy was conceived to measure diffusion coefficients and to deduce the hydrodynamic radii of molecules in solution by Stejskal and Tanner in the mid-1960s.¹ In 1992, the PGSE sequence was used in a two-dimensional NMR experiment by C. S. Johnson, in which one dimension represents the regular chemical shift and the second dimension separates species by particle size.² This 2D experiment is now referred to as diffusion-ordered NMR spectroscopy (DOSY).³ Our group has developed ^1H , ^{13}C and ^{31}P DOSY techniques and diffusion coefficient-formula weight (D-FW) analysis as useful tools for the measurement of formula weights of complexes in solution.⁴ Reliable predicted formula weights of target complexes can be calculated by the calibration curve of D-FW analysis from appropriate references.⁵ This referenced DOSY technique is

especially beneficial for studying various intermediates in solution and those systems not applicable to traditional mass spectrometric techniques, including air sensitive and reactive small molecules, such as organometallic compounds. According to our practical experience of this referenced DOSY method during recent decade, ^{13}C DOSY experiment is quite time-consuming for dilute samples, due to the low natural abundance of ^{13}C . ^{31}P DOSY is only applicable for phosphorus systems. Among all the nuclei, ^1H DOSY presents best accuracy, shortest time cost and widest application.⁶ However ^1H DOSY suffers from the potential drawback of overlapping resonances in the chemical shift dimension which lead to deceptive values in the diffusion dimension. In order to overcome these disadvantages, isotopically labeled references were introduced. Our group has developed isotopically enriched ^{13}C DOSY technique⁷ and successfully applied on the solution-state characterization of methyl lithium. Considering for most organic compounds, the cheapest and easiest isotopically labeling method is deuterium labeling, establishment of this referenced DOSY method on deuterium is a necessary and important extension for the DOSY toolbox. There are only a few of solution state ^2H NMR studies have been reported,⁸ including several self-diffusion coefficient measurements by the PGSE method.⁹ Here we report the first example of referenced ^2H DOSY method and its applications.

2.3 Results and Discussion

2.3.1 Experimental Temperature

Unlike the nuclei (^1H , ^{13}C , ^{31}P) we applied before, the nuclear spin quantum number (I) of deuterium is 1, which implies a quadrupole moment (Q) due to the non-spherically electron charge distribution around its nucleus. The dominant relaxation mechanism for a nucleus with quadrupole moment is quadrupolar relaxation (R_{QR}),

described by **equation 2.1**. T_1 is longitudinal (or spin-lattice) relaxation time, μ is asymmetry of electric field, q_z is electric field gradient and τ_c is molecular correlation time (molecular or segmental rotation). This equation represents that molecular shape, chemical environment around target deuterium nuclei and molecule tumbling rate will all be able to influence the relaxation time T_1 . However τ_c is more predicable and can be significantly influenced by experimental. Lower temperature leads to longer τ_c , shorter relaxation time and broader peaks. As shown in **Figure 2.1**, two commercially available perdeuterated compounds and two synthetically partially deuterated complexes, whose formula weights distribution is similar to the distribution of ^1H DOSY references, have been used to observe the dependence of relaxation time on temperature. Base on our current instrumental condition, a longer than 100 ms T_1 time is necessary to set up the appropriate diffusion time of DOSY experiment. Therefore the recommended experimental temperature for ^2H DOSY is not lower than $-20\text{ }^\circ\text{C}$. Moreover, considering larger molecular weight would also reduce τ_c , a more general recommended experiment temperature is ambient temperature or higher like normal body temperature $37\text{ }^\circ\text{C}$.

$$R(^2\text{H})_{\text{QR}} = \frac{1}{T_{1(\text{QR})}} = \frac{2}{2} \pi^2 \left(1 + \frac{\mu^2}{3} \right) \left(\frac{Qq_z e^2}{h} \right) \tau_c \quad (\text{eq. 2.1})$$

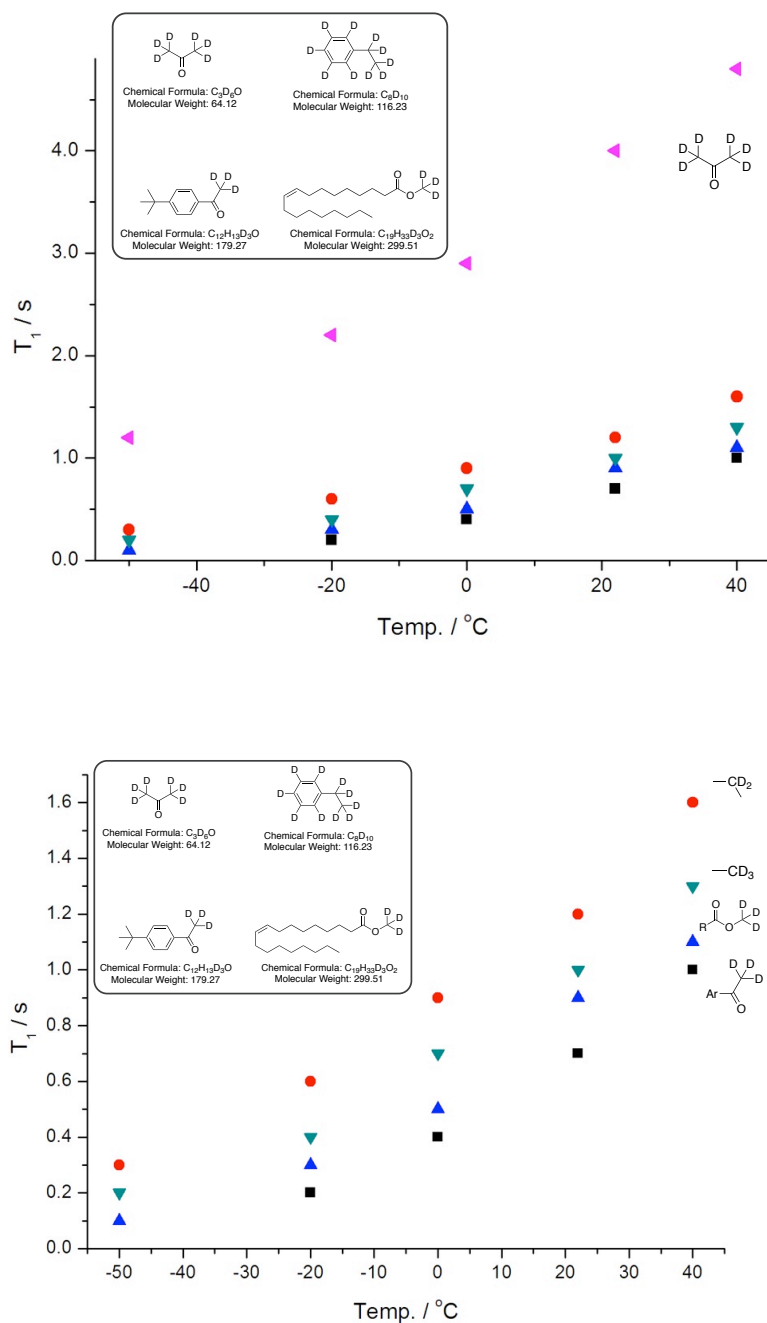


Figure 2.1. Dependence of T_1 on temperature

2.3.2 Internal References

There are a lot of commercial available perdeuterated compounds, which would be quite convenient internal references for ^2H DOSY experiment. However, most ^2H -labeled target complexes are partially deuterated, due to the consideration of synthetic

convenience and elusion of peaks overlap. It is questionable using perdeuterated references to measure partially deuterated compounds. According to the modified Stokes-Einstein equation (eq. 2.2),¹⁰ diffusion coefficient (D) will be influenced by temperature (T), viscosity (η), particle shape (f_s) and radius (r). Therefore using diffusion coefficient to predict molecular weight requires that all the complexes in the solution have similar densities.¹¹ Deuterium nucleus has identical size as proton but heavier mass. Thus in theory, introducing more deuterium nuclei to one compound will cause more increasing on density, then leads to larger error on prediction of molecular weight. On the other side, proton nuclei only take small part of MW for most of organic compounds. Hence, density change from introducing deuterium could be not significant enough to influence our DOSY result. Four commercial available perdeuterated compounds were mixed with synthetic methyl oleate- d_3 deuterated ester, and applied to ^2H DOSY, in order to test that if perdeuterated compounds can be employed as internal references for ^2H DOSY.

$$D = \frac{kT}{f_s(a, b)\pi\eta r} \quad (\text{eq. 2. 2})$$

As shown in **Figure 2.2 & 2.3**, perdeuterated actone, ethylbenzene and acenaphthene present quite good linear relationship with partially deuterated ester in D-FW analysis. This result indicates that both perdeuterated and partially deuterated compounds can be applied together in ^2H DOSY experiments, which is also confirmed in our application cases discussed later. The only exception we found is perdeuterated chrysene. This is probably because the diffusion-behavior description of chrysene would apply a dramatically different f_s value due to its distinctly flat molecular shape.

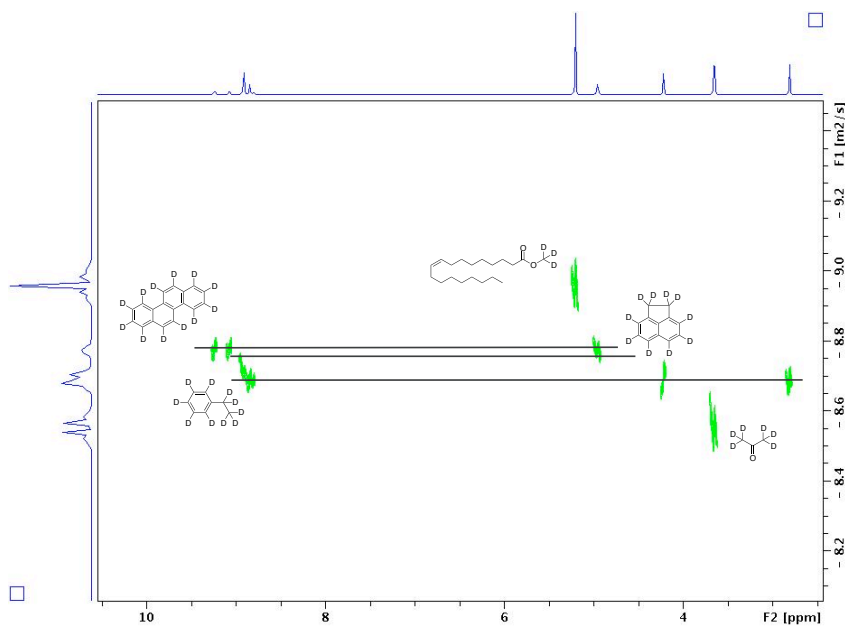


Figure 2.2. ^2H DOSY NMR in general THF for the test of internal references.

Table 2.1. D-FW analysis of ^2H DOSY data for the test of internal references

Entry	Compound	FW g/mol	D m^2/s	Predicted FW g/mol	% Error
1	Acetone- d_6	64.1	$2.82\text{E-}9$	67.3	5
2	ethylbenzene- d_{10}	116	$2.08\text{E-}9$	111	-4
3	acenaphthene- d_{10}	164	$1.70\text{E-}9$	155	-5
4	chrysene- d_{12}	240	$1.68\text{E-}9$	158	-34
5	Ester- d_3	300	$1.10\text{E-}9$	316	5

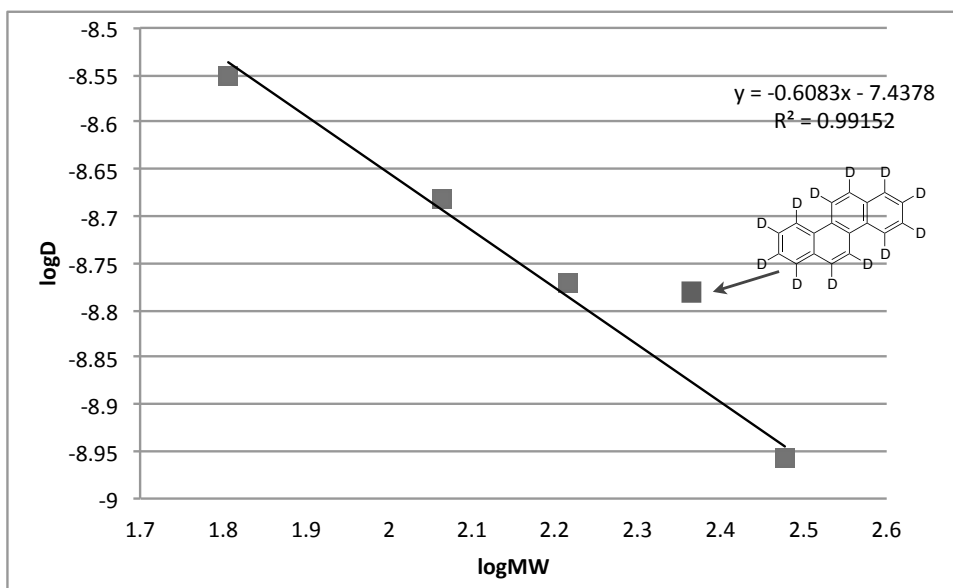


Figure 2.3. D-FW analysis of ^2H DOSY data for the test of internal references

2.3.3 Application on Organometallic Complex

LDA will form di-solvated dimer with THF in both solution state and solid state, which was supported by NMR study of $[^6\text{Li}, ^{15}\text{N}]$ -LDA,¹² x-ray crystallography structure¹³ and NMR study by $^1\text{H}/^{13}\text{C}$ DOSY with D-FW analysis.¹⁴ Hence LDA-*d*/THF/Tol system would be an ideal case to verify the reliability of D-FW analysis method via ^2H DOSY. The synthetic path of LDA-*d* is already available from previous literatures.¹⁵

Considering the molecular weight of target complex, di-THF solvated LDA-*d* dimer, is 360 g/mol, therefore the four chosen internal references have molecular weight from 100 g/mol to 371 g/mol and stay inert with organolithium reagents. As shown in **Figure 2.4**, the measured molecular weight of LDA-*d* is 366 g/mol (error 2%) with 10 eq of THF (averaged MW 104 g/mol, see **SI**) in general toluene solution, which is consistent with the fact that LDA forms di-solvated dimer with THF. Moreover, MWs of both LDA-*d* and THF-*d*₈ have been measured under various amount of THF (**SI**). These data can only be explained by the equilibrium between mono-THF solvated LDA dimer

and di-THF solvated LDA dimer and exclude the existence of LDA monomer. Hence, only THF solvated LDA dimer exists in hydrocarbon solvent at room temperature (**Scheme 2.1**).

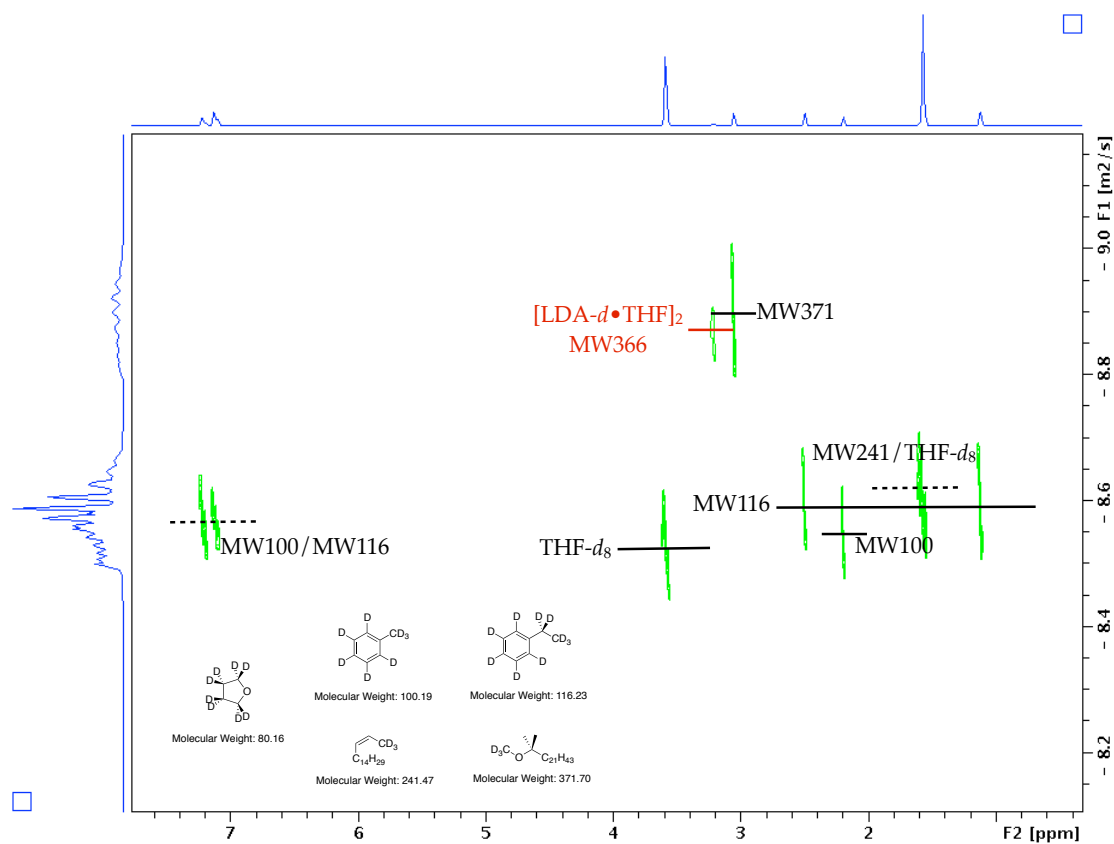
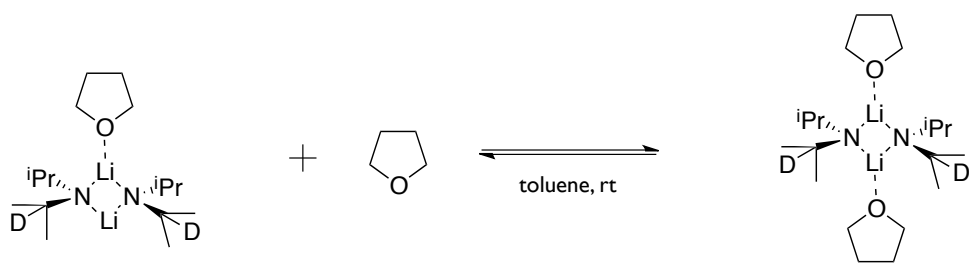


Figure 2.4. ^2H DOSY NMR of LDA-*d* in general toluene with 1 eq of THF- d_8 and 9 eq of general THF.

Scheme 2.1. Results of ^2H DOSY of LDA-*d* in general toluene with 1 ~ 20 eq of THF/THF- d_8 at room temperature



Molecular Weight: 288.36

Molecular Weight: 360.47

LDA : THF	Obs. MW _{LDA}	Obs. MW _{THF}	D ₁ /%	D ₂ /%
1 : 1	316	261	~75	~25
1 : 2	323	146	~60	~40
1 : 10	366	104	<5	>95
1 : 20	360	--	<5	>95

2.3.4 Application on amide via Hydrogen-Deuterium Exchange Labeling

The most convenient method of deuterium labeling is hydrogen-deuterium exchange. This method has been widely applied on the amides in the backbone of a protein, in order to study the structure and dynamic properties of proteins. Therefore, it is intriguing to know if ^2H DOSY can achieve reliable result for exchangeable deuterium. In the first experiment, 10 μl of D_2O was added to 0.5 ml of 0.4 M acetanilide/acetone- d_6 solution. Molecular weight of acetanilide was measured by ^1H DOSY as 181 g/mol (**Figure 2.5**), which is larger than its FW 135 g/mol, due to self-dimerization and solvation by water in the solution. We prepared another sample as the one in the first experiment, but using general acetone as the solvent instead of acetone- d_6 . Before being utilized in ^2H DOSY experiment, the second sample sit still for 1 h, in order to allow the H-D exchange achieve equilibrium. The only observable peak of acetanilide in ^2H NMR is from N-D group with T_1 relaxation time 0.5 s, which is long enough for setting the appropriate diffusion time (0.1 s) for ^2H DOSY. As shown in **Figure 2.6**, acetanilide- d has measured molecular weight 197 g/mol, within 10% error comparing with the result in ^1H DOSY experiment. Therefore, compounds with

exchangeable proton (with relatively long relaxation time for deuterium peak) can be applied in ^2H DOSY experiment via H-D exchange method.

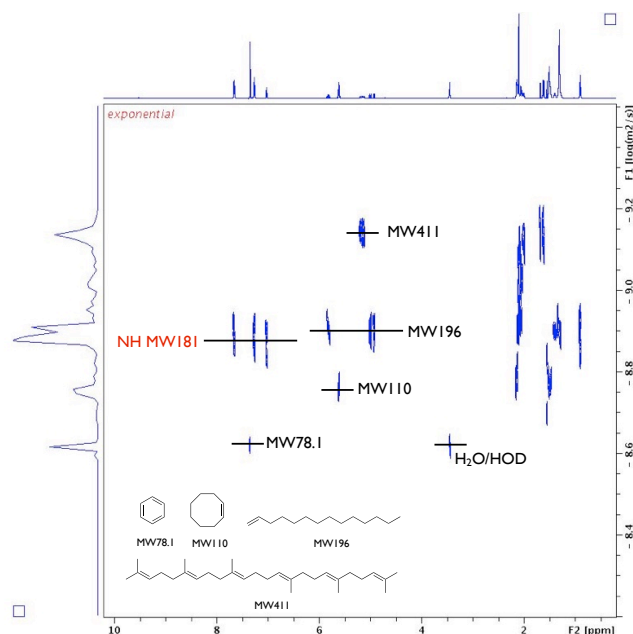


Figure 2.5. ^1H DOSY NMR of 0.4 M acetanilide in acetone- d_6 with 10 μl D_2O (2.5 eq).

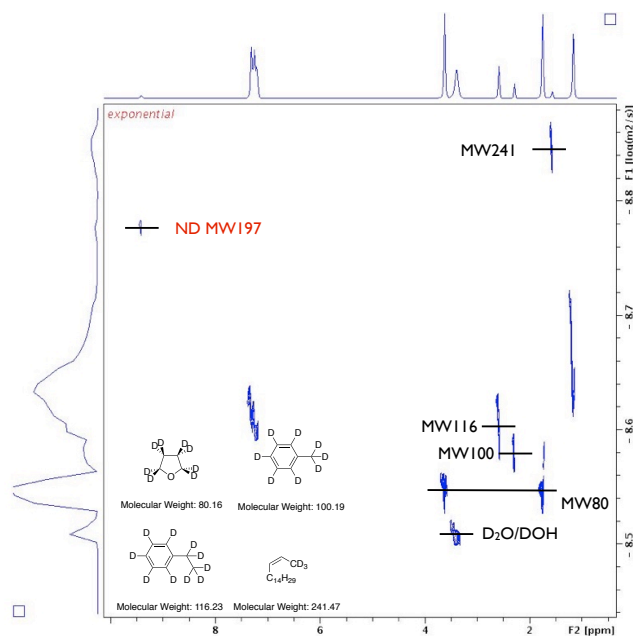


Figure 2.6. ^2H DOSY NMR of 0.4 M acetanilide in general acetone with 10 μl H_2O (2.5 eq).

2.4 Conclusion

Referenced ^2H DOSY method has been developed with both partially deuterated and perdeuterated internal references. The correlation between $\log D$ and $\log FW$ presents quite great linear relationship ($R^2 > 0.99$) in all ^2H DOSY experiments. Solution state structure of THF solvated LDA has been studied in hydrocarbon solvent via ^2H DOSY and an equilibrium between mono-solvated and di-solvated dimer is observed at room temperature. Finally, a non-deuterated compound with exchangeable proton is labeled by deuterium through proton-deuterium exchange process and applied in both ^1H and ^2H DOSY experiments with compatible predicted MW results.

2.5 Experimental Section

Procedures for NMR Experiments. ^1H chemical shifts were referenced to TMS (from CDCl_3) at 0.00 ppm and ^{13}C chemical shifts were referenced to CDCl_3 at 77.2 ppm. All NMR experiments were acquired on a 400 MHz spectrometer equipped with a z-axis gradient ATMA BBO probe. For DOSY experiments, a z-axis gradient amplifier was employed, with maximum gradient strength of 0.214 T/m. Spin-lattice relaxation time (T_1) was estimated by zero-crossing/null-time experiment after calibration of 90° pulse (P_1). ^1H and ^2H DOSY was performed using the standard ledbpgp2s pulse program, employing a bipolar gradient pulses for diffusion, and 2 spoil gradients. Diffusion time was 100 ms, and the rectangular gradient pulse duration was 1000 μs for ^1H DOSY and 3000 μs for ^2H DOSY. Gradient recovery delays were 200 μs . Individual rows of the quasi-2-D diffusion databases were phased and baseline corrected. Actual diffusion coefficients used for D-FW analysis were obtained using the T1/T2 analysis module in commercially available software.

Synthesis of 2,2,2- ^2H -4'-tert-butylacetophenone. Gibson's method¹⁶ has been applied here to label the α position of ketones by deuterium. 0.88 g of 4'-tert-

butylacetophenone (5 mmol, 1.0 eq) was added to a solution containing 3 ml of methanol-d (75 mmol, 15 eq), 0.9 ml of D₂O (50 mmol, 10 eq) and 30 mg of sodium metal (1.3 mmol, 0.26 eq) in a flamed-dried flask under argon atmosphere. The mixture was heated to reflux for 3 h, cooled and diluted with 20 ml diethyl ether. The organic phase was washed by 10 ml water twice, brine once and dried over anhydrous Na₂SO₄. After removal of solvent by rotary evaporation, 0.82 g of 2,2,2-²H-4'-tert-butylacetophenone (92%) was gained as colorless oil. ¹H NMR (CDCl₃, 600 MHz) δ 1.34 (s, 9H), 7.48 (d, 2H, J = 8.5 Hz), 7.95 (d, 2H, J = 8.5 Hz); ¹³C NMR (CDCl₃, 150 MHz) δ 31.1, 35.1, 125.5, 128.3, 134.6, 156.8, 198.0; HRMS-ESI m/z: [M]⁺ Calcd for C₁₂H₁₃D₃O: 179.1389, found [M+H]⁺ 180.1458.

Synthesis of cis-(methyl-²H)-oleate.¹⁷ 0.113 g of Oleic acid (0.4 mmol) was dissolved in 1 ml chloroform. 0.02 g methanol-d₄ (0.6 mmol, 1.5 eq) and 0.023 g trimethylsilyl chloride (0.2 mmol, 0.5 eq) have been slowly added to the solution. After stirring at room temperature for 12 h, the reaction mixture was quenched and washed by 1 ml of 0.5 M NaHCO₃, then washed by 1 ml of brine and dried over by anhydrous Na₂SO₄. After removal of solvent by rotary evaporation, 96 mg ester (80%) was obtained as colorless oil. ¹H NMR (CDCl₃, 600 MHz) δ 0.88 (t, 3H, J = 6.7 Hz), 1.15 ~ 1.40 (m, 20H), 1.62 (m, 2H), 2.01 (m, 4H), 2.30 (t, 3H, J = 7.6 Hz), 5.34 (m, 2H); ¹³C NMR (CDCl₃, 150 MHz) δ 14.1, 22.7, 24.9, 27.1, 27.2, 29.1, 29.1, 29.1, 29.3, 29.5, 29.6, 29.7, 31.9, 34.1, 129.7, 129.9, 174.2.

Synthesis of (Z)-Heptadec-2-ene-1,1,1-²H. 0.55 g of 1-hexadecyne (2.5 mmol, 1.0 eq) was dissolved in 20 ml dried THF in a flamed-dried flask under argon atmosphere. 1.4 ml of 2.2 M n-BuLi (3.0 mmol, 1.2 eq) was added slowly at -78 °C. After 10 min, the mixture was warmed up to 0 °C and stirred for 0.5 h. Then 0.54 g of CD₃I (3.75 mmol, 1.5 eq) was added and stirred at room temperature for 3 h. The resulting

solution was quenched with 5 ml of saturated ammonium chloride and extracted with 20 ml of hexanes three times. The combined organic phase was washed by brine and dried over anhydrous Na_2SO_4 . After removal of solvent by rotary evaporation, heptadec-2-yne-1,1,1- ^2H was gained and used in the next step without purification. Heptadec-2-yne-1,1,1- ^2H was reduced to (Z)-heptadec-2-ene-1,1,1- ^2H by Ashby's method.¹⁸ Under an atmosphere of nitrogen, 0.05 eq of Cp_2TiCl_2 was dissolved in THF. Crude heptadec-2-yne-1,1,1- ^2H was added at 0 °C, then 1.2 eq of LiAlH_4 was added. After stirring at room temperature for 3 h. the reaction was quenched by the successive addition of water, 5% NaOH (aq), and water. The mixture was filtered and then concentrated under reduced pressure. The crude product was purified via silica gel chromatography (100% hexanes) to gain transparent oil ^1H NMR (CDCl_3 , 600 MHz) δ 0.88 (t, 3H, $J = 6.8$ Hz), 1.10 ~ 1.60 (m, 24H), 2.02 (m, 2H), 5.41 (m, 2H); ^{13}C NMR (CDCl_3 , 150 MHz) δ 14.1, 22.7, 26.9, 29.3, 29.4, 29.6, 29.6, 29.7, 29.7, 31.9, 123.5, 131.0; MS m/z 241 $[\text{M}]^+$, 241, 213, 196, 171, 154, 128, 111, 83, 57.

Synthesis of 2-methyl-2-(methoxy- ^2H)-tricosane. 2-methyltricosan-2-ol was prepared by following previous reported method.¹⁹ 0.23 g of 60% sodium hydride in mineral oil (5.7 mmol, 4 eq) was placed in a flamed-dried flask under argon atmosphere. The grey mixture was washed by 3 ml dry pentane three times in order to remove mineral oil. Then 10 ml dried THF and 0.50 g 2-methyltricosan-2-ol (1.4 mmol, 1.0 eq) were added and the resulting solution was refluxed for 4 h. 0.30 g of CD_3I (2.1 mmol, 1.5 eq) has been added at 0 °C into the solution, before another 3 h of reflux. The reaction mixture was quenched with 5 ml of saturated ammonium chloride at 0 °C, then extracted by 10 ml of hexanes three times. The combined organic phase was washed by 30 ml of brine and dried over anhydrous Na_2SO_4 . After removal of solvent by rotary evaporation, the residue was purified

chromatographically on a flash column by hexanes. After the removal of solvent, 0.38 g of ether (1.0 mmol, 72%) was obtained as white solid. ¹H NMR (CDCl₃, 600 MHz) δ 0.88 (t, 3H, J = 6.8 Hz), 1.13 (s, 6H), 1.24 ~ 1.30 (br, 40H); ¹³C NMR (CDCl₃, 150 MHz) δ 14.1, 22.7, 23.9, 25.0, 29.4, 29.7, 29.7, 29.8, 29.8, 30.3, 32.0, 39.9, 74.6;

2.6 References

-
- ¹ (a) Stejskal, E. O.; Tanner, J. E. *J. Chem. Phys.* **1965**, *42*, 288-292. (b) Tanner, J. E. *Rev. Sci. Instrum.* **1965**, *36*, 1086-1087. (c) Stejskal, E. O. *J. Chem. Phys.* **1965**, *43*, 3597-3603.
- ² Morris, K. F.; Johnson, Jr., C. S. *J. Am. Chem. Soc.* **1992**, *114*, 3139-3141.
- ³ Johnson, Jr., C. S. *Prog. NMR Spectrosc.* **1999**, *34*, 203-256.
- ⁴ (a) Kagan, G.; Li, W.; Russell, H.; Williard, P. G. *Org. Chem.* **2010**, *12*, 50-53. (b) Li, W.; Kagan, G.; Yang, H.; Cai, C.; Hopson, R.; Dai, W.; Sweigart, D. A.; Williard, P. G. *Organometallics* **2010**, *29*, 1309-1311. (c) Li, W.; Kagan, G.; Yang, H.; Cai, C.; Hopson, R.; Sweigart, D. A.; Williard, P. G. *Org. Lett.* **2010**, *12*, 2698-2701. (d) Li, D.; Keresztes, I.; Hopson, R.; Williard, P. G. *Acc. Chem. Res.* **2009**, *42*, 270-280. (e) Li, D.; Kagan, G.; Hopson, R.; Williard, P. G. *J. Am. Chem. Soc.* **2009**, *131*, 5627-5634. (f) Kagan, G.; Li, W.; Hopson, R.; Williard, P. G. *Org. Lett.* **2009**, *11*, 4818-4821. (g) Li, D.; Hopson, R.; Li, W.; Liu, J.; Williard, P. G. *Org. Lett.* **2008**, *10*, 909-911. (h) Liu, J.; Li, D.; Sun, C.; Williard, P. G. *J. Org. Chem.* **2008**, *73*, 4045-4052. (i) Keresztes, I.; Williard, P. G. *J. Am. Chem. Soc.* **2000**, *122*, 10228-10229.
- ⁵ (a) Su, C.; Guang, J.; Li, W.; Wu, K.; Hopson, R.; Williard, P. G. *J. Am. Chem. Soc.* **2014**, *136*, 11735-11747. (b) Su, C.; Hopson, R.; Williard, P. G. *J. Am. Chem. Soc.* **2014**, *136*, 3246-7863. (c) Su, C.; Hopson, R.; Williard, P. G. *J. Am. Chem. Soc.* **2013**, *135*, 12400-12406. (d) Su, C.; Hopson, R.; Williard, P. G. *Eur. J. Inorg. Chem.* **2013**, *24*, 4136-4141. (e) Su, C.; Hopson, R.; Williard, P. G. *J. Org. Chem.* **2013**, *78*, 7288-7292. (f) Su, C.; Hopson, R.; Williard, P. G. *J. Am. Chem. Soc.* **2013**, *135*, 14367-14379. (g) Kagan, G.; Li, W.; Li, D.; Hopson, R.; Williard, P. G. *J. Am. Chem. Soc.* **2011**, *133*, 6596-6602. (h) Kagan, G.; Li, W.; Sun, C.; Hopson, R.; Williard, P. G. *J. Org. Chem.* **2011**, *76*, 65-70. (i) Socha, A. M.; Kagan, G.; Li, W.; Hopson, R.; Sello, J. K.; Williard, P. G. *Energy & Fuels* **2010**, *24*, 4518-4521.
- ⁶ (a) Armstrong, D. R.; Garcia-Alvarez, P.; Kennedy, A. R.; Mulvey, R. E.; Parkinson, J. A. *Angew. Chem. Int. Ed.* **2010**, *49*, 3185-3188. (b) Consiglio, G. B.; Queval, P.; Harrison-Marchand, A.; Mordini, A.; Lohier, J.-F.; Delacroix, O.; Gaumont, A.-C.; Gerard, H.; Maddaluno, J.; Ouyadi, H. *J. Am. Chem. Soc.* **2011**, *133*, 6472-6480. (c) Mulvey, R. E.; Armstrong, D. R.; Conway, B.; Crosbie, E.; Kennedy, A. R.; Robertson, S. D. *Inorg. Chem.* **2011**, *50*, 12241-12251. (d) Lecachey, B.; Duguet, N.; Ouyadi, H.; Fressigne, C.; Harrison-Marchand, A.; Yamamoto, Y.; Tomioka, K.; Maddaluno, J. *Org. Lett.* **2009**, *11*, 1907-1910. (e) Armstrong, D. R.; Garcia-Alvarez, P.; Kennedy, A. R.; Mulvey, R. E.; Robertson, S. D. *Chem. Eur. J.* **2011**, *17*, 6725-

6730. (f) Lecachey, B.; Oulyadi, H.; Lameiras, P.; Harrison-Marchand, A.; Gerard, H.; Maddaluno, J. *J. Org. Chem.* **2010**, *75*, 5976-5983. (g) Armstrong, D. R.; Kennedy, A. R.; Mulvey, R. E.; Parkinson, J. A.; Robertson, S. D. *Chem. Sci.* **2012**, *3*, 2700-2707. (h) Armstrong, D. R.; Clegg, W.; Garcia-Alvarez, P.; McCall, M. D.; Nuttall, L.; Kennedy, A. R.; Russo, L.; Hevia, E. *Chem. Eur. J.* **2011**, *17*, 4470-4479. (i) Tatic, T.; Hermann, S.; John, M.; Loquet, A.; Lange, A.; Stalke, D. *Angew. Chem. Int. Ed.* **2011**, *50*, 6666-6669. (j) Benndorf, P.; Schmitt, S.; Koppe, R.; Ona-Burgos, P.; Scheurer, A.; Meyer, K.; Roesky, P. W. *Angew. Chem. Int. Ed.* **2012**, *51*, 5006-5010. (k) Hevia, E.; Kennedy, A. R.; Mulvey, R. E.; Ramsay, D. L.; Robertson, S. D. *Chem. Eur. J.* **2013**, *19*, 14069-14075. (l) Lane, E. M.; Chapp, T. W.; Hughes, R. P.; Glueck, D. S.; Feland, B. C.; Bernard, G. M.; Wasylshen, R. E.; Rheingold, A. L. *Inorg. Chem.* **2010**, *49*, 3950-3957. (m) Munoz, M. T.; Urbaneja, C.; Temprado, M.; Mosquera, M. E. G.; Cuenca, T. *Chem. Commun.* **2011**, *47*, 11757-11759. (n) Tran, N. T.; Wilson, S. O.; Franz, A. K. *Chem. Commun.* **2014**, *50*, 3738-3740. (o) Hamdoun, G.; Sebban, M.; Cossoul, E.; Harrison-Marchand, A.; Maddaluno, J. Oulyadi, H. *Chem. Commun.* **2014**, *50*, 4073-4075. (p) Garcia-Rodriguez, R.; Liu, H. *Chem. Commun.* **2013**, *49*, 7857-7859.

⁷ Su, C.; Russell, H.; Williard, P. G. *J. Org. Chem.* **2013**, *78*, 11733-11746.

⁸ (a) Pitner, T. P.; Edwards, W. B.; Bassfield, R. L.; Whidby, J. F. *J. Am. Chem. Soc.* **1978**, *100*, 246-251. (b) Wolk, S. K.; Eisenhart, E. *Macromolecules* **1993**, *26*, 1086-1090. (c) Gusev, D. G.; Vymenits, A. B.; Bakhmutov, V. I. *Mendeleev Commun.* **1991**, *1*, 24-26. (d) Foston, M. B.; McGaughey, J.; O'Neil, H.; Evans, B. R.; Ragauskas, A. *Analyst* **2012**, *137*, 1090-1093. (e) Serhan, Z.; Borgogno, A.; Billault, I.; Ferrarini, A.; Lesot, P. *Chem. Eur. J.* **2012**, *18*, 117-126. (e) Guo, J.; Yang, D.-P.; Chari, R.; Tian, X.; Pavlopoulos, S.; Lu, D.; Makriyannis, A. *J. Med. Chem.* **2008**, *51*, 6793-6799. (f) Knorr, R.; Hauer, H.; Weiss, A.; Polzer, H.; Ruf, F.; Low, R.; Dvortsak, P.; Bohrer, P. *Inorg. Chem.* **2007**, *46*, 8379-8390. (g) Zhu, D.; Herbert, B. E.; Schlautman, M. A.; Carraway, E. R. *J. Environ. Qual.* **2004**, *33*, 276-284. (h) Bakhmutov, V. I. In: Roli, R.; Peruzzini, M. (eds). *Deuterium NMR Relaxation as a Method for the Characterization and Study of Transition Metal Hydride Systems in Solution*, in *Recent Advances in Hydride Chemistry*. Elsevier: Amsterdam, London, New York, Paris, Tokyo, **2001**, 375-390.

⁹ (a) Giordani, C.; Wakai, C.; Okamura, E.; Matubayasi, N.; Nakahara, M. *J. Phys. Chem. B* **2006**, *110*, 15205-15211. (b) Kriz, J.; Dybal, J. *J. Phys. Chem. B* **2005**, *109*, 13436-13444. (c) Kurkova, D.; Kriz, J.; Schmidt, P.; Dybal, J.; Rodriguez-Cabello, J.; Alonso, M. *Biomacromolecules* **2003**, *4*, 589-601. (d) Iannilli, E.; Tettamanti, E.; Galantini, L.; Magazu, S. *J. Phys. Chem. B* **2001**, *105*, 12143-12149.

¹⁰ (a) Perrin, F. J. *Phys. Radium*, 1936, *7*, 1-11; (b) Chen, H.; Chen, S. *J. Phys. Chem.* **1984**, *88*, 5118-5121.

¹¹ (a) Evans, R.; Deng, Z.; Rogerson, A. K.; McLachlan, A. S.; Richards, J. J.; Nilson, M.; Morris, G. A. *Angew. Chem. Int. Ed.* **2013**, *52*, 3199-3202. (b) Valencia, D. P.; Gonzalez, F. *J. Electrochem. Commun.* **2011**, *13*, 129-132. (c) Pregosin, P. S. *Spectrosc. Prop. Inorg. Organomet. Compd.* **2012**, *42*, 248-268.

¹² (a) Galiano, R.; Angela S.; Collum, D. B. *J. Am. Chem. Soc.* **1989**, *111*, 6772-6778. (b) Rutherford, J. L.; Collum, D. B. *J. Am. Chem. Soc.* **2001**, *123*, 199-202.

¹³ Williard, P. G.; Salvino, J. M. *J. Org. Chem.* **1993**, *58*, 1-3.

¹⁴ (a) Li, D.; Hopson, R.; Li, W.; Liu, J.; Williard, P. G. *Org. Lett.* **2008**, *10*, 909-911; (b) Li, D.; Kagan, G.; Hopson, R.; Williard, P. G. *J. Am. Chem. Soc.* **2009**, *131*, 5627-5634.

-
- ¹⁵ (a) Newcomb, M.; Varick, T. R.; Goh, S.-H. *J. Am. Chem. Soc.* **1990**, *112*, 5186-5193; (b) Williard, P. G.; Salvino, J. M. *J. Org. Chem.* **1993**, *58*, 1-3.
- ¹⁶ Gibson, T. *Org. Magn. Reson.* **1983**, *21*, 482-486.
- ¹⁷ Nakao, R.; Oka, K.; Fukumoto, T. *Bull. Chem. Soc. Jpn.* **1981**, *54*, 1267-1268.
- ¹⁸ Ashby, E. C.; Noding, S. A. *J. Org. Chem.* **1980**, *45*, 1035-1041.
- ¹⁹ Su, C.; Hopson, R.; Williard, P. *J. Org. Chem.* **2013**, *78*, 11733-11746.

Chapter 3 Lithium Pinacolone Enolate Solvated by Hexamethylphosphoramide (HMPA)

3.1 Abstract

We report the crystal structure of a substoichiometric, HMPA trisolvated lithium pinacolone enolate tetramer $(\text{LiOPin})_4 \cdot \text{HMPA}_3$ abbreviated as \mathbf{T}_3 . In this tetramer one HMPA binds to lithium more strongly than the other two causing a reduction in spatial symmetry with corresponding loss of C_3 symmetry. A variety of NMR experiments, including HMPA titration, diffusion coefficient-formula weight (D-FW) analysis and other multi-nuclear one- and two-dimensional NMR techniques reveal that \mathbf{T}_3 is the major species in hydrocarbon solution when more than 0.6 equivalents of HMPA are added. Due to a small amount of moisture from HMPA or air leaking into the solution, a minor complex was identified and confirmed by x-ray diffraction analysis as a mixed aggregate containing enolate, lithium hydroxide, and HMPA in a 4:2:4 ratio, $[(\text{LiOPin})_4 \cdot (\text{LiOH})_2 \cdot \text{HMPA}_4]$ that we refer to as pseudo- \mathbf{T}_4 . The tetra-HMPA solvated lithium cyclopentanone enolate tetramer was also prepared and characterized by x-ray diffraction leading to the conclusion that steric effects dominate the formation and solvation of the pinacolone \mathbf{T}_3 and pseudo- \mathbf{T}_4 aggregates. An unusual mixed aggregate consisting of pinacolone enolate, lithium diisopropyl amide, lithium oxide and HMPA in the ratio 5:1:1:2 is also described.

3.2 Introduction

Hexamethylphosphoramide (HMPA) as an additive or co-solvent plays an intriguing role in reactions of organolithium reagents by altering rates, yields and selectivity.¹ Its influence on selectivity is most striking and has been intensively

studied. For example, HMPA influences the regioselectivity of enolate addition reaction to α,β -unsaturated compounds.² It also influences the stereoselectivity of asymmetric addition and the enolization of carbonyl compounds.³ In many cases, addition of HMPA results in reaction rate acceleration and higher yields of thermodynamic products.⁴ An explanation for the differing reaction selectivity attributed to the presence or absence of HMPA involves deaggregation or formation of ion pairs.⁵ Steric effects are also invoked because HMPA is rather large compared to the typical ethereal solvents used with many organolithium reagents. HMPA is also believed to bind more strongly to lithium than THF or diethyl ether.⁶ However, recent studies serve to highlight the very complicated nature of HMPA's interaction with organolithium complexes. Thus the aggregation state of organolithium compounds was shown to increase⁷, decrease⁸, remain unchanged⁹ or form separated ion pairs¹⁰ (SIP) due to the introduction of HMPA. Aggregate behavior in the presence of HMPA is clearly sensitive to the amount added and to the temperature as well as being substrate specific. HMPA-Li interactions are convenient to study by NMR because the direct J-coupling between ^{31}P and $^6\text{Li}/^7\text{Li}$ is observable.¹¹

The mechanism of ketone enolization is clearly dependent upon solvation and aggregation state of the base.¹² Ultimately the observation that enolization leads to enolate aggregates and mixed aggregates both of which are also solvated prompted this study. In this paper, we utilize pinacolone enolate as a model to demonstrate the influence of HMPA upon the enolate aggregation state. Reich has gained deep and comprehensive insight into aggregation state, solvation and ion pair status for over 120 lithium species from HMPA titration experiments below -90°C .¹³ Reich's elegant spectroscopy study concluded that HMPA has only a minor effect on structure at sub-stoichiometric amounts.¹⁴ Thus for lithium enolates of simple ketones which form

cubic tetramers in THF, HMPA replaces THF during titration, but does not necessarily disaggregate, i.e. dissociation from tetramer to trimer, dimer or monomer, or generate SIP's. Nonetheless, with high concentration of HMPA, Reich noted dissociation and formation of ions for the lithium enolates of bisphenyl-2-propanone derivatives, reported as forming dimers and monomers in THF by Streitwieser.¹⁵

Thus spectroscopic studies led to different observations about aggregate structure.¹⁶ However single crystal structures of HMPA solvated lithium enolates do not exist. The only closely related structure is that of HMPA solvated lithium phenoxide complex $[(\text{PhOLi})_3 \cdot \text{LiNCS} \cdot \text{HMPA}_4]$ reported by Snaith.¹⁷ This mixed-anion complex forms a structurally similar tetrameric array with three phenoxides and four Li atoms, three of which bear terminal HMPA ligands, and the fourth HMPA forms a μ_3 bridge. A similar bridged HMPA has been observed in the structures of $(\text{KNCS})_3 \cdot \text{HMPA}_5$ (μ_3)¹⁸ and $(\text{LiBr})_2 \cdot \text{HMPA}_3$ (μ_2)¹⁹. Snaith also reported an unresolved disorder among HMPA ligands in a tetramer characterized as $(\text{PhOLi} \cdot \text{HMPA})_4$ by molecular mass measurement. This tetra-HMPA solvated tetrameric structure was assigned based on ^7Li and ^{31}P NMR spectroscopy.

This study targets HMPA solvated lithium enolate crystal structures and correlates these with their solution structures using diffusion NMR methods. Previous spectroscopic studies utilized HMPA in ethereal solvents, however in this paper the solution-state study is limited to hydrocarbon solvent.

3.3 Results and Discussion

3.3.1 Characterization of HMPA-solvated Lithium Pinacolone Enolate in the Solid State

Crystal Structure of tri-HMPA Solvated Lithium Pinacolone Enolate Tetramer.

Lithium pinacolone enolate (LiOPin) was generated *in situ* by slowly adding the ketone to a lithium amide base (1.05 equivalent) in hydrocarbon solvent at 0 °C. After adding HMPA, the solution was stored at low temperature to initiate crystallization. Two bases were utilized, lithium diisopropyl amide (LDA) and lithium bis(trimethylsilyl)amide (LHMDS). Pentane, heptane and toluene were used as solvents. Crystallization temperature ranged from -20 °C to -80 °C. The amount of HMPA was adjusted from 0.5 to 3.0 eq. After systemically monitoring all these combinations, we found that the amount of HMPA used was crucial for crystallization with 0.7 ~ 0.9 eq. HMPA providing the optimum result. Hence, adding 0.75 eq. HMPA to 1.0 M LiOPin in pentane yielded nicely shaped, colorless crystals suitable for x-ray diffraction analysis that grew overnight at -20 °C. No crystallization was observed if more than 1.5 eq. of HMPA was added even at -80 °C. In all cases, recrystallization from pentane provides very pure crystals suitable for x-ray diffraction and further NMR analysis.

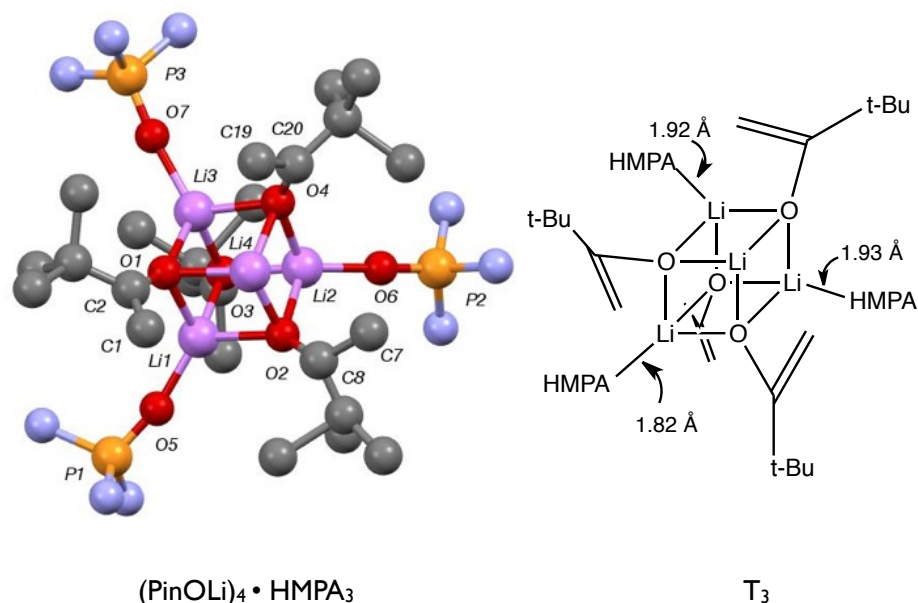


Figure 3.1. Crystal structure of $(\text{PinOLi})_4 \cdot \text{HMPA}_3$ - hydrogen atoms and methyl groups of HMPA are omitted for clarity.

As shown in **Figure 3.1**, the x-ray structure determination reveals that a coordinatively unsaturated tri-solvated cubic tetramer (T_3) formed bearing one tri-coordinate lithium site, *i.e.* Li4. One HMPA molecule binds more strongly (Li1- O_{HMPA} bond 1.82 Å) than the other two (Li2- O_{HMPA} bond 1.93 Å and Li3- O_{HMPA} bond 1.92 Å). The cubic framework is slightly distorted. The distance between the bare lithium, *i.e.* Li4, and one of the adjacent enolate oxygen atoms is only 1.81 Å, much shorter than the all other eleven $\text{Li-O}_{\text{enolate}}$ bonds (1.95 Å to 2.06 Å) in this structure. The only similar substoichiometric solvated tetrameric lithium enolate structure is tris-pyridine solvated lithium pinacolone enolate tetramer $(\text{PinOLi})_4 \cdot \text{Pyr}_3$ reported by Jacobsen and coworkers in 1992 by combining pinacolone, LiHMDS and pyridine in the ratio 1:1:0.65 in methylcyclohexane.²⁰ However in Jacobsen's structure the three Li-N_{pyr} bonds are approximately same (2.04 Å, 2.05 Å and 2.07 Å) with a triad symmetry axis through the bare lithium. Also in the Jacobsen structure the tri-coordinate lithium is more closely associated to adjacent enolate oxygen (avg. Li-

O_{enoalte} bonds 1.86 Å) than the other nine Li-O_{enoalte} bonds (avg. 1.97 Å) by approximately 0.1 Å.

The observation that the unsolvated lithium exhibits shorter Li- O_{enoalte} bonds is related to its smaller coordination number. The orientation of the terminal C-C double bond farthest from the bare lithium leads to unequal HMPA ligands as determined by the different Li-O_{HMPA} bond distances. It is important to note that in this T₃ aggregate, all the *tert*-butyl (*t*-Bu) groups and HMPA ligands are oriented as far away from the cubic core as possible to lower the steric interactions. Therefore each terminal C=C bond is directed towards a specific Li₂O₂ face of the tetramer. As depicted in **Fig. 3.2**, the coordinatively unsaturated lithium (Li4) is surrounded by three counterclockwise-rotating C=C bonds, each associated with one of the three faces of the cube adjacent to Li4. All three methylene carbons are closer to Li4 (2.97 Å, 2.92 Å, 2.59 Å) than to Li1, Li2 or Li3 (3.54 Å, 3.38 Å, 3.35 Å) respectively. The terminal C=C bond farthest from Li4 is directed toward the Li1-O2-Li2-O3 face, consequently the distance C13-Li1 (3.24 Å) is significantly shorter than C13-Li2 (3.73 Å). The average length of the other three C=C bonds is 1.35 Å. The equivalent average value is 1.33 Å in tri-pyridine-solvated lithium pinacolone enolate tetramer in which the lengths of four C=C bonds are identical, 1.33 Å in tetra-THF-solvated lithium pinacolone enolate tetramer²¹ and 1.34 Å in unsolvated lithium pinacolone enolate hexamer²². The comparison of C=C bond lengths in all these structures indicates that the Li1 atom or Li1-O_{HMPA} bond interacts with the C=C(13) double bond. Thus this interaction causes shortening of the Li1-O_{HMPA} bond and the elongation of the C=C(13) double bond. Although we still don't understand the nature of this Li – oxallyl anion π interaction, this crystal structure strongly supports the presence of such an interaction between the Li atom and oxallyl O-C=C system within this lithium enolate structure. We first

noticed this identical π -oxallyl – Li interaction in the crystal structure of hexameric, unsolvated $(\text{LiOPin})_6$. Clearly the tricoordinated lithium cations in these structures seek to interact with electron density in the π orbitals of the enolate. Moreover, in the hindered crystal structure of tetra-pyridine-solvated lithium pinacolone enolate tetramer $(\text{LiOPin} \cdot \text{Pyr})_4$, two Li-N bonds (aver 2.17 Å) are just slightly longer than the other two (aver 2.13 Å) and these correlate directly to two unusually long C=C bonds (1.45 Å) possibly due to disorder in this structure. Comparing the HMPA aggregate in **Fig. 3.1** to Jacobsen's $(\text{LiOPin})_4 \cdot \text{Pyr}_3$ crystal structural mentioned above, in which all C=C bonds (avg. 1.33 Å) and Li-N bonds (avg. 2.05 Å) are equal, we propose that an incremental steric effect is the major reason driving the interaction between lithium cation and C=C double bond.

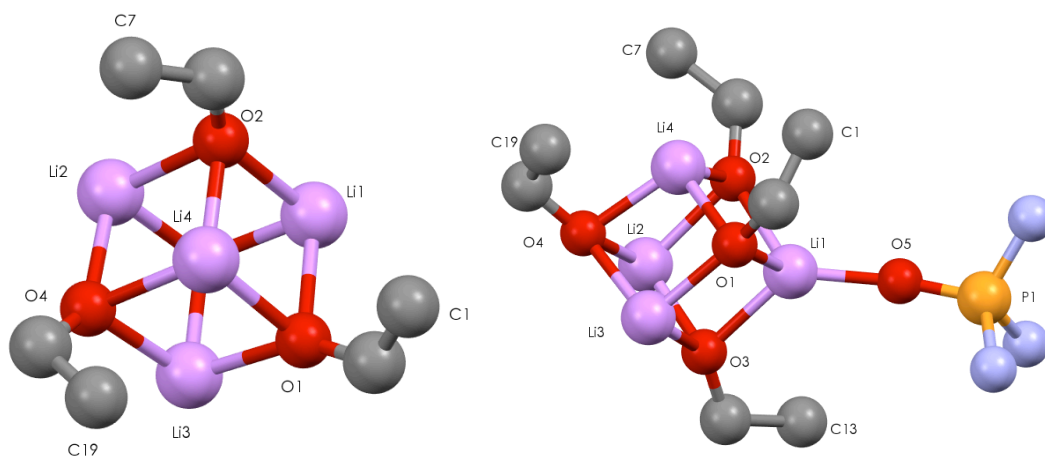


Figure 3.2. Simplified skeleton of $(\text{PinOLi})_4 \cdot \text{HMPA}_3$ tetrameric structure. Except the twisted Li_4O_4 cubic core, only four C=C double bonds and the “tight” HMPA molecule are shown. All the hydrogen atoms and methyl groups have been omitted.

3.3.2 Characterization of HMPA-solvated Lithium Pinacolone Enolate

Complexes in Solution

A series of NMR experiments were conducted to characterize these LiOPin -HMPA aggregates in hydrocarbon solution as described. Upon dissolving crystalline samples

of the $(\text{PinOLi})_4 \cdot \text{HMPA}_3$ in toluene- d_8 , one-dimensional NMR spectra indicate that there is only one dominant lithium enolate complex. It was not possible for us to distinguish free and bound HMPA from these one-dimensional spectra. Even at $-80\text{ }^\circ\text{C}$, only one set of HMPA peaks is observed as a ^1H (doublet, $^3J_{\text{H-P}} = 9.6\text{ Hz}$), ^{13}C (doublet, $^2J_{\text{C-P}} = 4.0\text{ Hz}$, decoupled by ^1H), ^{31}P (singlet) and ^6Li (singlet) in the respective NMR spectra, see supplementary material **Fig. S3.1** and **S3.2**. HSQC and HMBC spectra were also determined to confirm the assignments noted above, **Fig. S3.3** and **S3.4**. A few impurities coexist in these **T₃** spectra and were identified as pentane and diisopropylamine (DIPA) from the mother liquor in which the crystals were prepared. By integration of the proton spectrum, HMPA is always present at more than 0.75 eq., see **Figure 3.3**, no matter how carefully the crystals were washed with pentane, *i.e.* typically around 0.85 ~ 1.1 eq. was observed. Possibly the highly polar HMPA prefers to adhere to the crystal surface than to dissolve in non-polar pentane or alternatively some of the enolate is protonated during the washing and releases free HMPA that is not completely removed along with the free pinacolone. We also observed a significant resonance shift of the enolate terminal methylene peaks in both the ^1H and ^{13}C spectra depending on the amount of HMPA present that we characterized by titration experiments (*vide infra*).

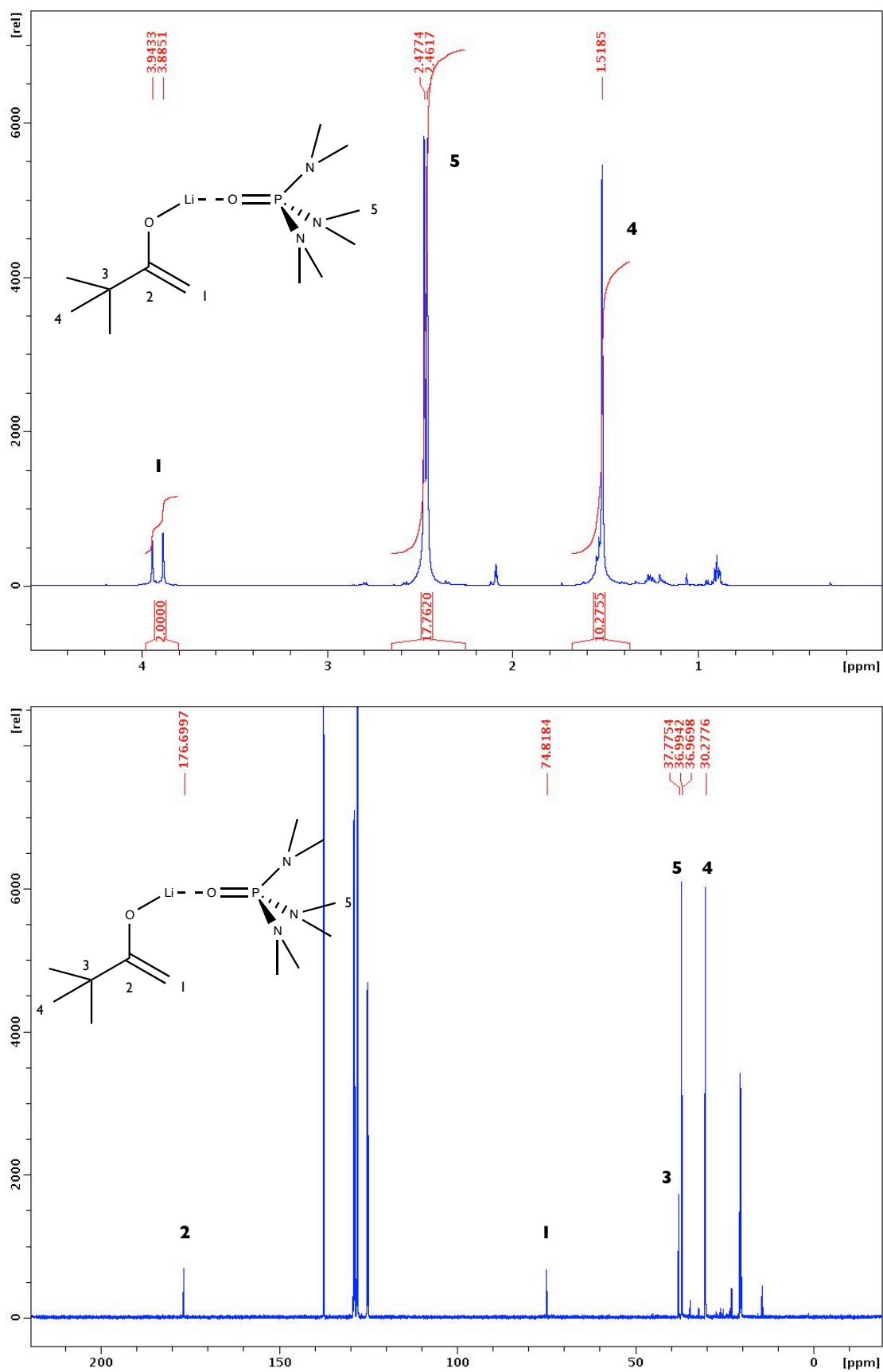


Figure 3.3. ¹H NMR (delay time 60 s) and ¹³C NMR of LiOPin/HMPA T₃ Complex in toluene-*d*₈ at -20 °C.

Characterization of Species in LiOPin/HMPA solution. A HMPA titration experiment was performed to better understand how HMPA influences the solution structure of lithium pinacolone enolate. Previously published crystal structures^{23,21} and HMPA titration studies suggest that lithium enolates of simple ketones preserve their cubic tetramer core aggregation state with many solvents in both solid and solution structures. Hence our first titration experiment was to add HMPA into a solution of LiOPin in cyclohexane-*d*₁₂, a non-aromatic hydrocarbon solvent, at room temperature. The results are depicted in **Fig 3.4**. LiOPin solution was generated *in-situ* by mixing pinacolone with 1.05 eq. of LDA to suppress self-aldol reaction. Upon titration of 0 ~ 1.0 eq. HMPA into the enolate solution, four different LiOPin/HMPA complexes appear in sequence. The third to appear in this sequence is identified as **T₃** by direct comparison of its spectrum with that of **T₃** obtained from dissolution of a crystalline sample that was characterized by diffraction analysis. Notably, **T₃** is the major component in solution once 0.6 ~ 1.0 eq. HMPA is added to the solution. Curiously this titration result matches our empirically optimized conditions for preparing **T₃** crystals with 0.7 ~ 0.9 eq. HMPA. When more than one equivalent HMPA had been added, a fifth unknown complex appeared. This titration experiment was repeated in toluene but much broad peaks were observed so the sample was cooled to -20 °C to achieve a reasonable resolution, **Fig 3.5**. Analogously we observed that a set of four different methylene carbon peaks emerged in sequence during titration and that these moved upfield with increasing HMPA. In light of Reich's titration experiments, this trend strongly suggests that all four complexes detected are tetrameric aggregates with a different solvation environment. Therefore, we label them **T₁** to **T₄**, with T indicating a tetrameric aggregation state and the subscript representing the number of HMPA molecules binding to the tetramer.

Owing to NMR peak line broadening in toluene solution, the fifth unknown peak shown in **Fig. 3.4** and labeled as U, overlaps with T₄ even at -60 °C in **Fig. 3.5**.

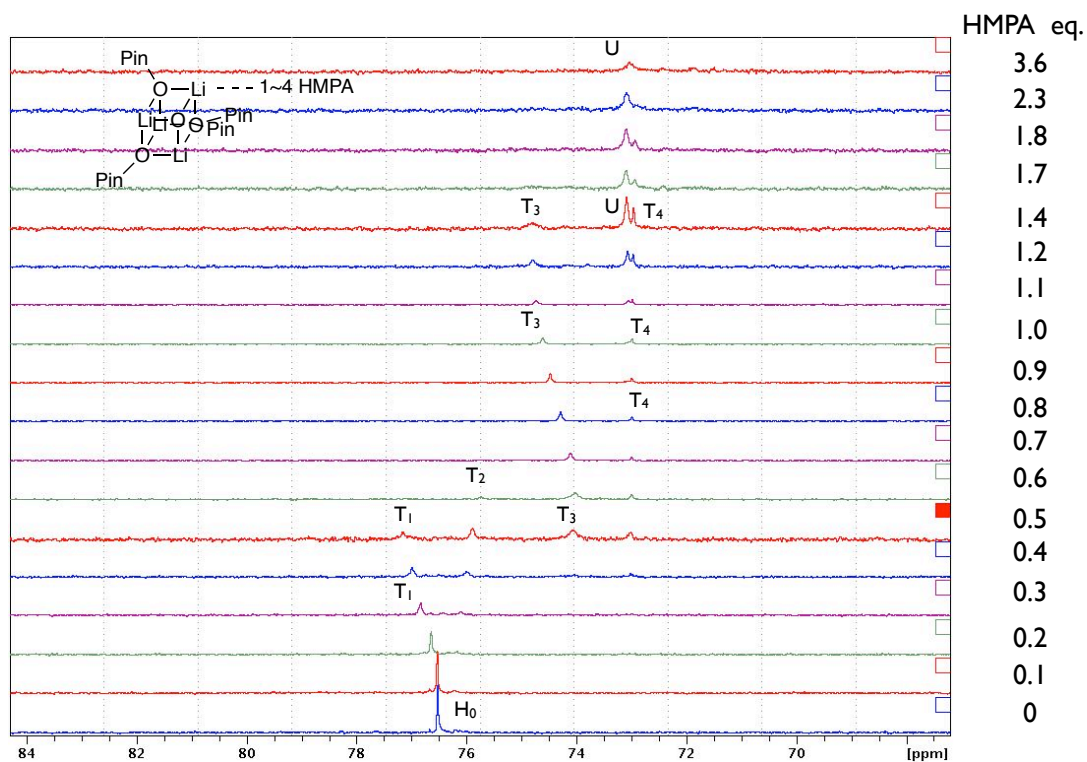


Figure 3.4. HMPA titration experiment of lithium pinacolone enolate in cyclohexane-*d*₁₂ at room temperature. 70~80 ppm region (=CH₂ carbon of enolate) of ¹³C NMR.

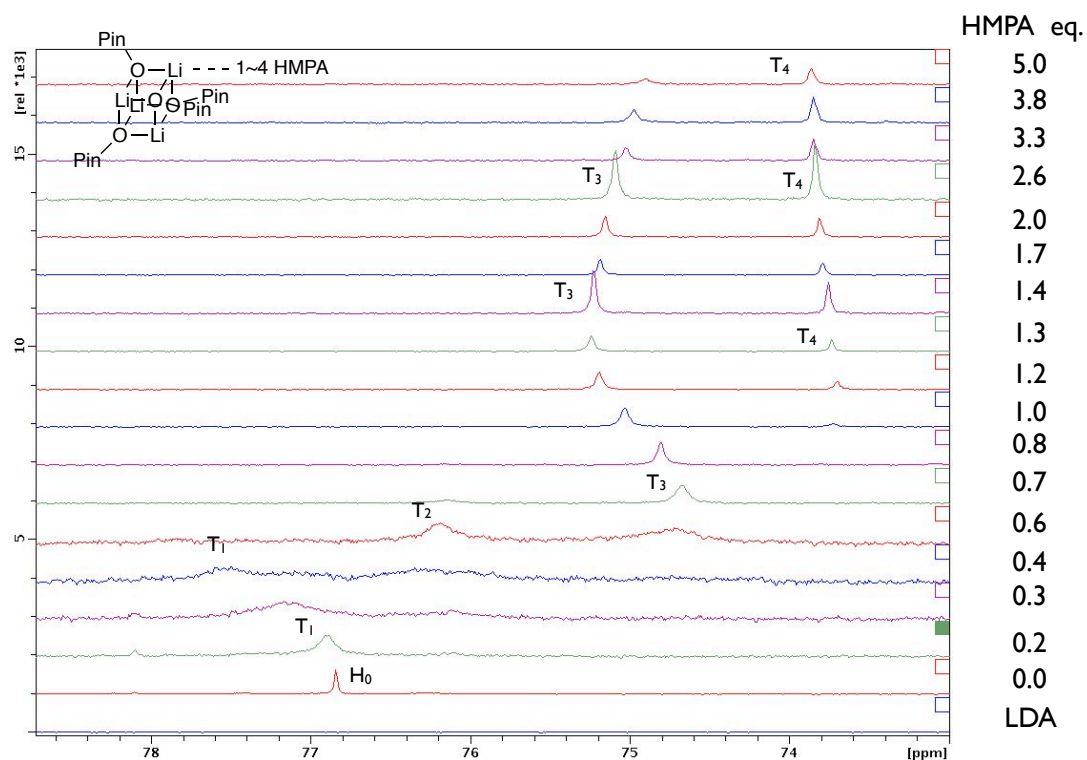


Figure 3.5. HMPA titration experiment of lithium pinacolone enolate in Toluene- d_8 at $-20\text{ }^\circ\text{C}$. 70~80 ppm region ($=\text{CH}_2$ carbon of enolate) of ^{13}C NMR.

The following additional observations are noteworthy. When a toluene solution of LiOPin unsolvated hexamer (H_0) prepared by dissolution of a crystalline sample was titrated by HMPA, **Figure 3.6-left**, only $\text{T}_1 \sim \text{T}_4$ were observed. When we titrated the toluene solution prepared directly from isolated T_3 crystals, **Figure 3.6-right**, only T_3 and a little bit of T_4 were observed. The methylene carbon peak of unknown complex (U) disappeared when we used samples prepared directly from crystals but did not disappear when the sample of LiOPin was prepared *in-situ* with a slight excess of LDA. This result can be rationalized by assigning the unknown compound (U) as a HMPA-solvated mixed aggregate of LiOPin and LDA $[(\text{LiOPin})_n \cdot (\text{LDA})_m \cdot \text{HMPA}_x]$. We assume that n is larger than m and also that x would not be smaller than n , due to the fact that only a slight excess of LDA remains in solution and also that there is no detectable U unless more than 1.0 eq. HMPA is added.

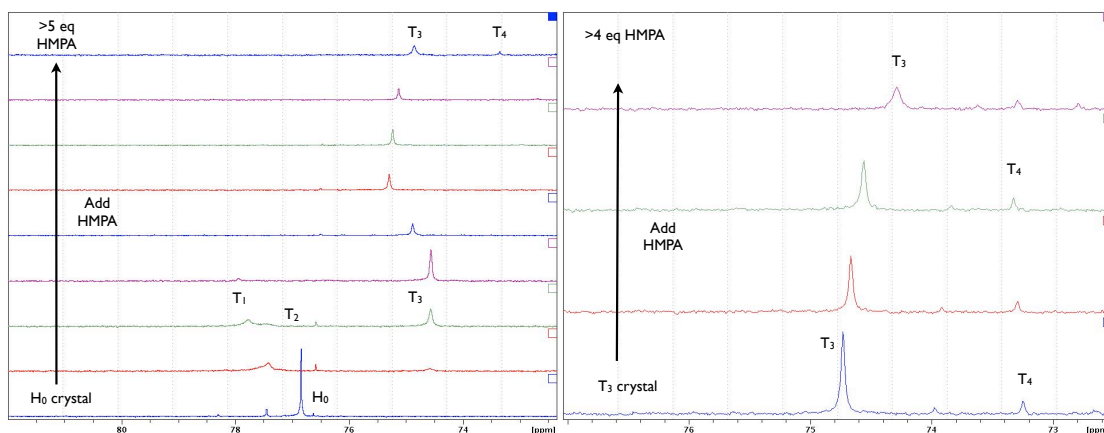


Figure 3.6. HMPA titration experiment of lithium pinacolone enolate in toluene- d_8 at $-20\text{ }^\circ\text{C}$. 70~80 ppm region ($=\text{CH}_2$ carbon of enolate) of ^{13}C NMR. Left: beginning with H_0 crystal; Right: beginning with T_3 crystal.

Our group has previously reported crystal structures of mixed aggregates consisting of enolates and amide bases such as $(\text{LiOPin} \cdot \text{LDA} \cdot \text{DME}_2)^{24}$ as well as

a lithium enolate/LiHMDS complex with internal chelation of an electron-donating heteroatom atom in the side chain²⁵. Collum's spectroscopic studies also confirm that LDA forms mixed aggregates with lithium enolate quantitatively in HMPA/THF solution.^{26,24} Unfortunately, our attempt to obtain a single crystal of the compound we've identified as U in the NMR spectra shown in **Fig. 3.4** and **3.5** was unsuccessful. However we have characterized a very unique mixed aggregate crystal obtained from solutions when only 0.2 ~ 0.3 eq. HMPA was added. This unique complex is depicted in Fig. 7. The composition of this aggregate is five pinacolone enolates, one LDA, two solvating HMPA's and a dilithium oxide, [(LiOPin)₅ • LDA • Li₂O • HMPA₂].²⁷ This result supports our assumption about compound U is most likely a mixed aggregate containing lithium enolate, LDA and HMPA but we do not directly assign the structure of the species depicted in **Fig. 3.7** to this complex identified as U in these NMR spectra. .

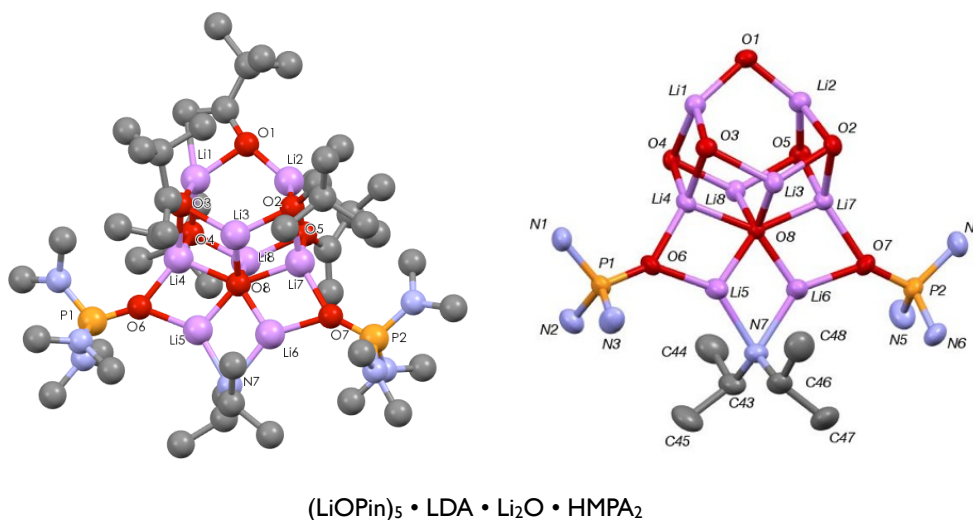


Figure 3.7. Crystal structure of [(LiOPin)₅ • LDA • Li₂O • HMPA₂] (hydrogen atoms omitted). A simplified skeleton with five Pin residues attached to O1 ~ O5 and HMPA methyl groups are omitted for clarity in the structure on the right.

An intriguing observation strongly encouraged us to pursue the crystal structure of **T₄**. When **T₃** crystals were grown to obtain samples for NMR studies, we noticed that

some crystalline samples had precipitates that appeared with the mother liquor for more than one day but subsequently redissolved in solution. These particular samples contained both a major component identified as T_3 and a minor component that we labeled T_4 as seen in **Fig. 3.6**. In contrast, the NMR samples of freshly prepared or re-crystallized T_3 crystals exhibited only T_3 peaks. Thus we concluded that, T_4 is generated and co-exists with T_3 in some samples after one day. Because T_3 is the dominant component in the mixture, we never detected T_4 from the precipitate. Therefore, if the crystallization of T_3 could be inhibited (by adding more than 1.5 eq. HMPA), we felt that it might be possible to collect T_4 crystals. Following this assumption, a delicate and tiny colorless crystal precipitated from 1.0 M LiOPin pentane solution with 3.0 eq. of HMPA at $-20\text{ }^\circ\text{C}$ after three days. X-ray diffraction analysis revealed an odd but not altogether surprising structure shown in **Figure 3.8**. We refer to this compound as **pseudo- T_4** , because two lithium hydroxide molecules insert into one normal cubic structure. Thus adding more HMPA and storing the sample for a longer time increases the possibility of absorbing moisture that we believe accounts for the presence of LiOH in this complex. This face-shared, double-cubic structure is unique for lithium enolates.²⁸ This structure is also the first mixed aggregate characterized that incorporates both lithium enolate and lithium hydroxide, although we have previously characterized a mixed aggregate consisting of pinacolone enolate, *t*-butoxide and KOH.²⁹ It is noteworthy that the four bulky *t*-Bu groups build up an outside hydrophobic shell. Considering our tris solvated T_3 structure and Jacobsen's slightly distorted tetra- pyridine solvated tetrameric structure combined with the fact that HMPA is larger than THF and pyridine, it is reasonable that a tetrasolvated $(\text{LiOPin} \cdot \text{HMPA})_4$ structure is very unstable due to steric constraints and thus has never been observed with this combination of reagents whereas Jacobsen

was able to characterize a T_4 aggregate solvated by pyridine. By inserting two unsolvated lithium hydroxides that serve to expand the cubic core, it is possible to achieve the more stable **pseudo- T_4** structure with stoichiometry $[(LiOPin)_4 \cdot (LiOH)_2 \cdot HMPA_4]$ depicted in **Fig. 3.8**.

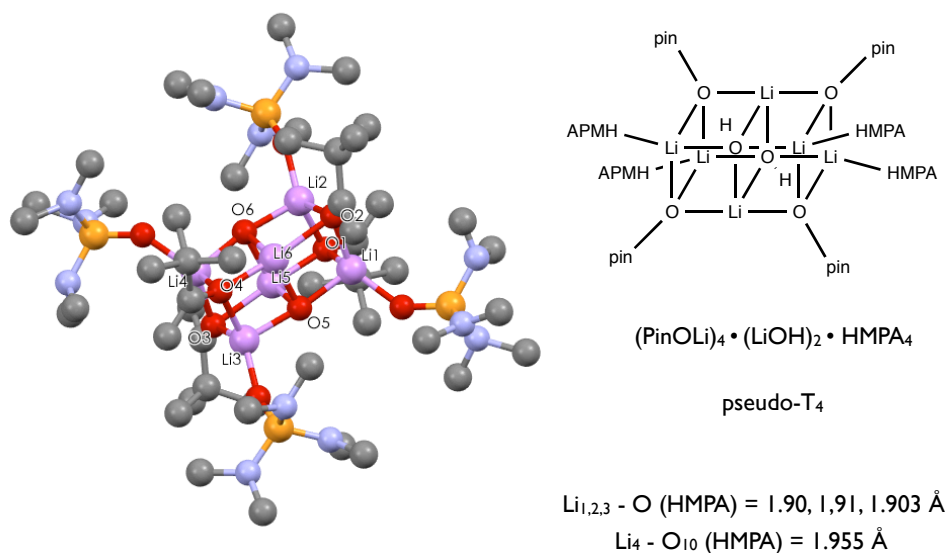
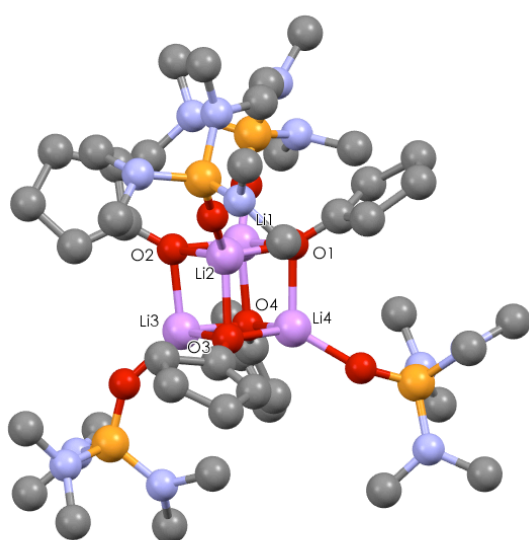


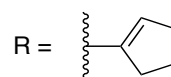
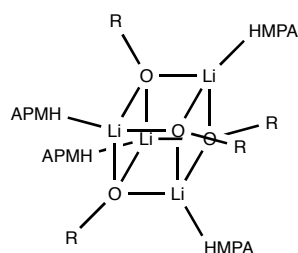
Figure 3.8. Crystal structure of $[(LiOPin)_4 \cdot (LiOH)_2 \cdot HMPA_4]$ (**pseudo- T_4**), each enolate is solvated by one HMPA (hydrogen atoms omitted).

To probe whether a steric effect is the major factor for **pseudo- T_4** formation, we prepared a HMPA-solvated lithium cyclopentanone enolate (LiOcP) crystal by adding 0.75 eq. HMPA to a 1.0 M pentane solution of lithium cyclopentanone enolate. We found that a tetra-HMPA solvated tetramer $(LiOcP \cdot HMPA)_4$ could be crystallized at $-20 \text{ }^\circ\text{C}$ and characterized by x-ray diffraction as shown in **Fig. 3.9**. The averaged $Li-O_{HMPA}$ bond is 1.90 \AA , which is still slightly shorter than the shortest $Li-O_{HMPA}$ bond found in **pseudo- T_4** . This crystal structure provides additional evidence that the driving force for the formation of these unusual T_3 and **pseudo- T_4** structures of LiOPin/HMPA is indeed steric hindrance. Hence, when the bulky pinacolate was replaced by the smaller cyclopentanone enolate residue and solvated by HMPA or

alternatively when HMPA is replaced by a sterically less demanding ligand such as THF or pyridine, a tetra-solvated cubic tetramer is easily formed. Alternatively, we also prepared a LiOPin solution with 0.75 eq. HMPA and 0.25 ~ 0.5 eq. THF to determine the solvation of the pinacolone enolate tetrameric aggregate with mixed solvents, for example possibilities include $[(\text{LiOPin})_4 \cdot \text{HMPA}_2 \cdot \text{THF}_2]$ or $[(\text{LiOPin})_4 \cdot \text{HMPA}_3 \cdot \text{THF}]$. The tri-HMPA solvated tetramer (**T₃**) is the only crystal we observed and this clearly did not incorporate THF as determined by the unique chemical shift of the unsolvated lithium due to the shielding effect from three OPin groups around it. It is noteworthy that as Collum has repeatedly pointed out in his elegant studies utilizing the bidentate ligand TMEDA, although deaggregation seems reasonable when bulky Lewis bases or bidentate ligands solvate organolithium aggregates, this is not a foregone conclusion given that we also have not observed the formation of HMPA solvated LiOPin aggregates smaller than the tetramer or separated ion pairs in this study. Thus **T₃** is always the major component of the LiOPin/HMPA complex in hydrocarbon solution when more than 0.6 eq. HMPA are present.



$\text{Li}_{1,2,3,4} - \text{O} (\text{HMPA}) = 1.892, 1.897, 1.895, 1.900 \text{ \AA}$
 avg. = 1.896 \text{ \AA}



$(\text{LiOcp} \cdot \text{HMPA})_4$

Figure 3.9. Crystal structure of $(\text{LiOcp} \cdot \text{HMPA})_4$, hydrogen atoms are omitted.

Solvation State of T_3 by Using DOSY. Diffusion-ordered ^1H NMR spectroscopy (DOSY) and diffusion coefficient-formula weight (D-FW) correlation analysis³⁰ were carried out to study the solvation state of T_3 complex in toluene solution. The FW of an unknown complex is determined by its diffusion coefficient (measured by DOSY) through the linear regression plot of the logarithms of diffusion coefficients against the known FWs of the references. Benzene (BEN, 78.11 g/mol), cyclooctene (COE, 110.2 g/mol), 1-tetradecene (TDE, 196.4 g/mol) and squalene (SQU, 410.7 g/mol) are added to T_3 solution as internal references. The resonances of the enolate terminal methylene protons (3.8 ~ 4.0 ppm) and also the HMPA methyl protons (2.45 ppm) were monitored for our D-FW analysis, **Fig. 3.10**.

We prepared the solution for D-FW analysis by dissolving T_3 in toluene. D-FW analysis of this solution reveals that the formula weight of the complex in solution is approx. 678 g/mol. We note that the formula weight of $[(\text{LiOPin})_4 \cdot \text{HMPA}_3]$, T_3 complex is 961 g/mol, while the formula weight of $[(\text{LiOPin})_4 \cdot \text{HMPA}_2]$, T_2 , is 782 g/mol and is 603 g/mol for the corresponding monosolvated T_1 complex. We also noted that the D-FW analysis for the resonance of HMPA in this solution yields an experimentally determined formula weight of 323 g/mol that is clearly significantly greater than the actual molecular weight of HMPA, 179 g/mol. We have previously observed such a disparity between the main component of an organolithium aggregate and the solvating Lewis acid coordinated to the Li. Presently we interpret this experimental result to suggest that each cubic tetramer has on the time scale of this diffusion experiment approx. one HMPA tightly bound to it and that around 70% of the HMPA exchanges with free HMPA in the solution. After repeating this experiment several times starting with T_3 crystalline samples with a total of 0.85~1.1 eq HMPA in

solution, we observe that the experimental FW determined by monitoring the enolate terminal methylene peak falls within the range of 580 ~ 750 g/mol and varies with the amount of HMPA present. Hence this experimental observation suggests an aggregate determined by diffusion analysis that is equal to or bigger than T_1 , but always somewhat smaller than T_2 . Thus we suggest that when the pure, crystalline $[(LiOPin)_4 \cdot HMPA_3]$, T_3 complex dissolves in solution, one of the three HMPA remains tightly bound to the LiOPin cubic core, while the remaining two HMPA are labile, **Scheme 3.1**. It is also noteworthy that in the crystal structure of the tris-solvated complex T_3 one Li-O_{HMPA} bond is much shorter than the other two Li-O_{HMPA} bonds by approx. 0.1 Å supporting our conclusion that one HMPA ligand in this complex is more tightly bound than the others.

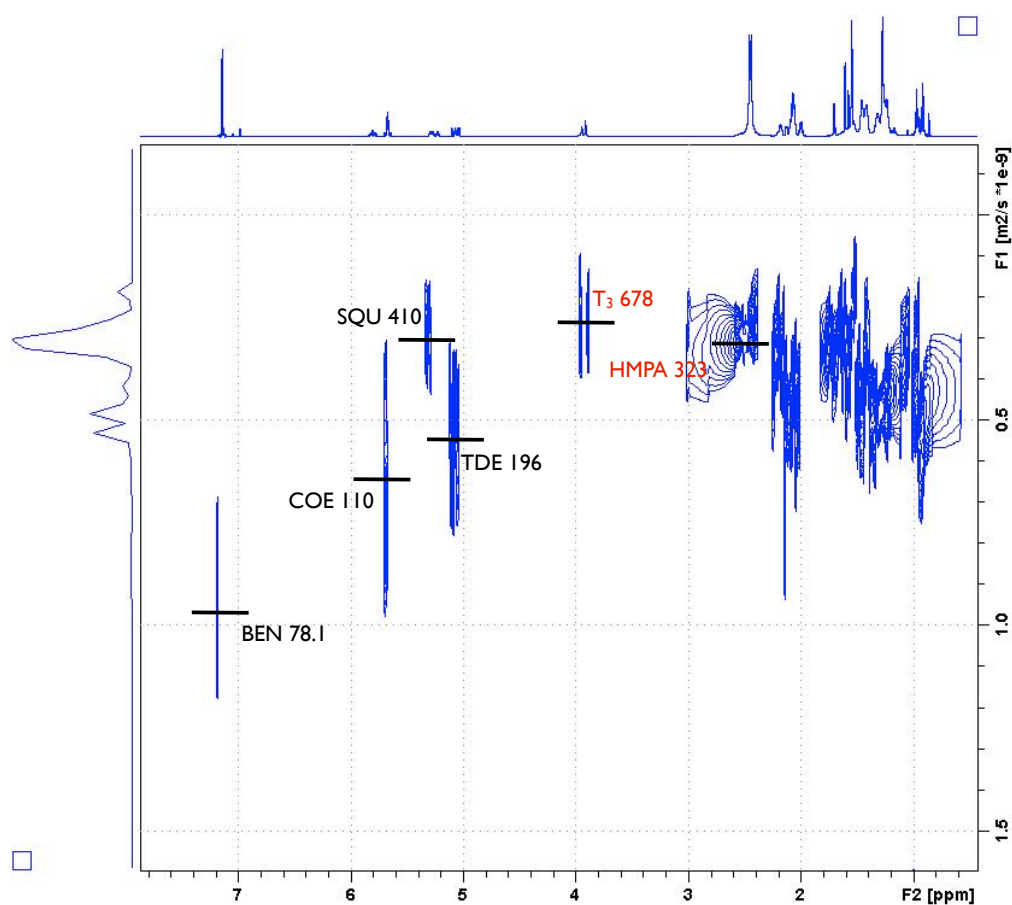
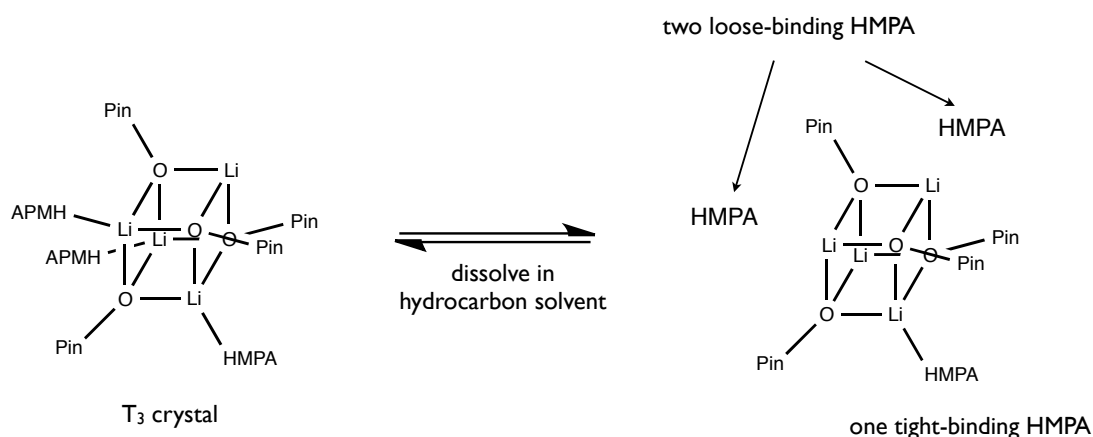


Figure 3.10. 1H DOSY of LiOPin/HMPA T_3 Complex in Toluene- d_8 at -20 °C.

Scheme 3.1. Dissolving LiOPin/HMPA T_3 Crystal in Hydrocarbon Solvents.



3.4 Conclusion

Crystal structures of HMPA solvated lithium simple ketone enolates are reported for the first time. These include a substoichiometric solvated tetramer; an unusual, face shared double-cube consisting of a mixed aggregate containing LiOPin and LiOH; a unique mix-aggregate consisting of LiOPin and LDA in the stoichiometric ratio 5:1; and a tetrasolvated tetramer of cyclopentanone enolate. Intensive NMR studies reveal that with the bulky lithium pinacolone enolate, tri-solvated tetramer, T_3 is the only major species in solution when more than 0.6 equivalents of HMPA are present. This tris-HMPA solvated tetramer, T_3 , consists of one tight-binding HMPA and two loose-binding HMPA ligands in both solid and solution structures. A fourth ligand such as HMPA, THF or pyridine is extremely difficult to approach the bare lithium in the T_3 aggregate because of the steric bulk of the pinacolone residue. Whereas for the less hindered cyclopentanone enolate, tetra-HMPA solvated tetramer forms easily in pentane and is more favorable than tri-solvated aggregate. Hence we conclude that a major factor controlling solvation of enolate aggregates is steric interaction within the aggregate.

3.5 Experimental Section

Procedures for NMR Experiments. NMR samples were prepared in tubes sealed with rubber septa cap and parafilm. NMR tubes were evacuated *in vacuo*, flame-dried and filled with argon before use. ^1H chemical shifts were referenced to toluene- d_8 at 7.00 ppm and ^{13}C chemical shifts were referenced to toluene- d_8 at 137.86 ppm. All NMR experiments were acquired on a Bruker Avance III HD 600 MHz spectrometer equipped with a z-axis gradient BBFO smartprobe. For DOSY experiments, a GRASP II 10A z-axis gradient amplifier was employed, with maximum gradient strength of 0.5 T/m. ^1H DOSY was performed using the standard Bruker pulse programs, employing a double stimulated echo sequence, bipolar gradient pulses for diffusion, and 3 spoil gradients. Diffusion time was 100 ms, and the rectangular gradient pulse duration was 1300 μs . Gradient recovery delays were 200 μs . Individual rows of the quasi-2-D diffusion databases were phased and baseline corrected. Actual diffusion coefficients used for D-FW analysis were obtained using the T1/T2 analysis module in commercially available software.

Materials and Methods. Pentane, hexamethylphosphoramide (HMPA) and diisopropylamine (DIPA) were dried by stirring with calcium hydride (CaH_2) under Ar atmosphere overnight then distillation. Unless otherwise stated, purchased chemicals were used as received. All reactions under anhydrous conditions were conducted using flame- or oven-dried glassware and standard syringe techniques under an atmosphere of argon.

General Procedures for the Crystallization of $(\text{LiOPin})_4 \cdot \text{HMPA}_3 (\text{T}_3)$ and Tetra-HMPA Solvated Lithium Cyclopentanone Enolate Tetramer $(\text{LiOcP} \cdot \text{HMPA})_4$. To a 1.1 M DIPA (5.5 mmol) solution in 5.0 ml pentane at 0 °C under Ar atmosphere was slowly added 2.1 ml 2.5 M *n*-BuLi (5.25 mmol). The reaction mixture was

allowed to stir at 0 °C for 10 minutes. Ketone (5 mmol) was then added dropwise and the mixture was allowed to stir at 0 °C for 15 minutes. Finally, HMPA 0.68 g (3.75 mmol, 0.75 eq.) was added and the solution was kept stirring for another 15 minutes at room temperature. The clear solution was then stored at -20 °C freezer and XRD quality crystals were grown after overnight.

General Procedures for the Crystallization of [(LiOPin)₅ • LDA • Li₂O • HMPA₂].

To a 1.1 M DIPA (5.5 mmol) solution in 5.0 ml pentane at 0 °C under Ar atmosphere was slowly added 2.0 ml 2.5 M *n*-BuLi (5.0 mmol). The reaction mixture was allowed to stir at 0 °C for 10 minutes. Pinacolone 0.5 g (5.0 mmol) was then added slowly and the mixture was allowed to stir at 0 °C for 15 minutes. Finally, HMPA 0.18 ~ 0.26 g (1.0 ~ 1.5 mmol, 0.2 ~ 0.3 eq.) was added and the solution was kept stirring for another 15 minutes at room temperature. The clear solution was then stored at -20 °C freezer and XRD quality crystals were grown after several days.

General Procedures for the Crystallization of (LiOPin)₄ • (LiOH)₂ • HMPA₄

(pseudo-T₄). To a 1.1 M DIPA (5.5 mmol) solution in 5.0 ml pentane at 0 °C under Ar atmosphere was slowly added 2.1 ml 2.5 M *n*-BuLi (5.25 mmol). The reaction mixture was allowed to stir at 0 °C for 10 minutes. Pinacolone 0.5 g (5.0 mmol) was then added slowly and the mixture was allowed to stir at 0 °C for 15 minutes. Finally, HMPA 0.54 g (15 mmol, 3.0 eq.) was added and the solution was kept stirring for another 15 minutes at room temperature. The clear solution was then stored at -20 °C freezer and XRD quality crystals were grown after three days.

3.6 References

¹ (a) Kolonko, K. J.; Guzei, I. A.; Reich, H. J. *J. Org. Chem.* **2010**, *75*, 6163-6172; (b) Reich, H. J.; Sanders, A. W.; Fiedler, A. T.; Bevan, M. J. *J. Am. Chem. Soc.* **2002**, *124*, 13386-13387; (c) Ahmed, A.; Clayden, J.; Yasin, S. A. *Chem. Commun.* **1999**, 231-232; (d) Reich, H. J.; Sikorski, W. H.; Gudmundsson, B. O.; Dykstra, R. R. *J. Am. Chem. Soc.* **1998**, *120*, 4035-4036; (e) Reich, H. J.; Green, D. P.; Medina, M. A.; Goldenberg, W. S.; Gudmundsson, B. O.; Dykstra, R. R.; Phillips, N. H. *J. Am. Chem. Soc.* **1998**, *120*, 7201-7210; (f) Reich, H. J.; Phillips, N. H. *J. Am. Chem. Soc.* **1986**, *108*, 2102-2103; (g) Takahashi, O.; Saka, T.; Mikami, K.; Nakai, T. *Chem. Lett.* **1986**, 1599-1602.

² (a) Blay, G.; Fernandez, I.; Monje, B.; Pedro, J. R. *Tetrahedron* **2004**, *60*, 165-170; (b) Sikorski, W. H.; Reich, H. J. *J. Am. Chem. Soc.* **2001**, *123*, 6527-6535; (c) Reich, H. J.; Borst, J. P.; Dykstra, R. R.; Green, D. P. *J. Am. Chem. Soc.* **1993**, *115*, 8728-8741; (d) Hunt, D. A. *Org. Prep. Proced. Int.* **1989**, *21*, 705-749; (e) Mulzer, J.; Steffen, U.; Zorn, L.; Schneider, C.; Weinhold, E.; Muench, W.; Rudert, R.; Luger, P.; Hartl, H. *J. Am. Chem. Soc.* **1988**, *110*, 4640-4646; (f) Binns, M. R.; Haynes, R. K. *J. Org. Chem.* **1981**, *46*, 3790-3795; (g) Brown, C. A.; Yamaichi, A. *J. Chem. Soc., Chem. Commun.* **1979**, 100-101.

³ (a) Riggs, J. C.; Singh, K. J.; Yun, M.; Collum, D. B. *J. Am. Chem. Soc.* **2008**, *130*, 13709-13717; (b) Ma, Y.; Collum, D. B. *J. Am. Chem. Soc.* **2007**, *129*, 14818-14825. (c) Ma, Y.; Ramirez, A.; Singh, K. J.; Keresztes, I.; Collum, D. B. *J. Am. Chem. Soc.* **2006**, *128*, 15399-15404; (d) Gawley, R. E.; Zhang, Q.; McPhail, A. T. *Tetrahedron: Asymmetry* **2000**, *11*, 2093-2106; (e) Sun, X.; Collum, D. B. *J. Am. Chem. Soc.* **2000**, *122*, 2459-2463; (f) Sun, X.; Collum, D. B. *J. Am. Chem. Soc.* **2000**, *122*, 2452-2458; (g) Kress, M. H.; Yang, C.; Yasuda, N.; Grabowski, E. J. *J. Tet. Lett.* **1997**, *38*, 2633-2636; (h) Romesberg, F. E.; Collum, D. B. *J. Am. Chem. Soc.* **1994**, *116*, 9198-9202; (i) Ando, K.; Takemasa, Y.; Tomioka, K.; Koga, K. *Tetrahedron* **1993**, *49*, 1579-1588; (j) Xie, L.; Saunders, W. H. *J. Am. Chem. Soc.* **1991**, *113*, 3123-3130; (k) Corey, E. J.; Gross, A. W. *Tet. Lett.* **1984**, *25*, 495-498; (l) Nakamura, E.; Hashimoto, K.; Kuwajima, I. *Tet. Lett.* **1978**, *19*, 2079-2082; (m) Ireland, R. E.; Mueller, R. H.; Willard, A. K. *J. Am. Chem. Soc.* **1976**, *98*, 2868-2877. (n) Romesberg, F. E.; Gilchrist, J. H.; Harrison, A. T.; Fuller, D. J.; Collum, D. B. *J. Am. Chem. Soc.* **1991**, *113*, 5751-5757

⁴ (a) Reich, H. J.; Sanders, A. W.; Fiedler, A. T.; Bevan, M. J. *J. Am. Chem. Soc.* **2002**, *124*, 13386-13387; (b) Harris, N. J.; Gajewski, J. J. *J. Am. Chem. Soc.* **1994**, *116*, 6121-6129.

⁵ (a) Scholz, R.; Hellmann, G.; Rohs, S.; Raabe, G.; Runsink, J.; Oezdemir, D.; Luche, O.; Hess, T.; Giesen, A. W.; Atodiresei, J.; Lindner, H. J.; Gais, H.-J. *Eur. J. Org. Chem.* **2010**, 4559-4587; (b) Scholz, R.; Hellmann, G.; Rohs, S.; Oezdemir, D.; Raabe, G.; Vermeeren, C.; Gais, H.-J. *Eur. J. Org. Chem.* **2010**, 4588-4616; (c) Jones, A. C.; Sanders, A. W.; Sikorski, W. H.; Jansen, K. L.; Reich, H. J. *J. Am. Chem. Soc.* **2008**, *130*, 6060-6061; (d) Fernandez, I.; Martinez-Viviente, E.; Breher, F.; Pregosin, P. S. *Chem. - Eur. J.* **2005**, *11*, 1495-1506; (e) Reich, H. J.; Sanders, A. W.; Fiedler, A. T.; Bevan, M. J. *J. Am. Chem. Soc.* **2002**, *124*, 13386-13387; (f) Reich, H. J.; Sanders, A. W.; Bevan, M. J.; Sikorski, W. H.; Dykstra, R. R. *Latv. Kim. Z.* **2002**, 93-103; (g) Sikorski, W. H.; Reich, H. J. *J. Am. Chem. Soc.* **2001**, *123*, 6527-6535; (h) Carlier, P. R.; Lo, C. W. S. *J. Am. Chem. Soc.* **2000**, *122*, 12819-12823; (i) Van Vliet, G. L. J.; De Kanter, F. J. J.; Schakel, M.; Klumpp, G. W.; Spek, A. L.; Lutz, M. *Chem. - Eur. J.* **1999**, *5*, 1091-1094; (j) Reich, H. J.; Sikorski, W. H. *J. Org. Chem.* **1999**, *64*, 14-15; (k) Leung, S. S.-W.; Streitwieser, A. *J. Org. Chem.* **1999**, *64*, 3390-

- 3391; (l) Reich, H. J.; Green, D. P.; Medina, M. A.; Goldenberg, W. S.; Gudmundsson, B. O.; Dykstra, R. R.; Phillips, N. H. *J. Am. Chem. Soc.* **1998**, *120*, 7201-7210; (m) Reich, H. J.; Kulicke, K. J. *J. Am. Chem. Soc.* **1995**, *117*, 6621-6622; (n) Reich, H. J.; Dykstra, R. R. *Organometallics* **1994**, *13*, 4578-4585; (o) Jackson, M. D.; Gilkerson, W. R. *J. Am. Chem. Soc.* **1979**, *101*, 328-333; (p) Gilkerson, W. R.; Jackson, M. D. *J. Am. Chem. Soc.* **1979**, *101*, 4096-4100.
- ⁶ (a) Reich, H. J.; Kulicke, K. J. *J. Am. Chem. Soc.* **1996**, *118*, 273-274; (b) Wang, J. S.; Jerome, R.; Warin, R.; Zhang, H.; Teyssie, P. *Macromolecules* **1994**, *27*, 3376-3382.
- ⁷ (a) Jackman, L. M.; Chen, X. *J. Am. Chem. Soc.* **1992**, *114*, 403-411; (b) Corset, J.; Froment, F.; Lautie, M.-F.; Ratovelomanana, N.; Seyden-Penne, J.; Strzaklo, T.; Roux-Schmitt, M.-C. *J. Am. Chem. Soc.* **1993**, *115*, 1684-1694; (c) Reich, H. J.; Borst, J. P.; Dykstra, R. R. *Organometallics* **1994**, *13*, 1-3.
- ⁸ (a) Jackman, L. M.; Chen, X. *J. Am. Chem. Soc.* **1992**, *114*, 403-411; (b) Reich, H. J.; Borst, J. P.; Dykstra, R. R.; Green, P. D. *J. Am. Chem. Soc.* **1993**, *115*, 8728-8741; (c) Reich, H. J.; Green, D. P.; Medina, M. A.; Goldenberg, W. S.; Gudmundsson, B. O.; Dykstra, R. R.; Phillips, N. H. *J. Am. Chem. Soc.* **1998**, *120*, 7201-7210.
- ⁹ (a) Romesberg, F. E.; Bernstein, M. P.; Fuller, D. J.; Harrison, A. T.; Collum, D. B. *J. Am. Chem. Soc.* **1993**, *115*, 3475-3483; (b) Romesberg, F. E.; Gilchrist, J. H.; Harrison, A. T.; Fuller, D. J.; Collum, D. B. *J. Am. Chem. Soc.* **1991**, *113*, 5751-5757.
- ¹⁰ (a) Carlier, P. R.; Lo, C. W.-S. *J. Am. Chem. Soc.* **2000**, *122*, 12819-12823; (b) Reich, H. J.; Green, D. P.; Phillips, N. H. *J. Am. Chem. Soc.* **1989**, *111*, 3444-3445.
- ¹¹ (a) Reich, H. J.; Borst, J. P.; Dykstra, R. R.; Green, P. D. *J. Am. Chem. Soc.* **1993**, *115*, 8728-8741; (b) Reich, H. J.; Borst, J. P. *J. Am. Chem. Soc.* **1991**, *113*, 1835-1837; (c) Reich, H. J.; Green, D. P.; Phillips, N. H. *J. Am. Chem. Soc.* **1989**, *111*, 3444-3445; (d) Reich, H. J.; Green, D. P. *J. Am. Chem. Soc.* **1989**, *111*, 8729-8731.
- ¹² (a) Ma, Y.; Collum, D. B. *J. Am. Chem. Soc.* **2007**, *129*, 14818-14825; (b) Ramirez, A.; Sun, X.; Collum, D. B. *J. Am. Chem. Soc.* **2006**, *128*, 10326-10336; (c) Zhao, P.; Lucht, B. L.; Kenkre, S. L.; Collum, D. B. *J. Org. Chem.* **2004**, *69*, 242-249; (d) Zhao, P.; Collum, D. B. *J. Am. Chem. Soc.* **2003**, *125*, 14411-14424; (e) Sun, X.; Collum, D. B. *J. Am. Chem. Soc.* **2000**, *122*, 2452-2458; (f) Romesberg, F. E.; Collum, D. B. *J. Am. Chem. Soc.* **1995**, *117*, 2166-2178.
- ¹³ Reich, H. J. *J. Org. Chem.* **2012**, *77*, 5471-5491.
- ¹⁴ (a) Kolonko, K. J.; Guzei, I. A.; Reich, H. J. *J. Org. Chem.* **2010**, *75*, 6163-6172; (b) Kolonko, K. J.; Biddle, M. M.; Guzei, I. A.; Reich, H. J. *J. Am. Chem. Soc.* **2009**, *131*, 11525-11534.
- ¹⁵ Gareyev, R.; Ciula, J. C.; Streitwieser, A. *J. Org. Chem.* **1996**, *61*, 4589-4593.
- ¹⁶ Suzuki, M.; Koyama, H.; Noyori, R. *Tetrahedron* **2004**, *60*, 1571-1579.
- ¹⁷ Raithby, P. R.; Reed, D.; Snaith, R.; Wright, W. S. *Angew. Chem. Int. Ed. Engl.* **1991**, *30*, 1011-1013.
- ¹⁸ Raithby, P. R.; Reed, D.; Snaith, R.; Wright, W. S. *Angew. Chem. Int. Ed. Engl.* **1991**, *30*, 1011-1013.
- ¹⁹ Barr, D.; Doyle, M. J.; Raithby, P. R.; Snaith, R.; Wright, D. S.; Mulvey, R. E.; Reed, D. *J. Chem. Soc. Chem. Commun.* **1989**, 318-319.
- ²⁰ Pospisil, P. J.; Wilson, S. R.; Jacobsen, E. N. *J. Am. Chem. Soc.* **1992**, *114*, 7585-7587.
- ²¹ Amstutz, R.; Schweizer, W. B.; Seebach, D.; Dunitz, J. D. *Helv Chim Acta* **1981**, *64*, 2617-2620.
- ²² Williard, P. G.; Carpenter, G. B. *J. Am. Chem. Soc.* **1985**, *107*, 3345-3346.

-
- ²³ Seebach, D. *Angew. Chem. Int. Ed. Engl.* **1988**, *27*, 1624-1654.
- ²⁴ Williard, P. G.; Hintze, M. J. *J. Am. Chem. Soc.* **1990**, *112*, 8602-8604.
- ²⁵ Williard, P. G.; Hintze, M. J. *J. Am. Chem. Soc.* **1987**, *109*, 5539-5541.
- ²⁶ (a) Romesberg, F. E.; Collum, D. B. *J. Am. Chem. Soc.* **1994**, *116*, 9198-9202; (b) Romesberg, F. E.; Collum, D. B. *J. Am. Chem. Soc.* **1995**, *117*, 2166-2178.
- ²⁷ Li₂O is a reasonable minor impurity generated during lithiation process due to contamination of moisture or air: Williard, P. G.; Jacobson, M. A. *Org. Lett.* **2000**, *2*, 2753-2755.
- ²⁸ (a) Henderson, K. W.; Williard, P. G.; Bernstein, P. R. *Angew. Chem. Int. Ed. Engl.* **1995**, *34*, 1117-1119; (b)
- ²⁹ Williard, P. G.; MacEwan, G. J. *J. Am. Chem. Soc.* **1989**, *111*, 7671-7672.
- ³⁰ Li, D.; Keresztes, I.; Hopson, R.; Williard, P. G. *Acc. Chem. Res.* **2009**, *42*, 270-280.

Chapter 4 Lithium Pinacolone Enolate Hexamer

4.1 Abstract

A metastable polymorphic hexameric crystal structure of lithium pinacolone enolate (LiOPin) is reported with three preparation methods. NMR-based structural characterization implies that lithium pinacolate hexamer will significantly deaggregate to tetramer in toluene but retain mainly the hexameric structure in non-aromatic hydrocarbon solvent like cyclohexane. Moreover, the existence of small amount of correlated lithium aldolate (LiOA) will dramatically affect the aggregation state of LiOPin by forming a mixed aggregate with a 1:3 ratio (LiOPin₃•LiOA).

4.2 Introduction

Lithium enolates play an important role in organic synthesis as nucleophiles with a complicated and partially understood mechanism in solution. In comparison with other organolithium reagents, such as lithium amide bases and alkyl lithium, structural information of lithium enolates is more challenging to obtain in both solution and solid state. The lack of Li-C or Li-N bonds limits the applications of NMR techniques on structural characterization of lithium enolates in solution. X-ray crystallography is a reliable tool to determine solid-state structures. Surprisingly, since Seebach reported the first two crystal structures of THF-solvated lithium enolates in 1981,¹ only xx solid-state structure containing lithium simple mono-carbonyl ketone enolates have been reported.² There are five involving lithium pinacolone enolate (LiOPin): an unsolvated hexamer,³ a THF-solvated tetramer,¹ a pyridine-solvated tetramer,⁴ a *N,N,N'*-trimethyl-1,2-ethanediamine solvated dimer,⁵ and a mixed aggregate with

lithium amide base.⁶ There is one containing lithium cyclopentanone enolate (LiOcP): THF-solvated tetramer¹ and three containing lithioisobutyrophenone:⁷ two unsolvated hexamers and TMEDA-solvated dimer. Here we reported another unsolvated lithium simple ketone enolate hexameric crystal structure and its solution-state structure, which, to the best of our knowledge, represents the first NMR-based aggregation study of unsolvated lithium enolate.

4.3 Results and Discussion

4.3.1 Polymorphic Crystal Structure of Unsolvated Lithium Pinacolone Enolate Hexamer

Crystal Preparation. Three decades ago, Williard reported a hexameric structure of unsolvated lithium pinacolone enolate, which is the first crystal structure of unsolvated lithium enolate. Several years later, Liu, a previous graduate student of Williard's group, observed a polymorphic crystal of this enolate via the recrystallization of Willard's hexamer. This new crystal is also a hexamer with triclinic space group. To distinguish between them, we name the published hexamer as **H₁**, and the newer polymorphic one as **H₂**. After the first-time observation of **H₂** by Liu, we were unable to obtain **H₂** for a long time. Only recently was a single crystal of **H₂** accidentally collected from pentane solution of lithium pinacolone enolate in the presence of 0.2 eq. HMPA at -20 °C. Crystallization of **H₂** has been repeated several times utilizing this condition with the presence of 0.1 ~0.2 eq. HMPA. Subsequently **H₂** was also prepared from a toluene solution of LiOPin at -20 °C without any additive. Finally, we also successfully repeated Dr. Liu's procedure of obtaining **H₂** crystal by recrystallization of **H₁** in pentane. Therefore, **H₂** has been observed repeatedly by X-ray analysis via three different preparation methods. However, crystal of **H₁** has also

been observed from all these three preparation procedures, which indicates that the controllable preparation of **H**₂ is still unpredictable. It is very difficult to predetermine whether the precipitated crystal will be **H**₁ or **H**₂ until X-ray analysis is applied. According to our experimental observation, **H**₁ would precipitate within overnight at -20 °C and **H**₂ crystals usually need more than one day to form at the same temperature. However, we are still not confident whether this is a reliable way to predict the conformer.

Structural Characterization. The crystallographic data is listed in **Table 4.1**. Both crystals exist in the space group P-1, which indicates that the only symmetry element is an inversion center. By overlaying two hexameric structures (**Figure 4.1**), we found the Li₆O₆ core has no significant change. The major difference between two hexamer is the conformation of the Pin groups. As shown in **Figure 4.2**, all six *tert*-Bu groups are oriented towards the top or bottom faces of the Li₆O₆ core in **H**₁. Hence, the six carbon-carbon double bonds will approach six side faces of the hexagonal prism. However in the structure of **H**₂, two of the carbon-carbon double bonds are oriented towards the top and bottom faces. Consequently the two *tert*-Bu groups from the correlated pinacolate are placed on two of the side faces. The most obvious result due to this structural change is losing two Li-oxallyl cation- π interactions. Williard noticed that in **H**₁ the terminal methylene carbon is around 0.7 Å closer to one specific lithium atom in the side Li₂O₂ face than the other lithium atom in the same face. This implies the existence of cation- π interaction between lithium atom and oxallyl group. In each hexameric unit of **H**₁, there are six Li-oxallyl pairs, which are characterized by the distances (2.42 Å ~ 2.58 Å) between terminal methylene carbon and lithium atom in the left part of **Figure 4.2**. However there are only four pairs of cation- π interactions in each hexamer of **H**₂, as shown in the right part of **Figure 4.2**. Due to the rotation of

two oxallyl groups, two carbon-carbon double bonds point away from lithium atoms. The distances between lithium and terminal methylene carbon are elongated to 3.72 Å.

Table 4.1. Selected Crystallographic Data of Two Hexameric LiOPin.

	H₁	H₂
Empirical Formula	C ₃₆ H ₆₆ Li ₆ O ₆	C ₃₆ H ₆₆ Li ₆ O ₆
Crystal System	Triclinic	Triclinic
Space Group	P-1	P-1
Cell Lengths (Å)	a 11.686(8)	a 10.3259(14)
	b 11.822(7)	b 10.7672(14)
	c 17.144(17)	c 10.8895(15)
Cell Angles (°)	α 80.56(7)	α 102.936(3)
	β 74.08(5)	β 115.200(3)
	γ 66.35(5)	γ 99.243(3)
R Factor (%)	7.81	5.51
Density (g • cm ⁻³)	1.02	1.035

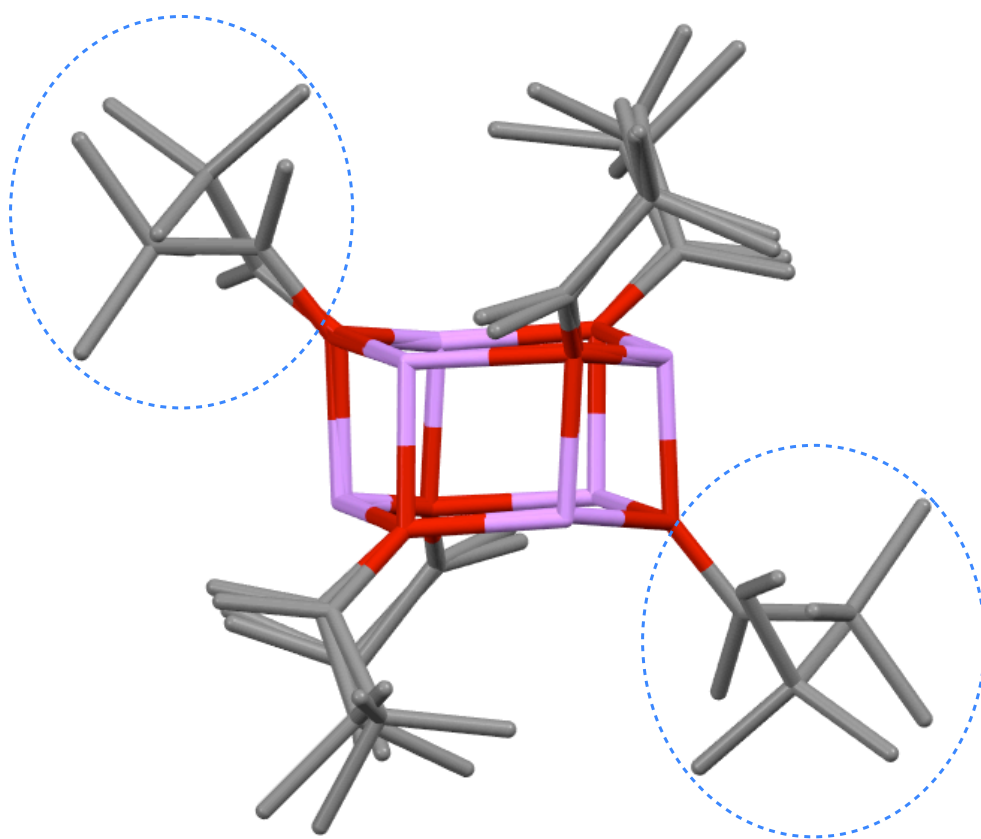


Figure 4.1. H₁/H₂ overlay: structural differences between two LiOPin hexamers. Hydrogen atoms have been omitted for clarity.

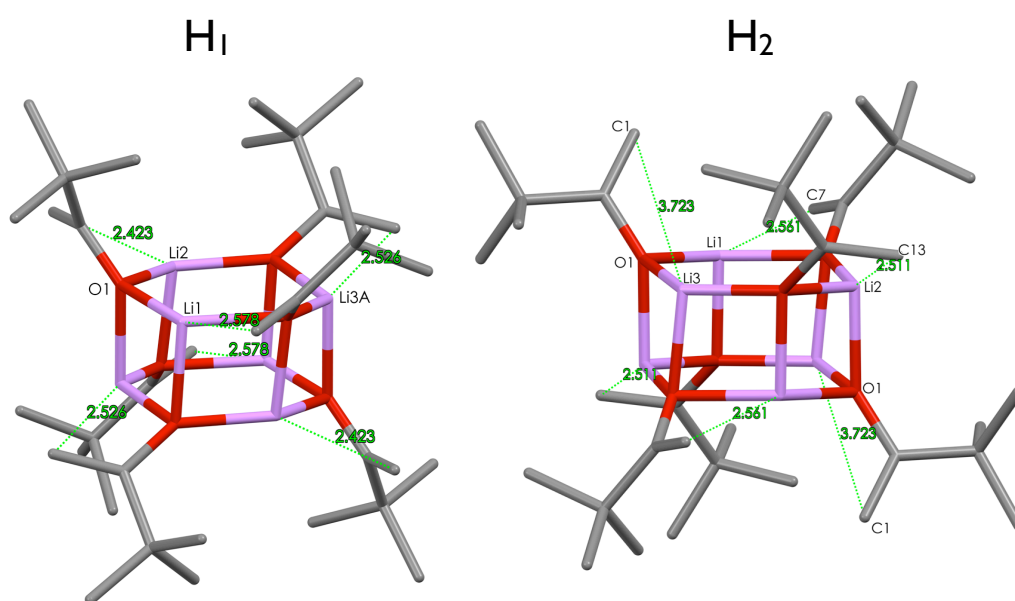


Figure 4.2. Short distances between lithium atoms and terminal methylene carbons indicate the existence of cation- π interactions. Distances are marked in green values

with units shown as Å.

Another structural consequence of the oxallyl group rotation is the steric effect between *tert*-Bu groups. As shown in **Figure 4.3**, if we observe the two structures from the top of hexamers, i.d. by viewing a hexagonal face of the aggregate, six *tert*-Bu groups array clockwise in **H₁** wherein each two *tert*-Bu group is separated by a carbon-carbon double bond. However this clockwise symmetry does not appear in **H₂**. In the structure of **H₂** (**Figure 4.3** right), the potential steric effect due to two head-to-head *tert*-Bu groups is circled by blue dashed line. Based on the consideration of cation- π interactions and steric effects between *tert*-Bu groups, **H₁** should be slightly more stable than **H₂**.

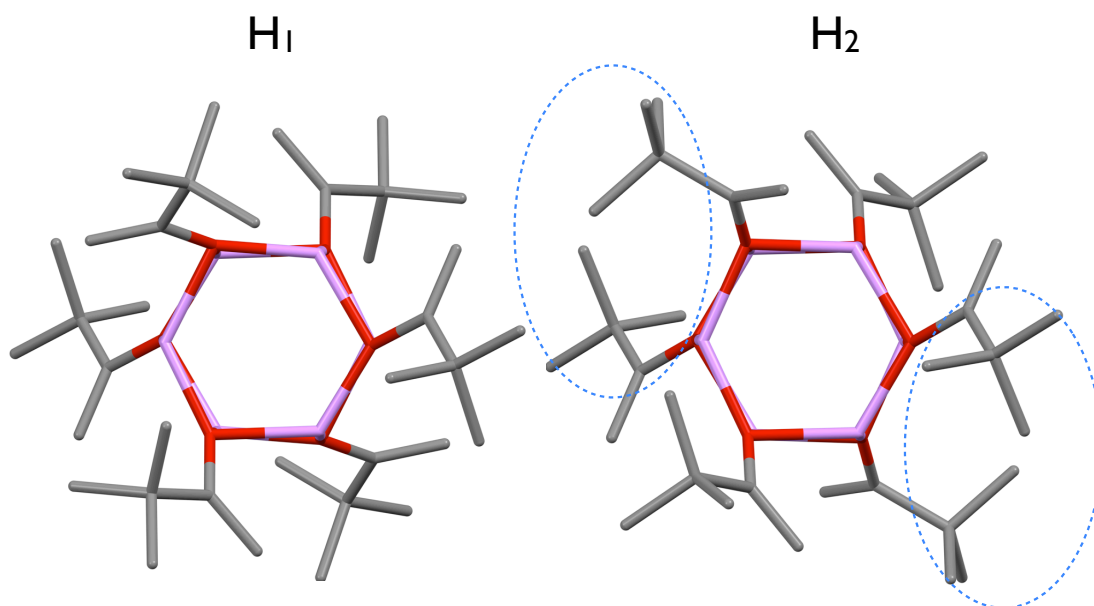


Figure 4.3. Hexameric structure of **H₁** and **H₂**, observed from top. Hydrogen atoms have been omitted for clarity.

4.3.2 Solution-state Structure of Unsolvated Lithium Pinacolone Enolate

Discrimination of H₁ and H₂ by NMR. Dissolving either crystal of H₁ or H₂ in Toluene-*d*₈ yields identical 1D NMR (¹H, ¹³C, ⁶Li) spectra. However, at least three different terminal methylene carbons are observed from ¹³C NMR (**Figure 4.4**) at -20 °C. These correlate with three pairs of terminal methylene proton peaks in the ¹H NMR (**Figure 4.5**), as confirmed by {¹H, ¹³C} HSQC (**SI**). These NMR results indicate that at least three lithium pinacolone enolates co-exist in the solution and bear different chemical environments. We name them E, E' and E'': E and E' are the two major species and E is more than E'; E'' is a minor complex. Above 0 °C, peaks belonging to E'' will overlap with E', then only two major intermediates can be observed.

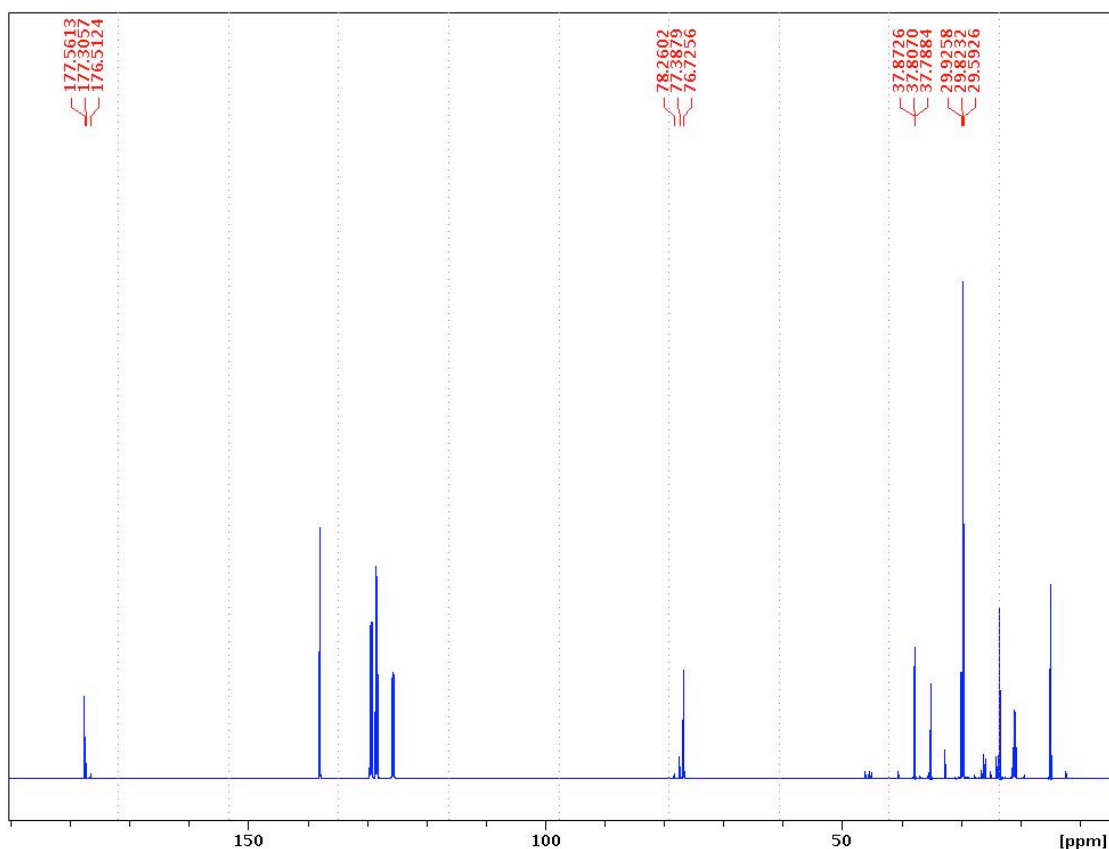


Figure 4.4. ¹³C NMR of LiOPin hexamer crystal dissolving in toluene-*d*₈ at -20 °C. Three groups of LiOPin peaks are labeled with their chemical shift values.

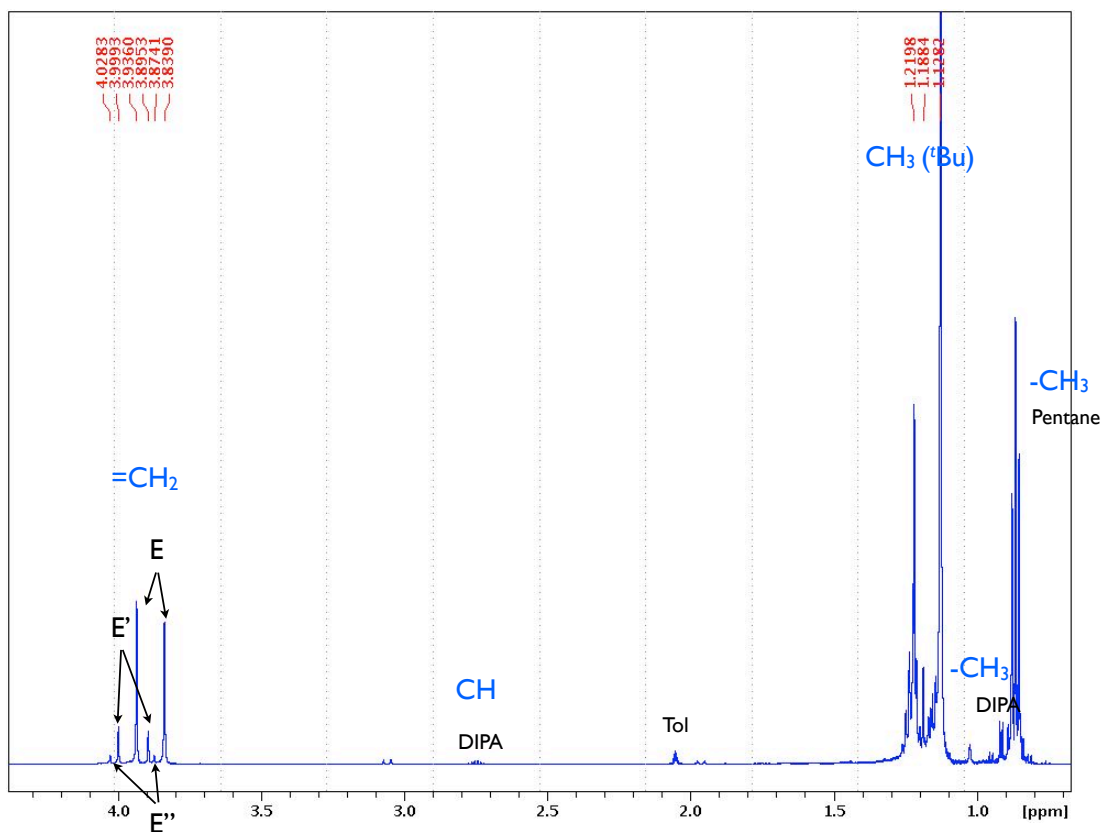


Figure 4.5. ^1H NMR of LiOPin hexamer crystal dissolving in toluene- d_8 at $-20\text{ }^\circ\text{C}$. Three groups of LiOPin peaks are labeled with their chemical shift values. A little of diisopropylamine (DIPA) and solvent pentane are also observed as impurities.

Our first idea about E and E' is that they are two different hexamers in solution, E is probably \mathbf{H}_1 and E' is \mathbf{H}_2 . E'' is not available at high enough concentration to collect accurate integration in ^1H NMR. However we suggest that it is likely to be a mixed aggregate with some undetectable impurities. Moreover, we assume E and E' will build up equilibrium in the solution, which can explain that \mathbf{H}_1 and \mathbf{H}_2 samples offer identical NMR spectra. However this assumption is not consistent with two additional experimental facts. First, the integration ratio of terminal methylene protons of E and E' has no observable change in VT NMR experiment from $-20 \sim -70\text{ }^\circ\text{C}$. Second, the self-diffusion coefficient values of E and E', measured via PGSE, always indicate that E' is slightly heavier and larger than E. The first fact rejects the existence of an NMR observable equilibrium between E and E'. The second

observation conflicts with the hypothesis that E and E' are both LiOPin hexamer. Therefore, using NMR to distinguish H₁ and H₂ is still not workable.

Spectra interpretation. The second proposal is that the two major components are tetramer and hexamer. Considering molecular size of E is smaller than E' such that E could be assigned as a tetramer and E' is a hexamer. In order to test this assignment, a referenced DOSY experiment^s was introduced to measure the MWs of E and E' in toluene. As shown in **Figure 4.6 & 4.7**, the diffusion coefficient values of four internal references and E/E' were measured and MWs of E and E' was predicted based on D-FW analysis (**Table 4.1**). MW of LiOPin tetramer is 424 g/mol and hexamer is 636 g/mol. Predicted MW of E is 416, which is quite close to the value of tetramer with a -2% error. However, if E' is a hexamer, then the experimental error is -24%. Based on our previous experience on referenced DOSY experiments, the experimental absolute error is usually less than 10%. Thus our second assumption is also not fully consistent with that E' assigned as a hexamer. Even though the predicted MW of E' (483 g/mol) approaches the MW of LiOPin pentamer (530 g/mol), we are hesitant to assign E' as a pentamer because pentameric organolithium reagents have never been observed in either the solid and solution state previously.

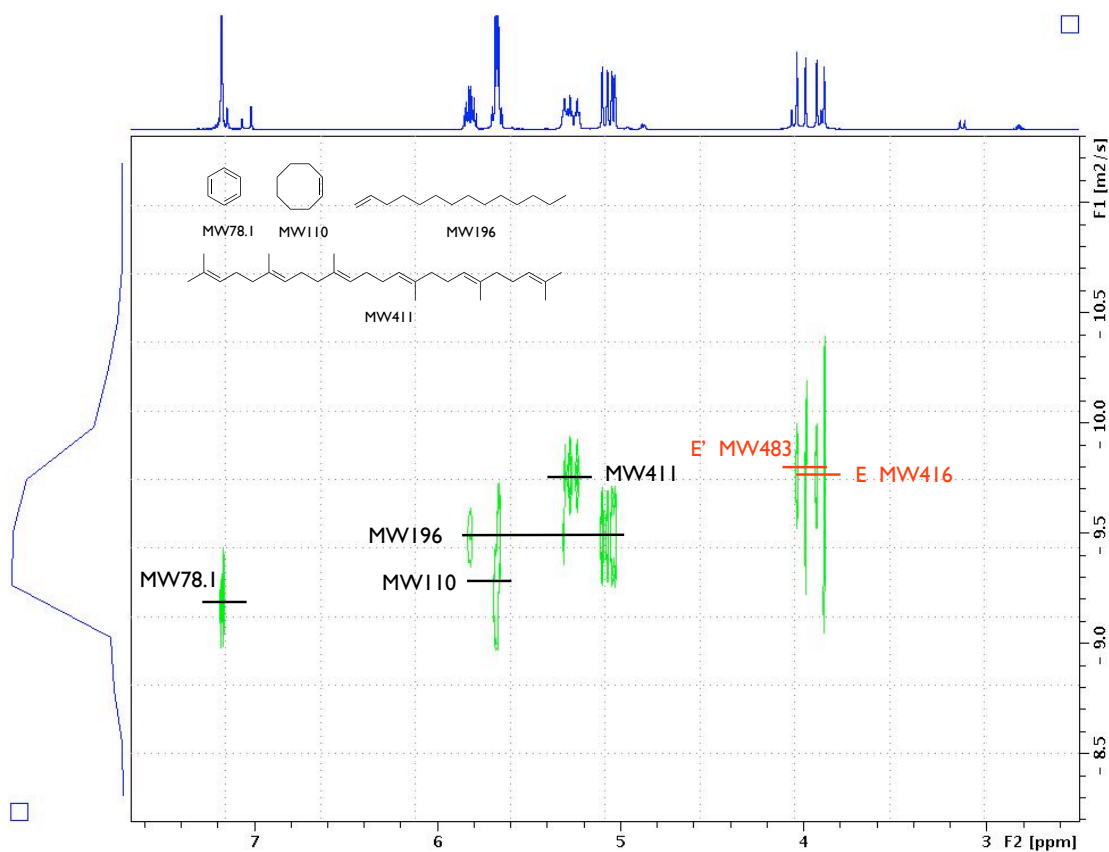


Figure 4.6. ^1H DOSY spectra of LiOPin hexamer crystal dissolved in $\text{Tol-}d_8$ at -20 $^\circ\text{C}$.

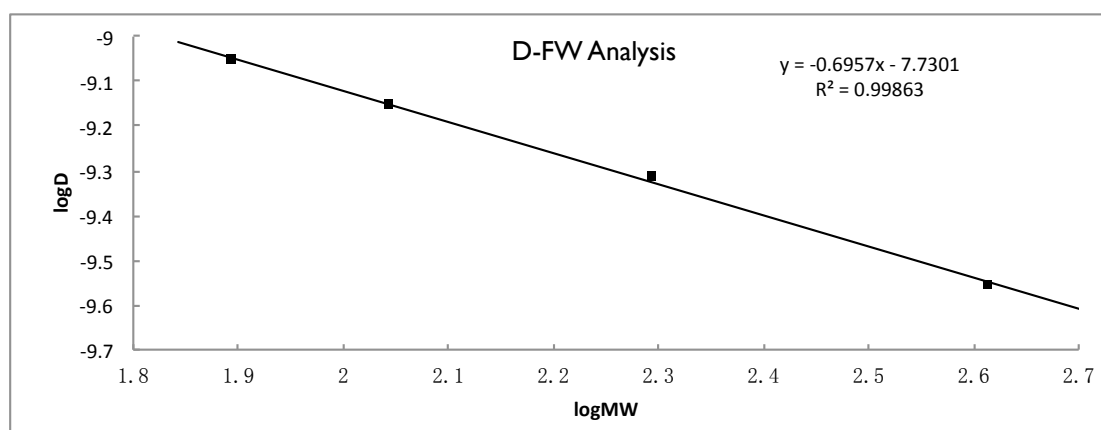


Figure 4.7. D-FW analysis of ^1H DOSY data of LiOPin hexamer crystal dissolved in $\text{Tol-}d_8$ at -20 $^\circ\text{C}$.

Table 4.1. D-FW analysis of ^1H DOSY data of LiOPin hexamer crystal dissolved in Tol- d_8 at $-20\text{ }^\circ\text{C}$

Entry	Compound	FW	D	Predicted FW	% Error
		g/mol	m^2/s	g/mol	
1	BEN	78.1	8.895E-10	79.2	1
2	COD	110	7.041E-10	111	1
3	TDE	196	4.858E-10	189	-4
4	SQU	411	2.789E-10	419	2
5	E	424	2.802E-10	416	-2
6	E'	--	2.528E-10	483	--

Carefully review of all the spectra reveals an interesting quaternary carbon peak besides the three $=\text{CH}_2$ carbons by overlaying ^{13}C spectra with DEPT135 spectra (**Figure 4.8**). A quaternary carbon peak appearing at 76.5 ppm implies that this quaternary carbon is adjacent to electron-withdrawing atoms or groups. We immediately realized this quaternary carbon is quite possible from lithium aldolate, the aldol product from LiOPin and pinacolone. Aldolate is a reasonable byproduct or impurity in this system, because during wash or transfer procedures, small amount of LiOPin can be quenched to form pinacolone followed by self-aldol reaction proceeding very fast at room temperature. We had not considered the possibility of aldolate until observation of this quaternary carbon. Because only three carbonyl carbons are present in the ^{13}C spectra (**Figure 4.4**) and these are correlated to three terminal methylene carbons, they all must belong to lithium enolates. However the existence of lithium aldolate requires a fourth carbonyl peak in the ^{13}C spectra. Our default spectral width (sw) of ^{13}C NMR is 240 ppm, spectral center (o1p) is 100 ppm, so our spectral range for ^{13}C spectra is from -20 ppm to 220 ppm. After expansion of

the SW to 260 ppm, we did observe the missing carbonyl carbon peak at 224.4 ppm (Figure 4.9). Thus all other carbon and proton peaks belonging to lithium aldolate are assignable in both ^{13}C and ^1H spectra (Figure 4.9 ~ 4.11), with the help of HSQC/HMBC/NOESY spectra (SI).

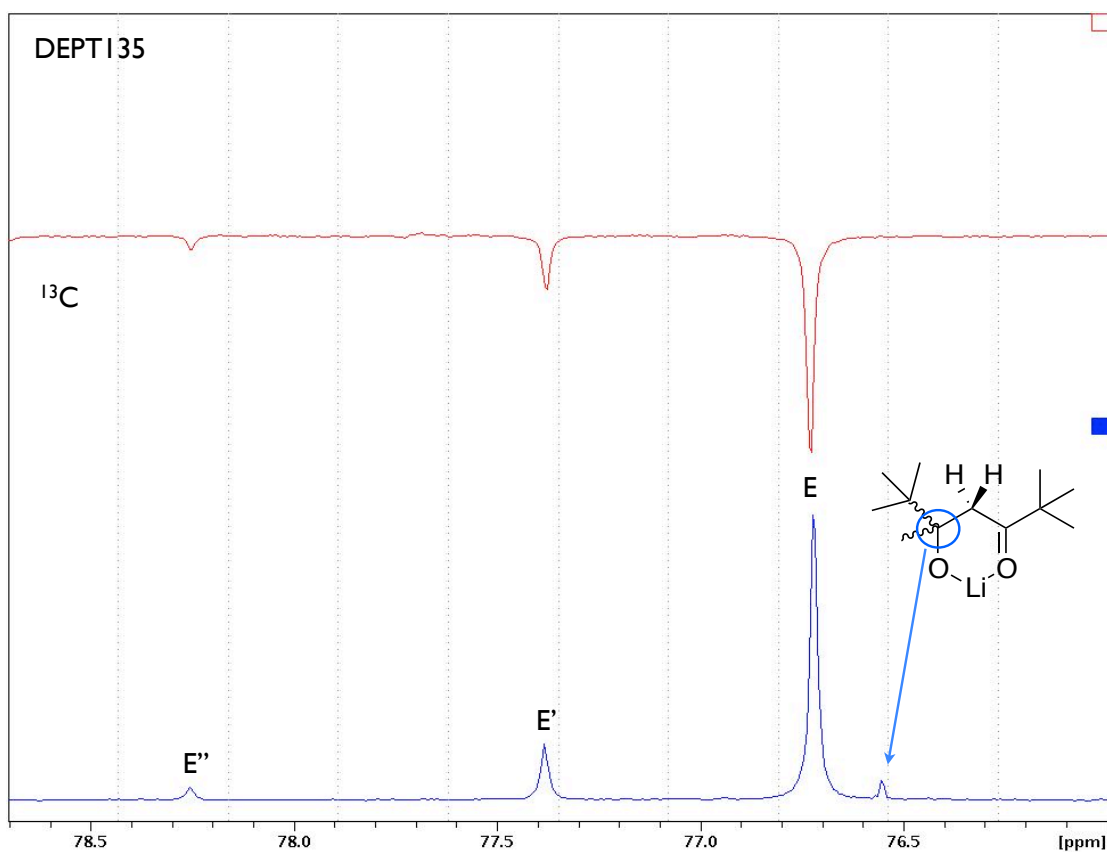


Figure 4.8. Overlay of ^{13}C NMR and DEPT135 spectra. Three terminal methylene carbon from three different enolates show negative phase in DEPT135 and a quaternary carbon from aldolate would only present in ^{13}C NMR but not DEPT135 spectra.

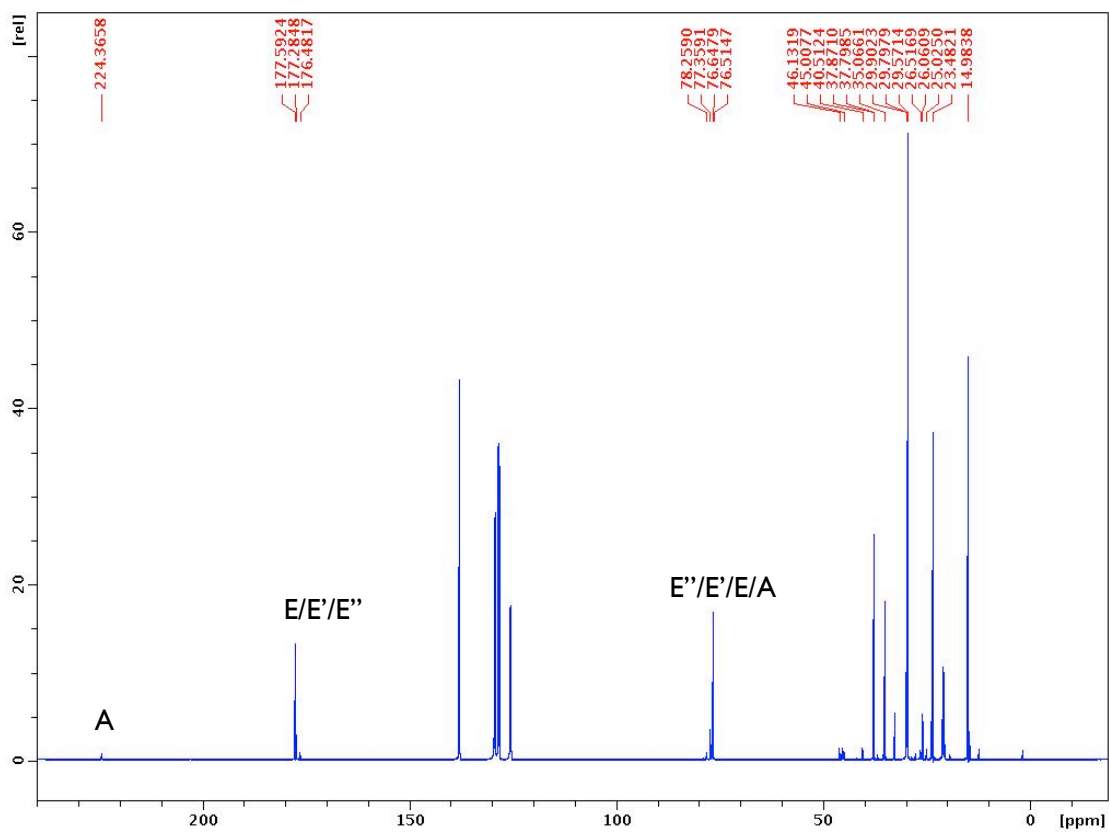


Figure 4.9. ^{13}C NMR of LiOPin hexamer crystal dissolving in Tol- d_8 at $-20\text{ }^\circ\text{C}$ with sw 260ppm and o1p 100 ppm.

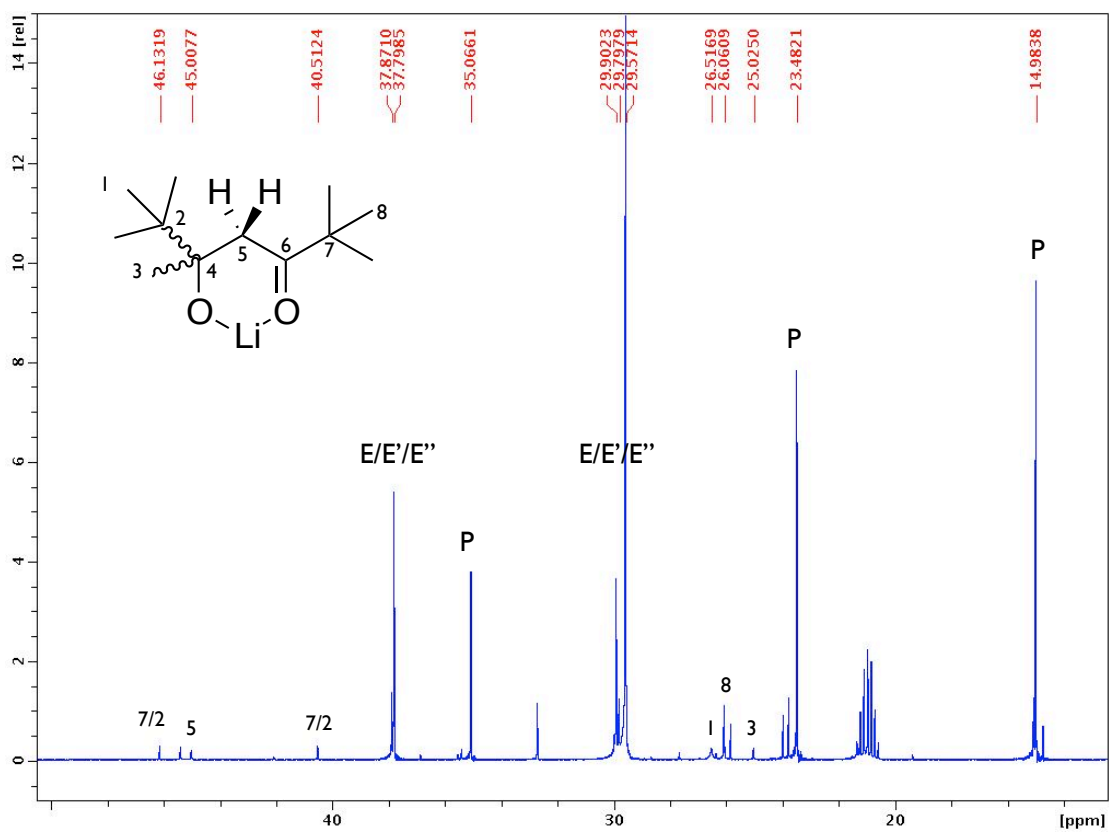


Figure 4.10. Up-field region (10 ~50 ppm) of ^{13}C NMR of LiOPin hexamer crystal dissolving in $\text{Tol-}d_8$ at $-20\text{ }^\circ\text{C}$.

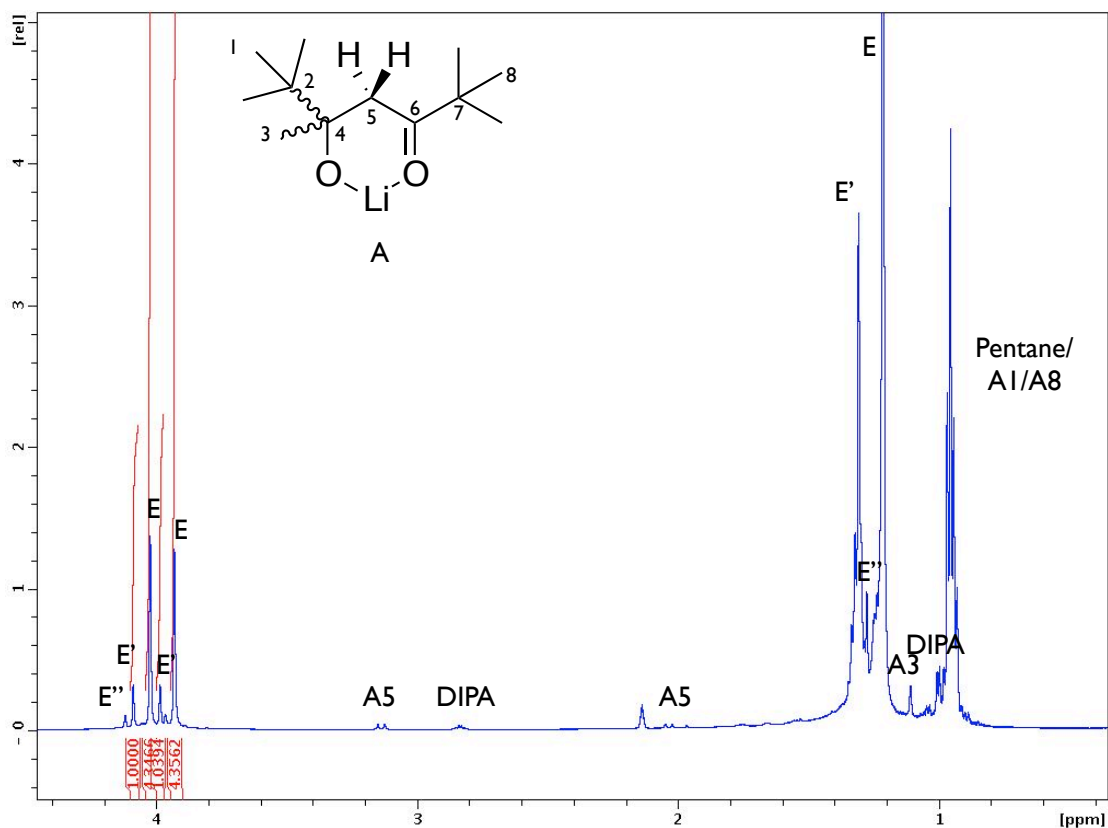


Figure 4.11. ^1H NMR of LiOPin hexamer crystal dissolving in $\text{Tol-}d_8$ at $-20\text{ }^\circ\text{C}$.

Since all the data now support the existence of lithium aldolate, therefore we deduced that E' is a mixed aggregate of lithium pinacolone enolate (LiOPin) and lithium pinacolone aldolate (LiOA). This assumption is confirmed by a NOE peak observed in $\{^1\text{H}, ^1\text{H}\}$ NOESY spectra. As shown in **Figure 4.12**, one of the two protons on carbon 5 of lithium aldolate exhibits an NOE with one of the two methylene protons from E'. This means E' binds with lithium aldolate and forms a mixed aggregate. This conclusion is also supported by the fact that methylene peak of E' will increase and the one from E will decrease if small amount of pinacolone is added to the solution (SI).

Considering the predicted MW of E' is 483 g/mol from the referenced DOSY experiment, we concluded that E' is a mixed tetramer of LiOPin and LiOA with ratio 3:1 (theoretical MW is 524 g/mol). This assignment is not only based on our referenced DOSY result, but is also supported by other two facts. First, there are two crystal structures of unsolvated lithium aldolate have been reported, both of which are tetramers.⁹ Considering that LiOPin forms a tetrameric structure in toluene, it is not surprising that the mixed complex of LiOA and LiOPin is also a tetramer. Second, excess LiOPin tetramer E coexists with E' so a likely ratio between LiOPin and LiOA is 3:1.

The solid-state crystal structure of mixed aggregate of lithium enolate and lithium aldolate is still undetermined. However the observation of this mixed aggregate is intriguing.¹⁰ Reich and co-workers¹¹ have reported an excellent work on the aldol reaction between acetophenones and 4-fluorobenzaldehyde utilizing LDA in ethereal solvent. The authors found that both lithium enolate dimer and tetramer are able to react with aldehyde to give mixed enolate-aldolate complexes that are more reactive than the homo-aggregates. According to their ¹⁹F NMR results, they observe two mixed aggregates: a 1:1 ratio dimer and a 3:1 enolate-aldolate tetramer. Thus the characterization of enolate-aldolate mixed compounds is still ongoing.

Since peaks of E'' are too small and partially overlap with E' and E, we cannot reliably assign a structure to E''.

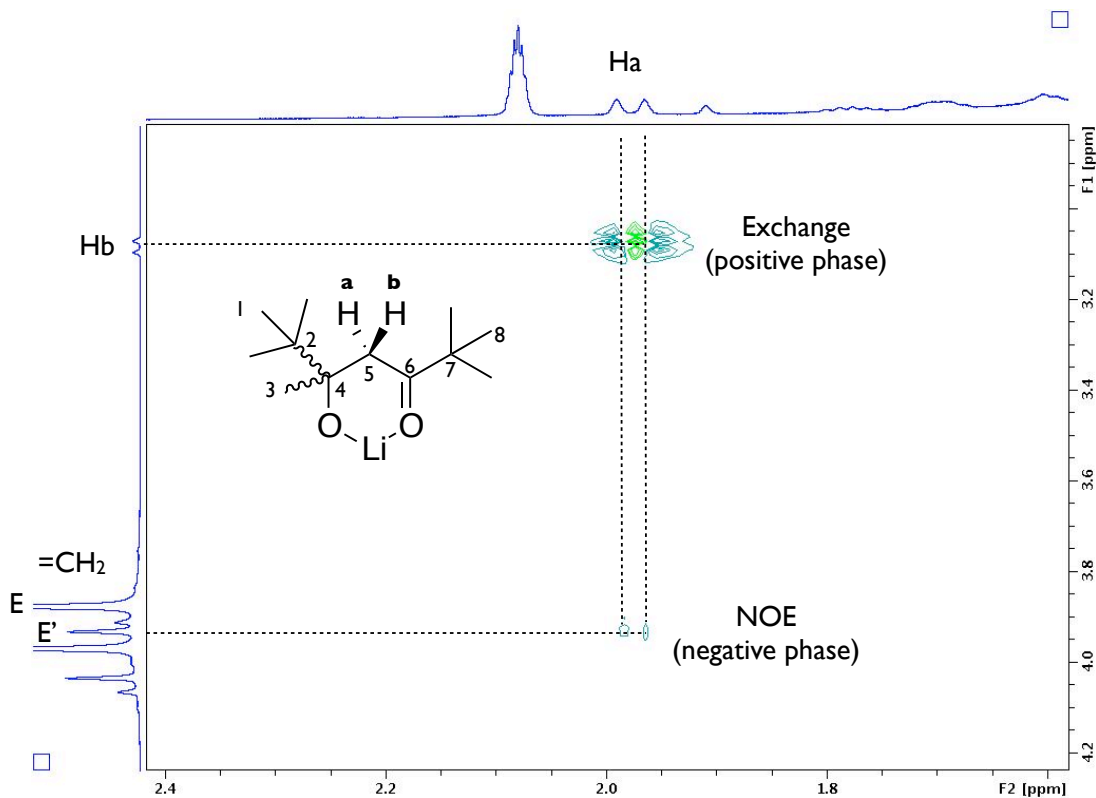


Figure 4.12. $\{^1\text{H}, ^1\text{H}\}$ NOESY spectra of LiOPin and lithium pinacolone aldolate in $\text{Tol-}d_8$ at $-20\text{ }^\circ\text{C}$.

The last question is why the LiOPin hexamer crystal dissolved in toluene deaggregates to form a tetramer? Our explanation is that this represents a solvent effect such that toluene deaggregates hexamer to tetramer. Even though there is no enolate crystal structure containing benzene or toluene as donating ligands to lithium atoms, lithium is known to sit in the center of an aromatic ring (lithium- π interaction) as has been observed in solid state.¹² Moreover, when we dissolving LiOPin Hexamer crystal in cyclohexane- d_{12} , E presents a much larger MW 548 g/mol even at room temperature (**Figure 4.13** and **SI**). These observations all suggest that toluene can stabilize bare lithium atoms in tetramer via a cation- π interaction.

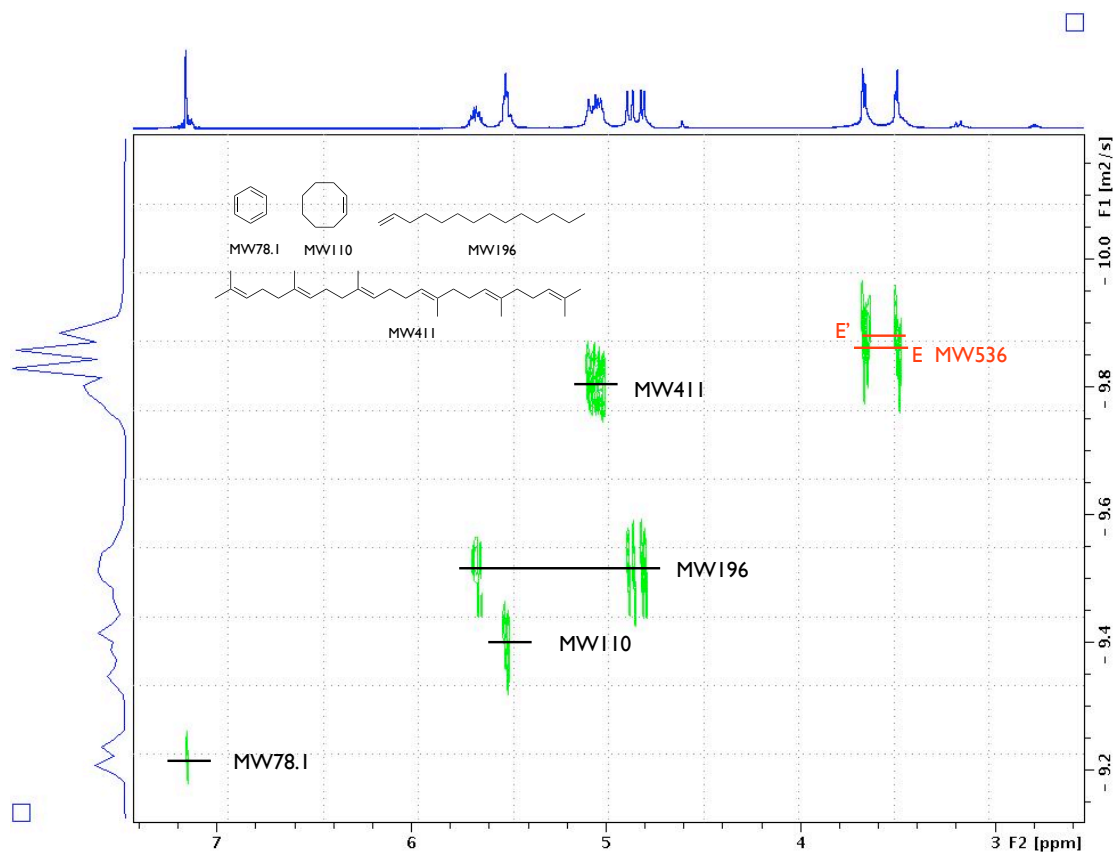
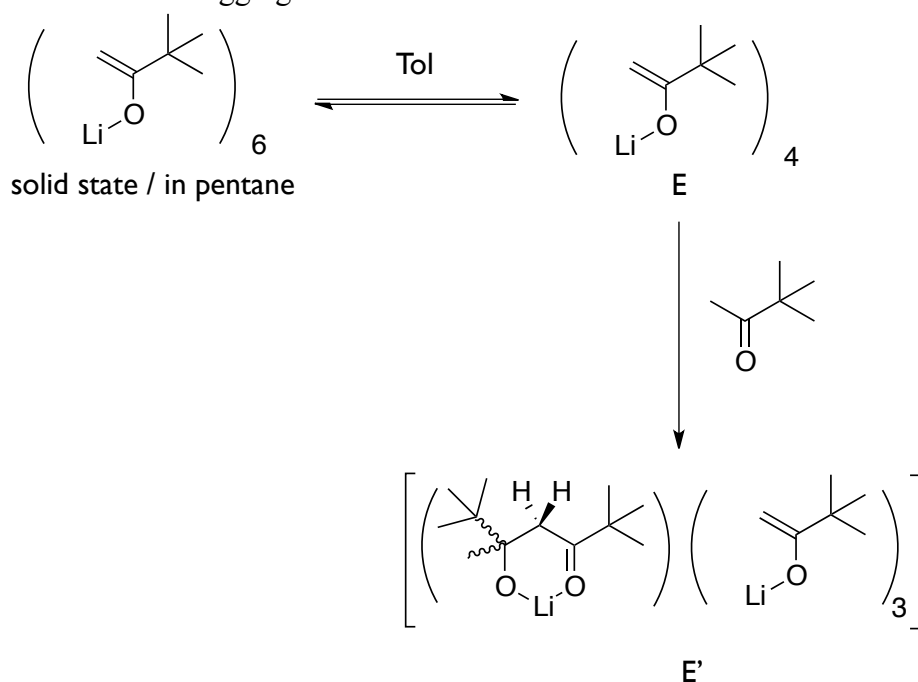


Figure 4.13. ^1H DOSY spectra of LiOPin hexamer crystal dissolved in cyclohexane- d_{12} at 23 °C.

4.4 Conclusion

A polymorphic crystal of lithium pinacolone enolate hexamer was prepared via three methods. It is a metastable structure due to the lost of partial Li-oxallyl cation- π interactions. An NMR study suggests that lithium pinacolone enolate hexamer will deaggregate to mainly tetramer in toluene solution but will remain mainly as a hexamer in cyclohexane solution. We invoke a cation- π interaction between lithium and toluene to explain this behavior. A small amount of lithium aldolate was observed and this forms a mixed tetrameric aggregate with lithium enolate in a 1:3 ratio.

Scheme 4.1. Lithium pinacolone enolate hexamer deaggregate to tetramer in toluene and form mixed aggregate with lithium aldolate.



4.5 Experimental Section

Procedures for NMR Experiments. NMR samples were prepared in tubes sealed with rubber septa cap and parafilm. NMR tubes were evacuated *in vacuo*, flame-dried and filled with argon before use. ^1H chemical shifts were referenced to toluene- d_8 at 7.00 ppm and ^{13}C chemical shifts were referenced to toluene- d_8 at 137.86 ppm. All NMR experiments were acquired on a Bruker Avance III HD 600 MHz spectrometer equipped with a z-axis gradient BBFO smartprobe. For DOSY experiments, a GRASP II 10A z-axis gradient amplifier was employed, with maximum gradient strength of 0.5 T/m. ^1H DOSY was performed using the standard Bruker pulse programs, employing a double stimulated echo sequence, bipolar gradient pulses for diffusion, and 3 spoil gradients. Diffusion time was 100 ms, and the rectangular gradient pulse duration was 1300 μs . Gradient recovery delays were 200 μs . Individual rows of the quasi-2-D diffusion databases were phased and baseline corrected. Actual diffusion

coefficients used for D-FW analysis were obtained using the T1/T2 analysis module in commercially available software.

Materials and Methods. Pentane, pinacolone and diisopropylamine (DIPA) were dried by stirring with calcium hydride (CaH_2) under Ar atmosphere overnight then distillation. Toluene was gained from dry solvent system. Unless otherwise stated, purchased chemicals were used as received. All reactions under anhydrous conditions were conducted using flame- or oven-dried glassware and standard syringe techniques under an atmosphere of argon.

General Procedures for the Crystallization of H_2 . Method 1: To a 1.1 M DIPA (5.5 mmol) solution in 5.0 ml pentane at 0 °C under Ar atmosphere was slowly added 2.1 ml 2.5 M *n*-BuLi (5.25 mmol). The reaction mixture was allowed to stir at 0 °C for 10 minutes. 0.5 g of pinacolone (5 mmol) was then added dropwise and the mixture was allowed to stir at 0 °C for 15 minutes. Finally, HMPA 0.18 g (1.0 mmol, 0.15~0.2 eq.) was added and the solution was kept stirring for another 15 minutes at room temperature. The clear solution was then stored at -20 °C freezer and XRD quality crystals were collected after two days.

Method 2: To a 1.1 M DIPA (5.5 mmol) solution in 5.0 ml of toluene at 0 °C under Ar atmosphere was slowly added 2.1 ml 2.5 M *n*-BuLi (5.25 mmol). The reaction mixture was allowed to stir at 0 °C for 10 minutes. 0.5 g of pinacolone (5 mmol) was then added dropwise and the mixture was allowed to stir at 0 °C for 15 minutes. The clear solution was then stored at -20 °C freezer and XRD quality crystals were collected after two days.

Method 3: To a 1.1 M DIPA (5.5 mmol) solution in 5.0 ml of pentane at 0 °C under Ar atmosphere was slowly added 2.1 ml 2.5 M *n*-BuLi (5.25 mmol). The reaction mixture was allowed to stir at 0 °C for 10 minutes. 0.5 g of pinacolone (5 mmol) was

then added dropwise and the mixture was allowed to stir at 0 °C for 15 minutes. The clear solution was then stored at -20 °C freezer and XRD quality crystals were collected after overnight. Mother liquor was removed via syringe and dried pentane was added dropwise at 0 °C to fully re-dissolve the crystals. Then the clear solution was put back to at -20 °C freezer and XRD quality crystals were collected after two days.

4.6 References

-
- ¹ Amstutz, R.; Seebach D.; Schweizer, W. B.; Dunitz, J. D. *Helv. Chim. Acta.* **1981**, *64*, 2617-2622.
- ² Cambridge Structural Database, updates through xx 2015. (waiting for software updates)
- ³ Williard, P. G.; Carpenter, G. B. *J. Am. Chem. Soc.* **1985**, *107*, 3345-3346.
- ⁴ Pospisil, P. J.; Wilson, S. R.; Jacobsen, E. N. *J. Am. Chem. Soc.* **1992**, *114*, 7585-7587.
- ⁵ Laube, T.; Dunitz, J. D., Seebach, D. *Helv. Chim. Acta.* **1985**, *68*, 1373-1393.
- ⁶ Williard, P. G.; Hintze, M. J. *J. Am. Chem. Soc.* **1990**, *112*, 8602-8604.
- ⁷ Nichols, M. A.; Leposa, C. M.; Hunter, A. D.; Zeller, M. *J. Chem. Crystallogr* **2007**, *37*, 825-829.
- ⁸ Li, D.; Keresztes, I.; Hopson, R.; Williard, P. G. *Acc. Chem. Res.* **2009**, *42*, 270-280.
- ⁹ (a) Berke, H. *Main Group Metal Chemistry*, **1991**, *14*(3), 137-152. (b) Williard, P. G.; Salvino, J. M. *Tetrahedron Lett.* **1985**, *26*, 3931-3934.
- ¹⁰ (a) Collum, D. B.; McNeil, A. J.; Ramirez, A. *Angew. Chem. Int. Ed.* **2007**, *46*, 3002-3017. (b) Jones, A.; C.; Sanders, A. W.; Bevan, M. J.; Reich, H. J. *J. Am. Chem. Soc.* **2007**, *129*, 3492-3493. (c) Larranaga, O.; Cozar, A.; Bickelhaupt, F. M.; Zangi, R.; Cossio, F. P. *Chem. Eur. J.* **2013**, *19*, 13761-13773.
- ¹¹ Kolonko, K.; Wherritt, D. J.; Reich, H. J. *J. Am. Chem. Soc.* **2011**, *133*, 16774-16777.
- ¹² (a) Schiemenz, B.; Power, P. P. *Angew. Chem. Int. Ed. Engl.* **1996**, *35*, 2150-2152. (b) Jonas, K.; Russeler, W.; Angermund, K.; Kruger, C. *Angew. Chem. Int. Ed.* **1986**, *25*, 927-928.

Chapter 5 Chiral Lithium Diamides Derived from Linked *N*- Isopropyl Valinol or Alaninol

5.1 Abstract

Four different chiral diamino diethers synthesized from *N*-isopropyl valinol or *N*-isopropyl alaninol were lithiated with *n*-butyllithium in tetrahydrofuran or diethyl ether. Crystal structures of the dilithiated diamino diethers are determined by X-ray diffraction. The solution structures of the dilithiated diamino diethers are characterized by a variety of NMR experiments including diffusion-ordered NMR spectroscopy (DOSY) with diffusion coefficient-formula (*D*-FW) weight correlation analyses as well as other one- and two-dimensional NMR techniques. Coexistence of monomer and dimer has been proved by both X-ray crystallography and NMR spectroscopy.

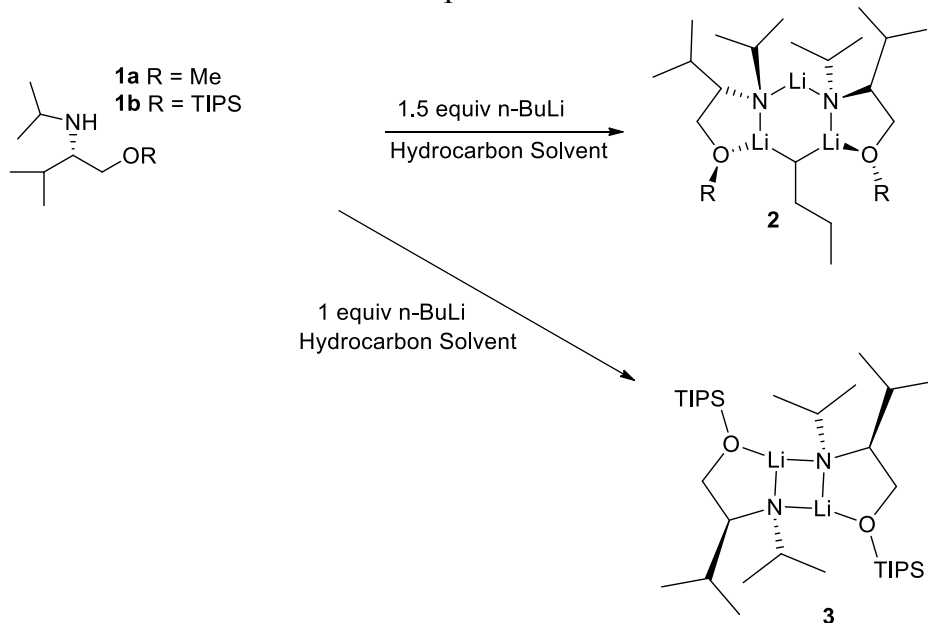
5.2 Introduction

Non-nucleophilic organolithium amide bases such as lithium diisopropylamide (LDA) and lithium hexamethyldisilazide (LHMDS) have long been widely employed in the deprotonation of various organic compounds.¹ Chiral lithium amide bases were also developed for asymmetric addition and deprotonation.² Recently, chiral lithium amide bases have also proven useful in catalytic dynamic resolution in enantioselective synthesis.³ Current research suggests that the aggregation state of chiral amide bases affects its reactivity and stereoselectivity.⁴ Thus, it is crucial to

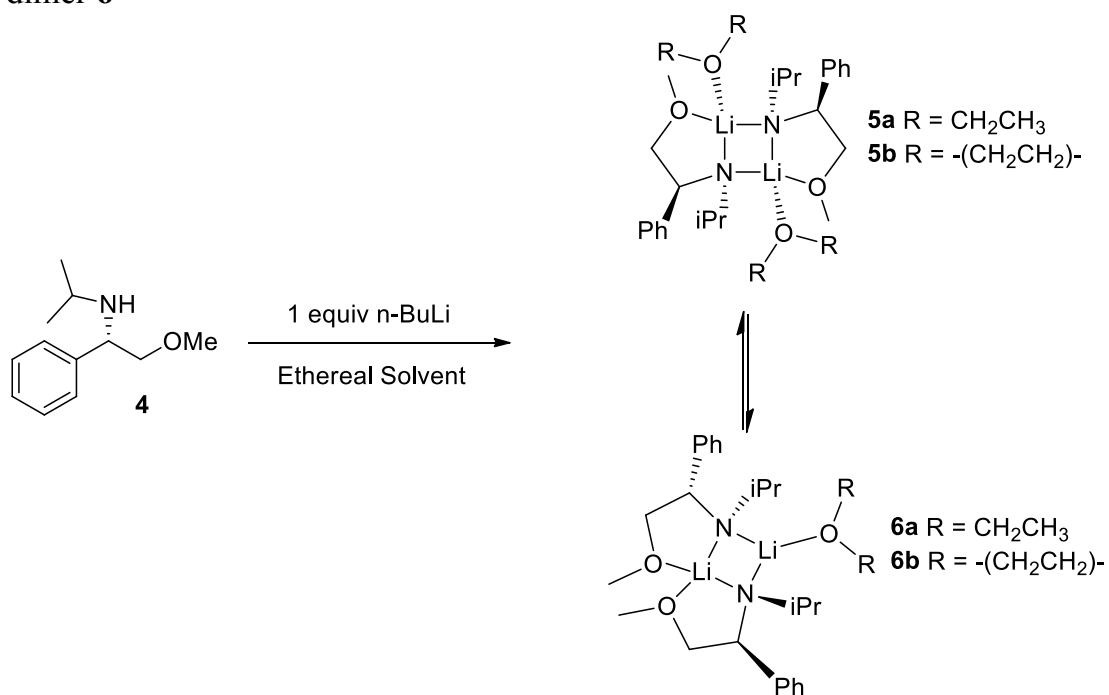
determine the aggregation state of chiral lithium amides as well as the solvation to reveal a reaction mechanism and to design more efficient chiral amines.

In 1997, we reported the crystal structures of a mixed trimer containing commercially available butyllithium with 2 eq of a lithiated chiral amino ether derived from *N*-isopropyl valinol **1a** (Scheme 5.1).⁵ Later, we carried out solution state characterization of a lithiated chiral amino ether **1b** which is structural similar to **1a**.⁶ We also reported the asymmetric addition to aldehydes with these reagents.^{4f} The result showed that lithiated chiral amino ether **1b** formed a 2:1 mixed trimer with *n*-butyllithium (*n*-BuLi) in toluene when there was excess *n*-BuLi in the solution.⁶ However, a ladder-type dimer is formed if there is only lithiated chiral amino ether **1b** in the solution without excess *n*-BuLi.⁷ In ethereal solution, lithiated chiral amino ether **4** existed as both a symmetrically solvated dimer **5** and non-equivalently solvated dimer **6** by Hilmersson and his coworkers (Scheme 5.2).⁸ Herein we reported the syntheses, as well as the solid and solution state characterization of four structurally related chiral diamino ethers derived from *N*-isopropyl valinol or alaninol.

Scheme 5.1. The Trimeric Complexes **2** and the Homodimer **3**



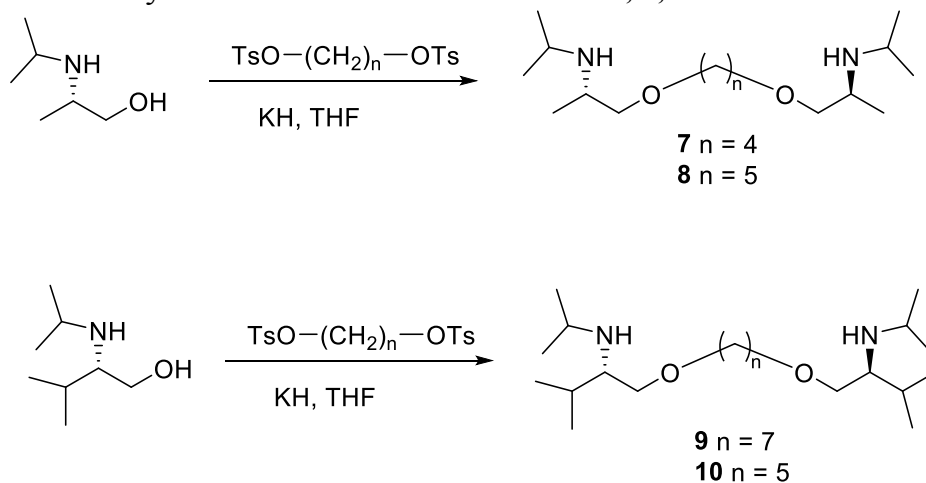
Scheme 5.2. The equivalently solvated dimer **5** and non-equivalently solvated dimer **6**



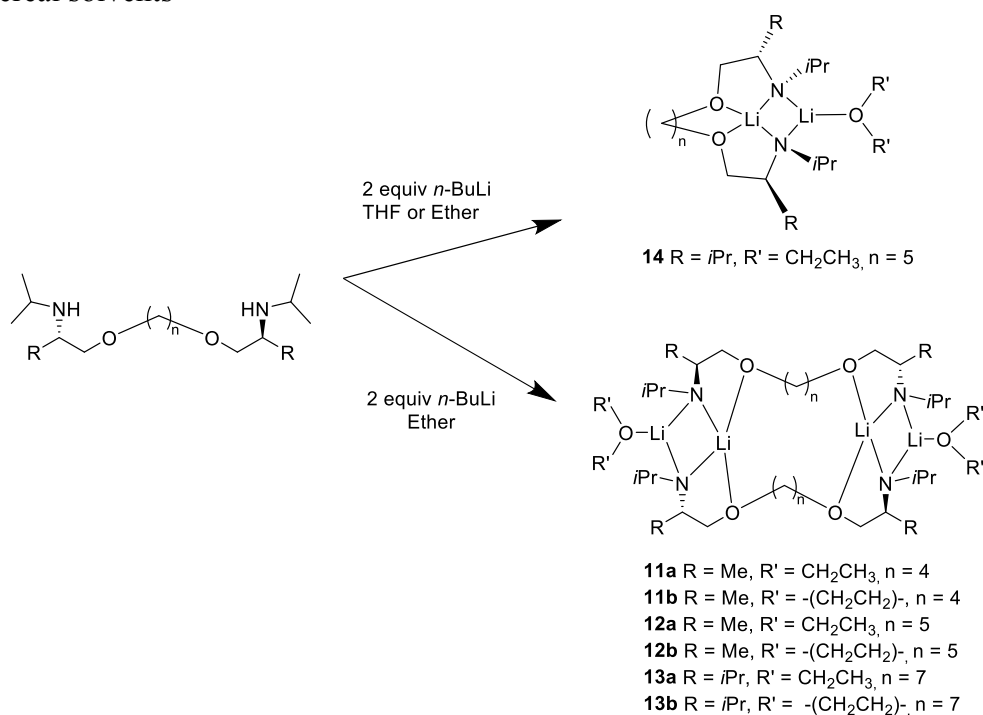
5.3 Background

(2*S*, 2'*S*)-1,1'-(butane-1,4-diylbis(oxy))bis(*N*-isopropylpropan-2-amine) **7** and (2*S*, 2'*S*)-1,1'-(pentane-1,5-diylbis(oxy))bis(*N*-isopropylpropan-2-amine) **8** were synthesized from *N*-isopropyl alaninol, whereas (2*S*,2'*S*)-1,1'-(heptane-1,7-diylbis(oxy))bis(*N*-isopropyl-3-methylbutan-2-amine) **9** and (2*S*,2'*S*)-1,1'-(pentane-1,5-diylbis(oxy))bis(*N*-isopropyl-3-methylbutan-2-amine) **10** were synthesized from *N*-isopropyl valinol as depicted in **Scheme 5.3**. Reaction of the chiral diamino diethers **7**, **8**, **9** or **10** with 2 eq of *n*-BuLi yielded products whose crystal structures were determined. These structures incorporated tetrahydrofuran (THF) and diethyl ether (DEE). Dilithiated chiral chiral diamino ethers **7**, **8**, and **9** form dimers in solid state, whereas dilithiated chiral diamino ethers **10** is a monomer, as shown in **Scheme 5.4**. These synthesis and crystallization were completed by Dr. Chicheung Su, Dr. Weibin Li and Dr. Kuiwang Wu.

Scheme 5.3. Synthesis of chiral diamino ethers 7, 8, 9 and 10



Scheme 5.4. Crystallization of dilithiated chiral diamino ethers 7, 8, 9 and 10 in ethereal solvents



5.4 Results and Discussion

5.4.1 Solution-state Characterization of Lithiated Diamino Ethers 9

The solution structure of dilithiated-9 was investigated by multinuclear magnetic

resonance spectroscopy. A 0.2 M solution of dilithiated-**9** in toluene- d_8 (0.4 ml) / THF- d_8 (0.1 ml) was prepared by adding ligand **9** (0.1 mmol) to n -Bu 6 Li (0.2 mmol). At low temperature, three peaks appear in 6 Li NMR spectrum excluding n -Bu 6 Li (Figure 10). However, if dilithiated-**9** has a similar di-solvated dimer structure in solution as its solid-state structure **13b**, we expected to observe a pair of 6 Li peaks with integration ratio 1:1. After repeating this experiment several times to exclude the possibility that the three observed peaks arose from variable impurities, e.g n -BuO 6 Li, CD $_2$ CD $_2$ O 6 Li, *etc.*, the integration ratio of three peaks was consistently around 3.5:2.3:1, clearly indicating that the integration of the biggest peak was nearly equal to the sum of the other two.

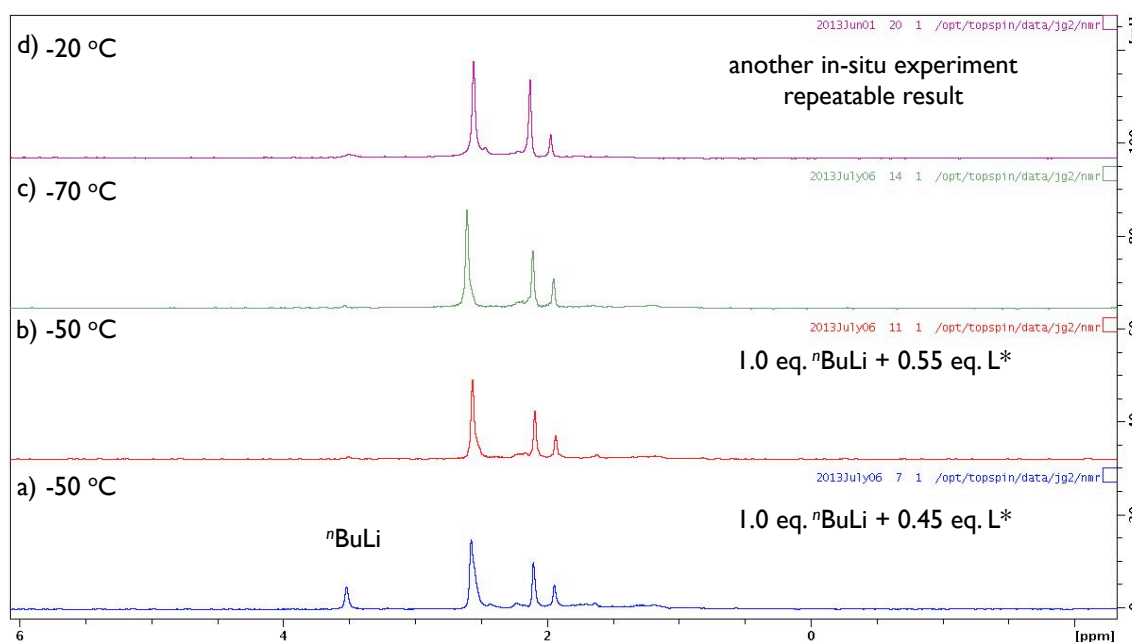


Figure 5.1. 6 Li NMR of dilithiated-**9** in Tol- d_8 /THF- d_8 (4:1). L* is chiral ligand **9**. In all four spectrums (a ~ d), the integration of the highest peak is close to the sum integrations of the other smaller peaks (relaxation delay is 10 s, equals to 5 times T1 relaxation time). Moreover, spectrum b, c and d were taken at different low temperatures without significant difference, which indicate this system is not temperature sensitive.

Reducing the temperature from -20 °C to -70 °C had no obvious effect on the frequency of the 3 resonances or their integrals. Surprisingly, changing the solvent to

100% THF-*d*₈, shifted all the peaks slightly upfield while the biggest peak separated into two peaks (**Figure 5.2a**). Now two sets of peaks with a 1:1 ratio appeared in the ⁶Li NMR spectrum, Li(x,x') and Li(y,y'). Similarly, two sets of signals were also found in ¹³C NMR (**Figure 5.3**). The multiplicity edited ¹H-¹³C HSQC (**Figure 5.4**) and COSY spectra (**Figure 5.5**), allowed us to assign the four methylene carbons (72.1 ppm, 72.4 ppm, 74.2 ppm, 74.2 ppm) adjacent to oxygen and the four methine carbons (50.8 ppm, 52.3 ppm, 66.5 ppm, 67.4 ppm) adjacent to nitrogen for dilithiated-**9**. Prior to lithiation, only two methylene carbon chemical shifts adjacent to oxygen and two methine carbon peaks adjacent to nitrogen were observed. This suggests an additional dilithiated molecule in solution. Further support for a second structure is evidenced in the ⁶Li DOSY (**Figure 5.2b**) where the two sets of resonances, Li (y,y') and Li(x,x') share similar diffusion coefficient values. Moreover, the diffusion coefficient of Li (y,y') is smaller than the diffusion coefficient of Li(x,x') implying that Li(y,y') belongs to a heavier complex than Li(x,x'). In the ⁶Li EXSY spectrum (**Figure 5.6**), there are cross peaks between Li(x) and Li(x'), and also between Li(y) and Li(y'), but not between the x and y species. All these observations support the existence of two different dilithiated complex molecules in solution.

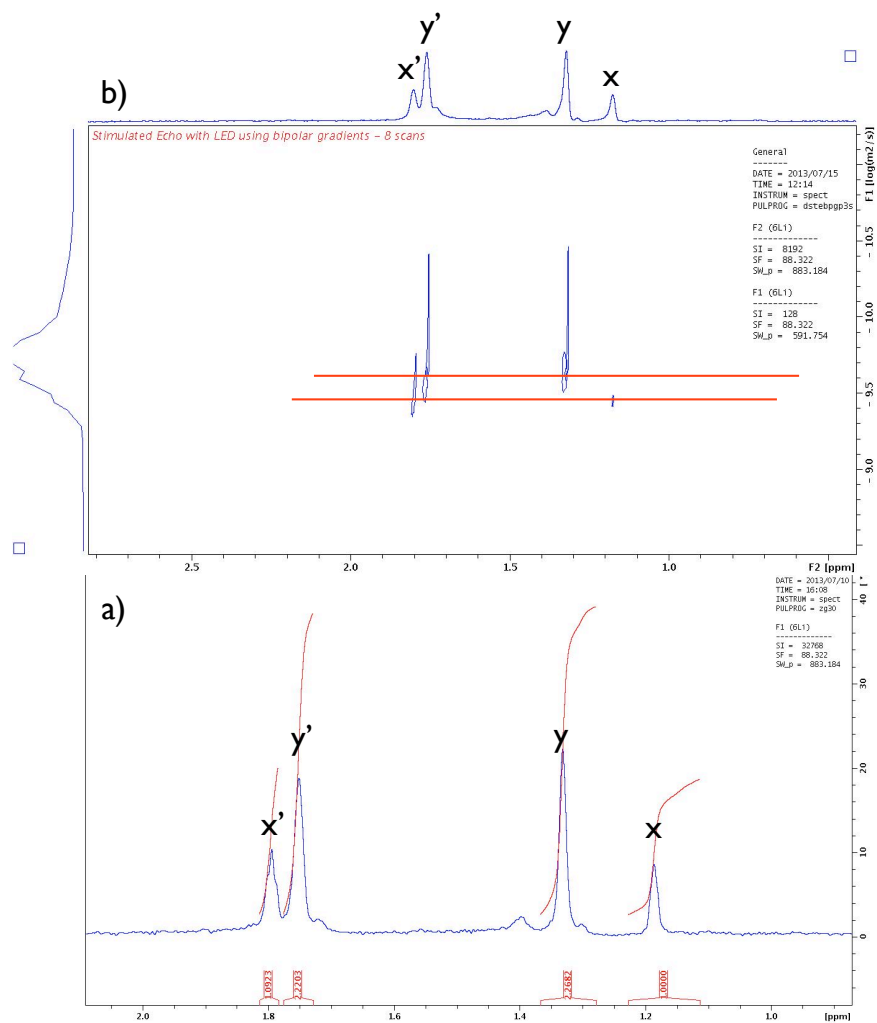


Figure 5.2. ${}^6\text{Li}$ NMR (a) and ${}^6\text{Li}$ DOSY (b) of dilithiated-9 in $\text{THF-}d_8$ at $-30\text{ }^\circ\text{C}$;

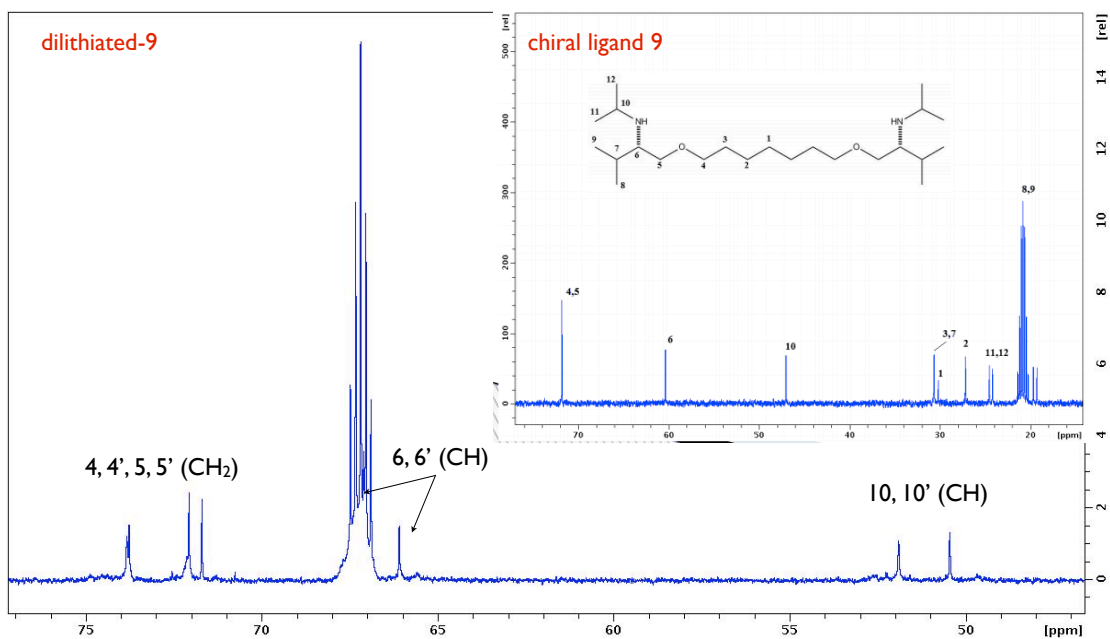


Figure 5.3. ${}^{13}\text{C}$ NMR of chiral ligand 9 and dilithiated-9. After lithiation, the number

of carbons beside oxygen atom or nitrogen atom (40-80 ppm region) was doubled.

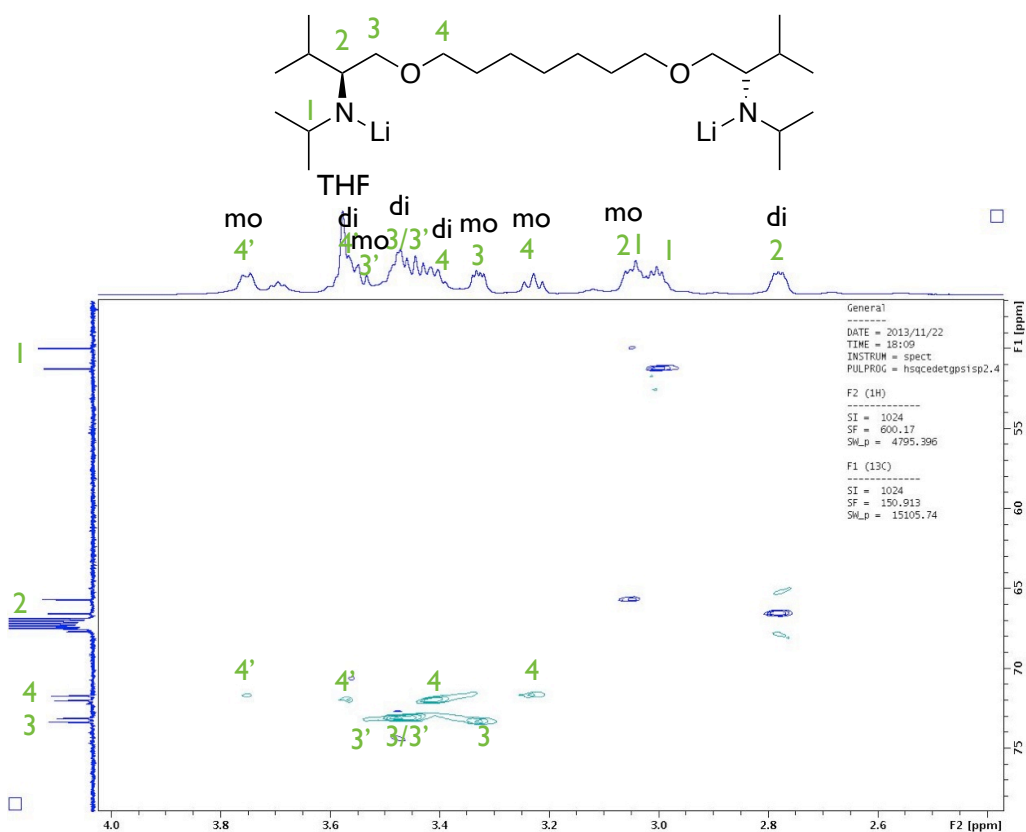


Figure 5.4. Multiplicity edited ^1H - ^{13}C HSQC spectrum of dilithiated-9 in $\text{THF-}d_8$ at -30°C . Blue spots indicate CH_3 or CH ; Green cross-peaks indicate CH_2 . “mo” means mono-THF solvated dilithiated-9 monomer; “di” means di-THF solvated dilithiated-9 dimer (Scheme 5.4).

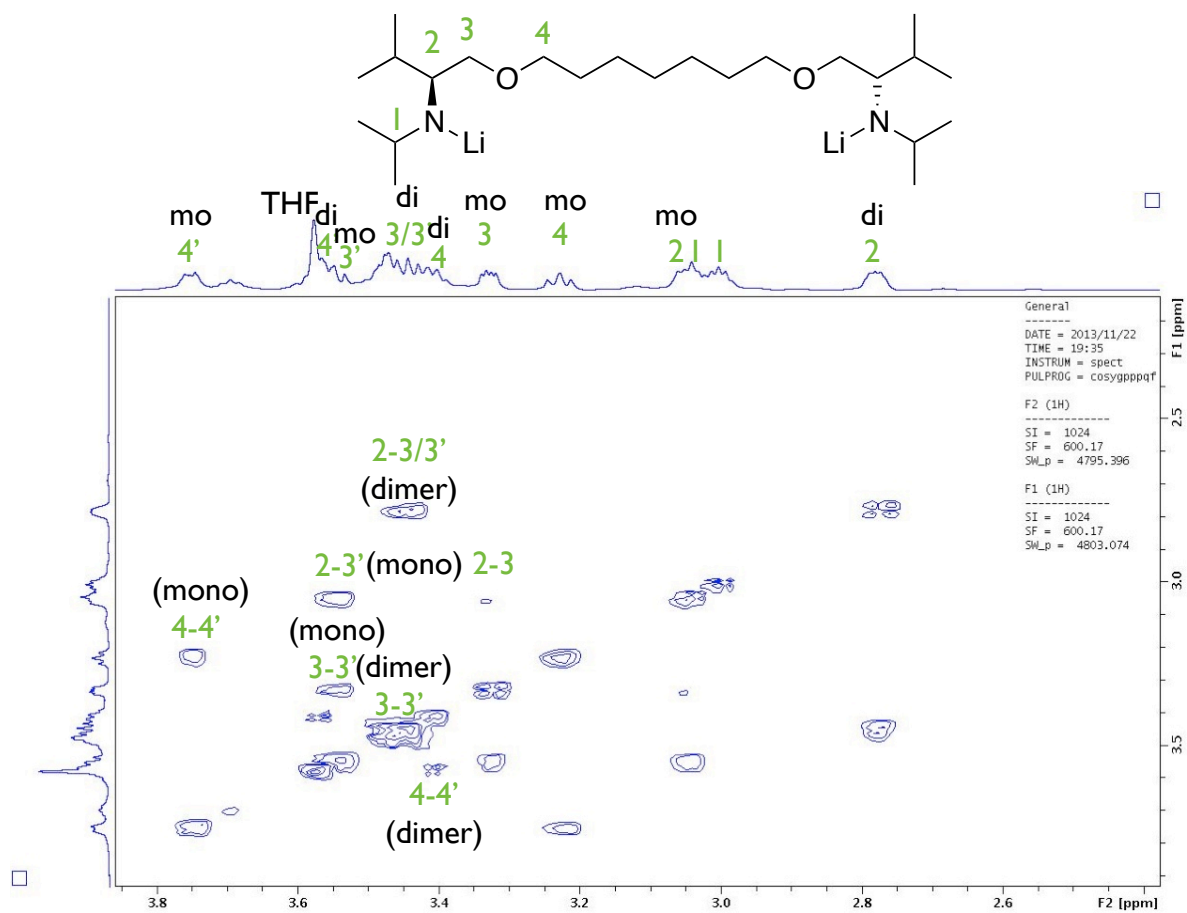


Figure 5.5. ^1H - ^1H COSY spectrum of dilithiated-**9** in $\text{THF-}d_8$ at $-30\text{ }^\circ\text{C}$. “mo” means mono-THF solvated dilithiated-**9** monomer; “di” means di-THF solvated dilithiated-**9** dimer (Scheme 5.4).

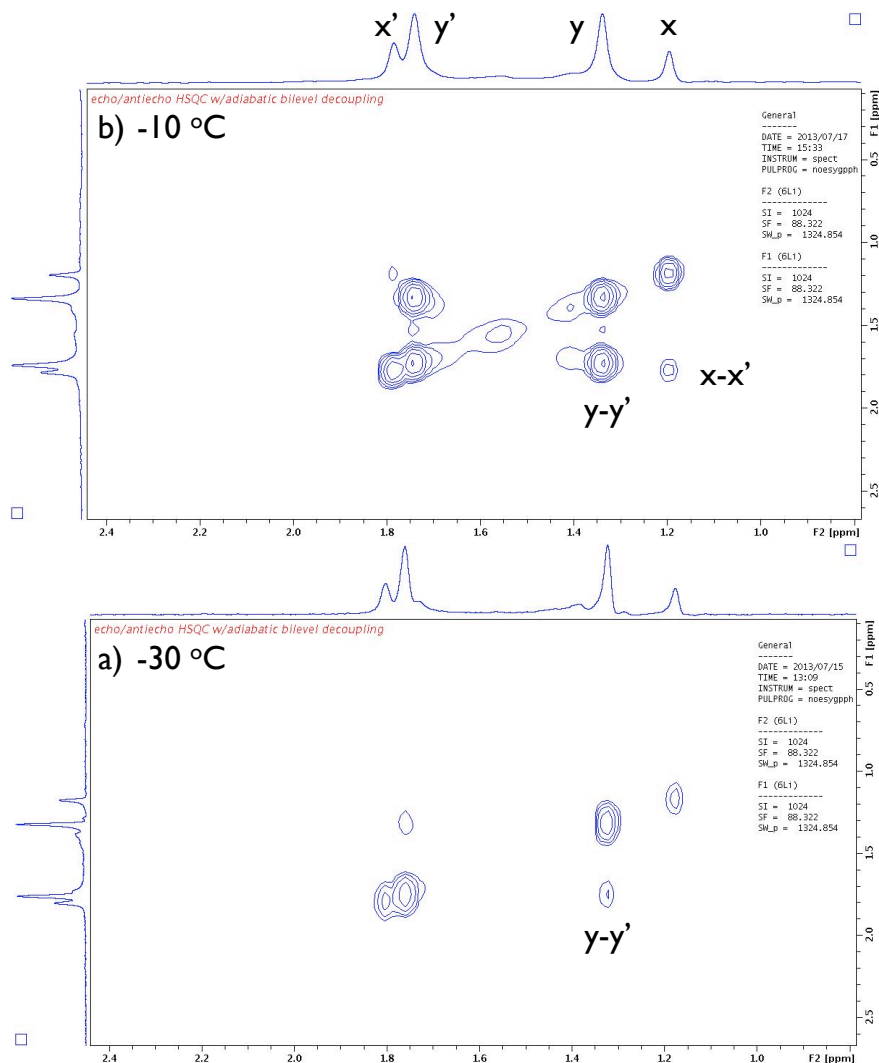


Figure 5.6. ${}^6\text{Li}$ EXSY NMR of dilithiated-9 in $\text{THF-}d_8$ at $-30\text{ }^\circ\text{C}$ (a) and $-10\text{ }^\circ\text{C}$ (b). Mixing time of spectrum (a) is 1 s and only cross peak between y and y' is observed. Mixing time of spectrum (b) is 2.4 s and cross peak between x and x' is also observed, due to higher temperature and longer mixing time.

A better understanding of the molecular weights of the two dilithiated complexes in solution comes from the diffusion – formula weight, D-FW experiment with internal references (Figure 5.7 and 5.8, Table 5.1).⁹ Consequently, we add benzene (BEN, 78.1 g/mol), cyclooctene (COE, 110 g/mol), 1-tetradecene (TDE, 196 g/mol) and squalene (SQU, 410 g/mol) as internal references (with a molar ratio around 1:3:3:1 for BEN, COE, TDE, SQU) to the sample solution of dilithiated-9 in order to carry out D-FW correlation analysis. At $-70\text{ }^\circ\text{C}$, the experimentally determined FW of the smaller

complex is 462 g/mol, while the larger one is 941 g/mol. In the solid state, dilithiated-**9** forms a di-solvated dimer (**13b**) with a FW of 952 g/mol. Therefore, we assumed that complex **13b** is larger. According to the D-FW analysis, the smaller complex is nearly half the FW of the larger one, and it has two ^6Li peaks with similar intensity and integration. In analogy to Hilmersson's non-equivalently solvated dimer **6**, we surmised that the smaller complex has a similar structure. This conclusion was then supported by the crystal structure of mono-solvated **14** (*vide infra*). If the mono-solvated **13b** has a similar structure to **14**, then its FW should be 476 g/mol (mono-solvated by THF), which is quite close to our experimentally determined DOSY result of 462 g/mol (error -3%). Hence we conclude that dilithiated-**9** exists as both dimer **13b** and monomer **13c** in ethereal solution as depicted in **Scheme 5.5**, and that di-solvated dimer **13b** is the major species.

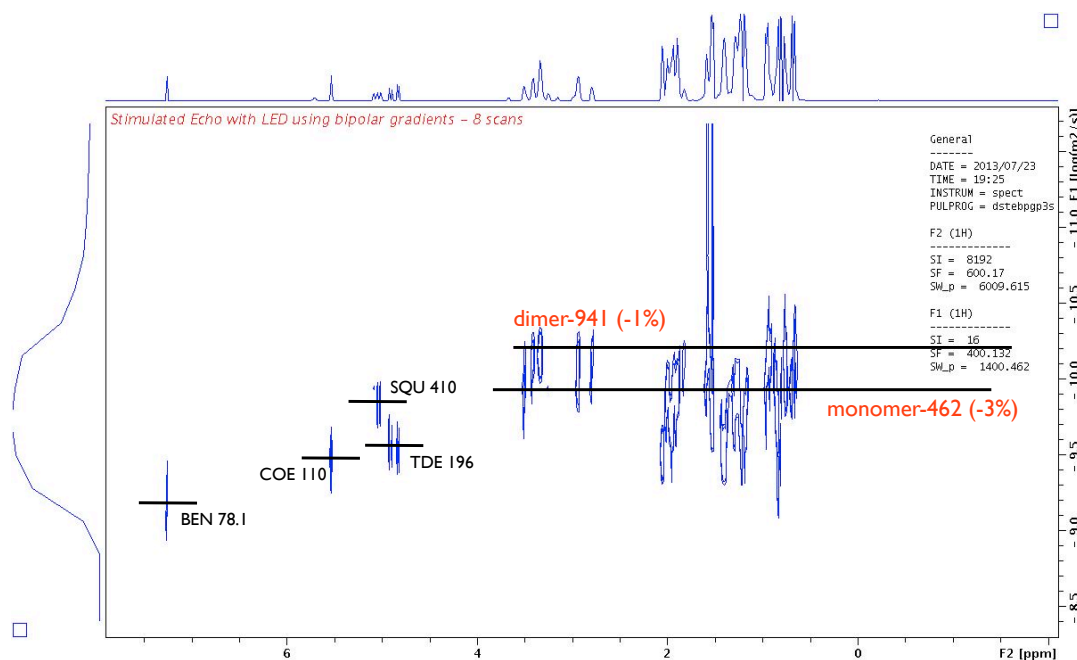
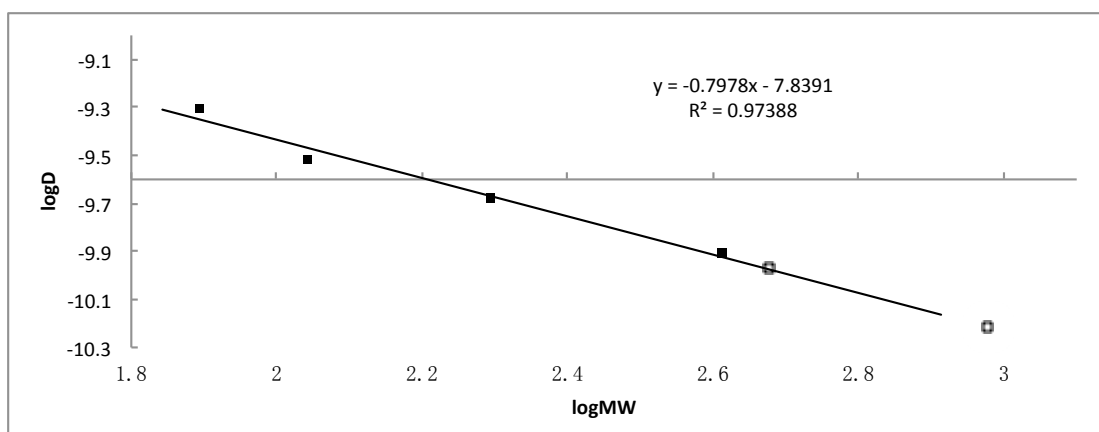


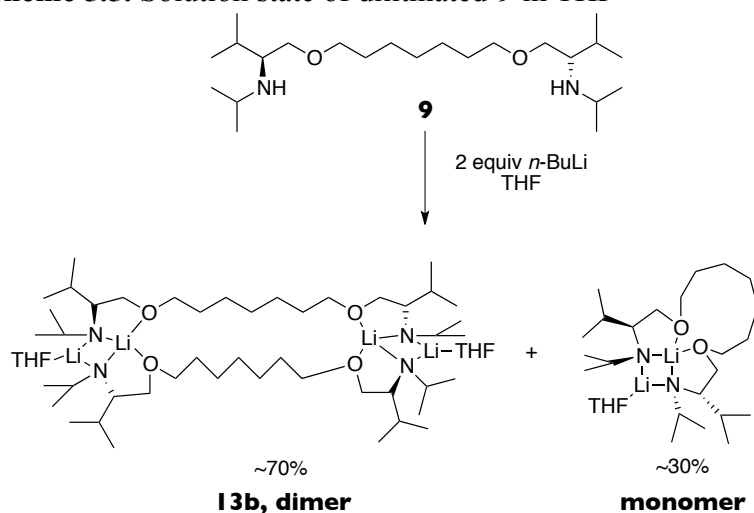
Figure 5.7. ^1H DOSY (with internal references) of dilithiated-**9** in $\text{THF-}d_8$ at -70°C ;

Table 5.1. D-FW analysis of ¹H DOSY data of dilithiated-9

Entry	Compound	FW	D	Predicted FW	% Error
		g/mol	m ² /s	g/mol	
1	BEN	78.1	4.97E-10	68	-12
2	COD	110	3.02E-10	128	16
3	TDE	196	2.10E-10	202	3
4	SQU	410	1.24E-10	392	-4
5	monomer	476	1.08E-10	462	-3
6	dimer	952	6.15E-11	941	-1

**Figure 5.8.** D-FW analysis of ¹H DOSY data. Four internal references are shown as solid squares; monomer and dimer of dilithiated-9 are shown as open squares.

Scheme 5.5. Solution state of dilithiated-9 in THF



5.4.2 Solution-state Characterization of Lithiated Diamino Ethers 10

On the basis of multiplicity edited HSQC (**Figure 5.9**), we observe only one dominant complex in the solution. ^6Li NMR and ^6Li DOSY (**Figure 5.10**) indicates that around 90% of dilithiated-10 exists as monomer **14** in ethereal solution with an experimentally determined FW of 403 g/mol (error -9%) by the ^1H DOSY D-FW analysis (**Figure 5.11** and **5.12**).

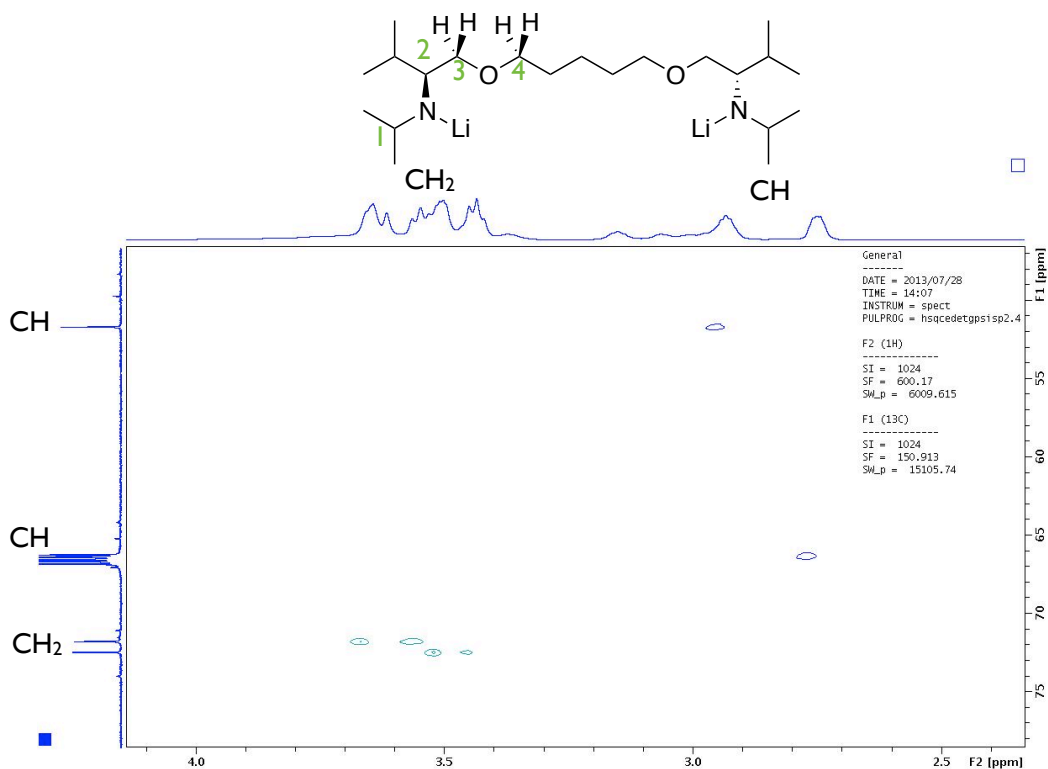


Figure 5.9. Multiplicity Edited ^1H - ^{13}C HSQC spectrum of dilithiated-**10** in $\text{THF-}d_8$ at $-50\text{ }^\circ\text{C}$. Blue spots indicate CH_3 or CH ; Green cross-peaks indicate CH_2 .

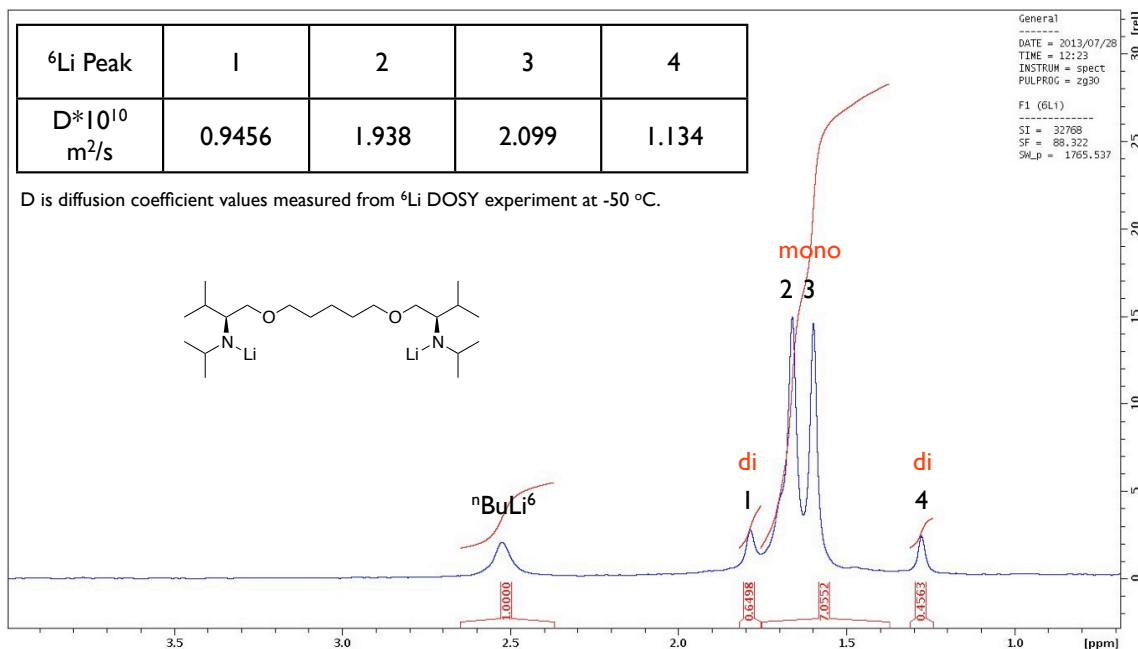


Figure 5.10. ^6Li NMR of dilithiated-**10** in $\text{THF-}d_8$ at $-50\text{ }^\circ\text{C}$ and diffusion coefficient values of each ^6Li peaks. “mono” means mono-THF solvated dilithiated-**10** monomer; “di” means di-THF solvated dilithiated-**10** dimer (Scheme 5.4).

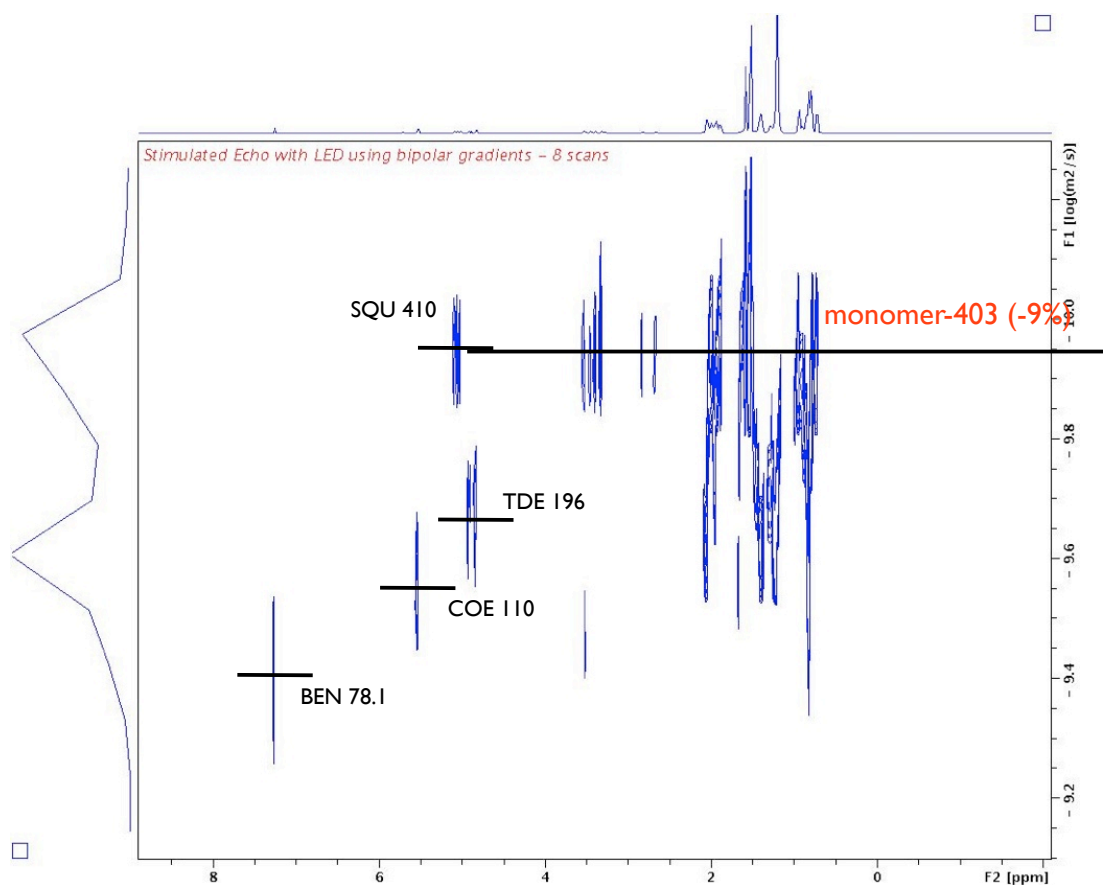


Figure 5.11. ^1H DOSY (with internal references) of dilithiated-**10** in $\text{THF-}d_8$ at $-70\text{ }^\circ\text{C}$;

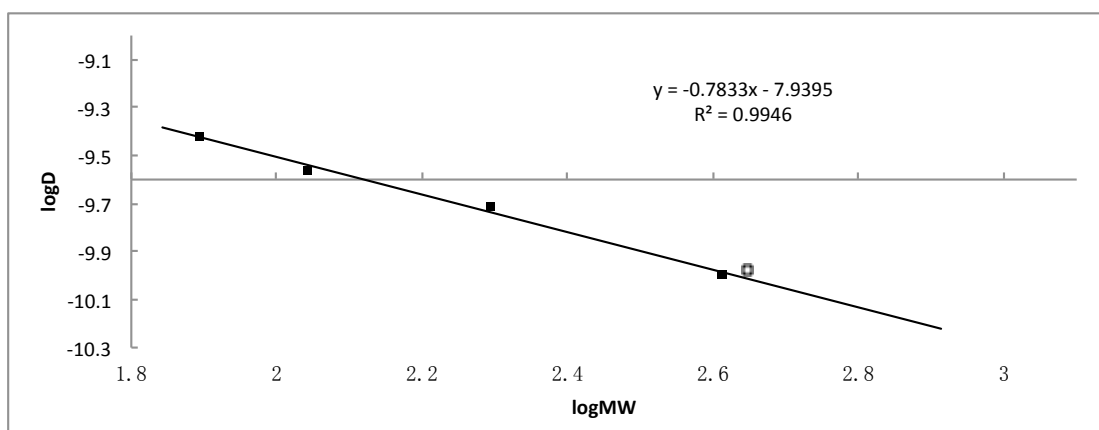


Figure 5.12. D-FW analysis of ^1H DOSY data. Four internal references are shown as solid squares; monomer of dilithiated-**10** is shown as open squares.

5.5 Conclusion

A chiral diamino diether ligand with a seven-methylene linker forms a dimeric structure after lithiation. The NMR-based study reveals an equilibrium between a

dimer and a monomer in THF solution and dimer is the major component in the solution. Thus we monitored other similar dilithiated complexes by NMR, and found monomer will become the dominant species in solution when its linker chain has five methylene carbons. Thus a monomer crystal was successfully obtained from this five-carbon linker ligand which strongly support our NMR interpretation of the monomer.

5.6 Experimental Section

Procedures for NMR Experiments. NMR samples were prepared in tubes sealed with rubber septa cap and parafilm. NMR tubes were evacuated *in vacuo*, flame-dried and filled with argon before use. ^1H chemical shifts were referenced to toluene- d_8 at 7.09 ppm or to THF- d_8 at 3.58 ppm; ^{13}C chemical shifts were referenced to toluene- d_8 at 137.86 ppm or to THF- d_8 at 67.57 ppm. All NMR experiments were acquired on a 600 MHz spectrometer. For DOSY experiments a z-axis gradient amplifier was equipped with a z-axis gradient coil with maximum gradient strength 0.5 T/m. Both ^1H and ^6Li DOSY were performed using the standard programs, employing a double stimulated echo sequence, bipolar gradient pulses for diffusion, and 3 spoil gradients. For ^1H DOSY: Diffusion time was 100 ms, and the rectangular gradient pulse duration was 1300 μs . Gradient recovery delays were 200 μs . For ^6Li DOSY: Diffusion time was 1500 ms, and the rectangular gradient pulse duration was 1300 μs . Individual rows of the quasi-2-D diffusion databases were phased and baseline corrected. Actual diffusion coefficients used for D-FW analysis were obtained using the T1/T2 analysis module in commercially available software.

The $n\text{-Bu}^6\text{Li}$ sample was prepared by laboratory synthesized $n\text{-Bu}^6\text{Li}$ heptane solution. About 100 - 200 μL of the $n\text{-Bu}^6\text{Li}$ heptane solution was added via syringe to a NMR tube. After the addition, the NMR tube was evacuated *in vacuo* for 5 - 10

minutes at 0 °C in order to remove the hydrocarbon solvent. After filling with argon, deuterium-labeled solvent was added via syringe to bring the total volume up to 500 - 600 µL.

Synthesis of *n*-Bu⁶Li. The *n*-Bu⁶Li solution was prepared in heptane according to the method that our group has published previously.¹⁰

5.7 References

¹ (a) Collum, D.; McNeil, A. J.; Ramirez, A. *Angew. Chem. Int. Ed.* **2007**, *46*, 3002-3017. (b) Lucht, B.; Collum, D. *Acc. Chem. Res.* **1999**, *32*, 1035-1042. (c) Snieckus, V. *Chem. Rev.* **1990**, *90*, 879-933. (d) Trost, B. M., Fleming, I., Eds. *Comprehensive Organic Synthesis*; Pergamon: Oxford, 1991. (e) Wu, G.; Huang, M. *Chem. Rev.* **2006**, *106*, 2596-2616.

² (a) Whitesell, J. K.; Felman, S. W. *J. Org. Chem.* **1980**, *45*, 755-756. (b) Eleveld, M. B.; Hogeveen, H. *Tetrahedron Lett.* **1984**, *45*, 5187-5190. (c) Shirai, R.; Tanaka, M.; Koga, K. *J. Am. Chem. Soc.* **1986**, *108*, 543-545. (d) Cain, C. M.; Cousins, R. P. C.; Coumbarides, G.; Simpkins, N. S. *Tetrahedron* **1990**, *46*, 523-544. (e) Bhuniya, D.; DattaGupta, A.; Singh, V. K. *J. Org. Chem.* **1996**, *61*, 6108-6113. (f) Corruble, A.; Valnot, J.-Y.; Maddaluno, J.; Duhamel, P. *Tetrahedron: Asymmetry* **1997**, *8*, 1519-1523. (g) Simpkins, N. S.; Hume, S. C. *J. Org. Chem.* **1998**, *63*, 912-913. (h) Corruble, A.; Valnot, J.-Y.; Maddaluno, J.; Duhamel, P. *J. Org. Chem.* **1998**, *63*, 8266-8275. (i) Matsuo, J.; Odashima, K.; Kobayashi, S. *Org. Lett.* **1999**, *1*, 345-348. (j) Arvidsson, P. I.; Davidsson, O.; Hilmersson, G. *Tetrahedron: Asymmetry* **1999**, *10*, 527-534. (k) De Sousa, S. E.; O'Brien, P.; Pilgram, C. D. *Tetrahedron* **2002**, *58*, 4643-4654. (l) Flinois, K.; Yuan, Y.; Bastide, C.; Harrison-Marchand, A.; Maddaluno, J. *Tetrahedron* **2002**, *58*, 4707-4716. (m) Rodeschini, V.; Simpkins, N. S.; Wilson, C. *J. Org. Chem.* **2007**, *72*, 4265-4267. (o) Stivala, C. E.; Zakarian A. *J. Am. Chem. Soc.* **2011**, *133*, 11936-11939.

³ (a) Beng, T. K.; Gawley, R. E. *J. Am. Chem. Soc.* **2010**, *132*, 12216-12217. (b) Beng, T. K.; Tyree, W. S.; Parker, T.; Su, C.; Williard, P. G.; Gawley, R. E. *J. Am. Chem. Soc.* **2012**, *134*, 16845-16855.

⁴ (a) Sato, D.; Kawasaki, H.; Shimada, I.; Arata, Y.; Okamura, K.; Date, T.; Koga, K. *J. Am. Chem. Soc.* **1992**, *114*, 761-763. (b) Arvidsson, P. I.; Hilmersson, G.; Ahlberg, P. *J. Am. Chem. Soc.* **1999**, *121*, 1883-1887. (c) Arvidsson, P. I.; Hilmersson, G.; Davidsson, O. *Chem.—Eur. J.* **1999**, *5*, 2348-2355. (d) Sott, R.; Granander, J.; Hilmersson, G. *Chem.—Eur. J.* **2002**, *8*, 2081-2087. (e) Pate, F.; Duguet, N.; Oulyadi, H.; Harrison-Marchand, A.; Fressigne, C.; Valnot, J.; Lasne, M.; Maddaluno, J. *J. Org. Chem.* **2007**, *72*, 6982-6991. (f) Liu, J.; Li, D.; Sun, C.; Williard, P. G.; *J. Org. Chem.* **2008**, *73*, 4045-4052. (g) Lecachey, B.; Duguet, N.; Oulyadi, H.; Fressigne, C.; Harrison-Marchand, A.; Yamamoto, Y.; Tomioka, K.;

Maddaluno, J. *Org. Lett.* **2009**, *11*, 1907-1910.

⁵ Williard, P. G.; Sun, C. *J. Am. Chem. Soc.* **1997**, *119*, 11693-11694.

⁶ Li, D.; Sun, C.; Liu, J.; Hopson, R.; Li, W.; Williard, P. G. *J. Org. Chem.* **2008**, *73*, 2373-2381.

⁷ Kagan, G.; Li, W.; Li, D.; Hopson, R.; Williard, P. G. *J. Am. Chem. Soc.* **2011**, *133*, 6596-6602.

⁸ Granander, J.; Sott, R.; Hilmersson, G. *Chem.—Eur. J.* **2006**, *12*, 4191-4197.

⁹ Li, D.; Keresztes, I.; Hopson, R.; Williard, P. G. *Acc. Chem. Res.* **2009**, *42*, 270-280.

¹⁰ Yu, K. H.; Kim, Y. S.; Kim, S. W.; Park, J. H.; Yang, S. D.; Herdering, W.; Knoechel, A. *J. Label. Compd. Radiopharm.* **2003**, *46*, 1151-1160.

Chapter 6 Perfluoroalkyl Grignard Reagents: NMR Study of 1-Heptafluoropropylmagnesium Halide in Solution

6.1 Abstract

The process of generating perfluoroalkyl Grignard reagent (R_fMgX) by exchange reaction between perfluoroalkyl iodide (R_fI) and Grignard reagent ($RMgX$) was studied. ^{19}F NMR was applied to monitor the generation process of C_3F_7MgCl . Other NMR techniques, including ^{19}F COSY, NOESY and PGSE, were invoked to elucidate the assignment of peaks observed in ^{19}F spectrum. Schlenk equilibrium was observed and was significantly influenced by solvent (diethyl ether or THF).

6.2 Introduction

The first synthesis of perfluoroalkyl Grignard reagent (R_fMgX) was developed by Haszeldine via using perfluoroalkyl iodide reacting with magnesium metal.¹ R_fMgX reacts with CO_2 , ketone and aldehyde similar to normal Grignard reagents. The major difference is that R_fMgX has much poorer thermal stability than the corresponding $RMgX$. Hence it would be better to produce and use R_fMgX at low temperature. However the reaction between perfluoroalkyl iodide and magnesium needs to be warmed to initiate and this causes part of the R_fMgX to decompose. To overcome this drawback, McBee and co-workers² developed a fast and convenient method to generate R_fMgX at low temperature. By mixing perfluoroalkyl iodide (R_fI) and $RMgX$ in ethereal solvent and an unusual Grignard exchange happens quickly leading

to R_fMgX and alkyl iodide (RI). This exchange reaction is fast and quantitative even at $-78\text{ }^\circ\text{C}$.³

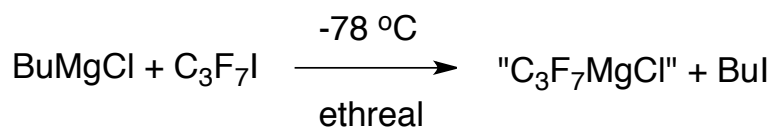
Like normal Grignard reagents, R_fMgX is applied to form carbon-carbon bonds of fluorofunctionalized intermediates leading to organofluorine compounds. However, the applications are quite limited due to poor stability and reactivity. Decomposition of R_fMgX yields a protonated product (R_fH), perfluoroalkene and traces of coupling product (R_f-R_f) as well as perfluoroalkene polymer.^{1b} Generation of perfluoroalkene involves α or β magnesium-fluoride elimination. A single electron transfer (SET) pathway was suggested which indicated the existence of a radical intermediate ($R_f\bullet$) to explain the formation of other byproducts from decomposition.

Mechanistic studies of R_fMgX are still insufficient. In the solid state, structural characterization of R_fMgX is lacking. ^{19}F NMR has been applied several decades ago⁴ but even clear chemical shift values of R_fMgX cannot be found due to poor instrumentation used in the earliest studies. However, mechanistic study is crucial for the improvement of stability and reactivity. For example, synthetic methodology development involving R_fMgX reagents shows that some additives can significantly stabilize R_fMgX or improve the performance but the reasons for improvements is unclear.⁵ Therefore, we tried to directly observe and assign various intermediates of R_fMgX and to supply NMR data in this study. Studies on additive effects and solid-state structural information are ongoing.

6.3 Results and Discussion

In order to simplify the spectra, perfluoropropyl magnesium chloride ($^f\text{PrMgCl}$) has been selected as the model of perfluoroalkyl Grignard reagents. Preparation is

described in **Figure 6.1**, with chemical shift values (^{19}F) of reactant and major byproducts listed. Chemical shift values are measured in general diethyl ether at -78 °C and calibrated by C_6F_6 at -164.9 ppm.



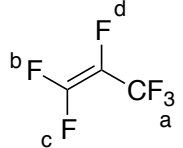
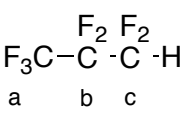
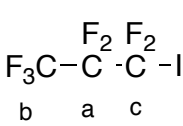
	-70.9ppm (a); -91.6ppm (b); -106.1ppm (c); -195.7ppm (d)
	-84.5ppm (a); -135.4ppm (b); -141.5ppm (c)
	-69.2ppm (a), -81.4ppm (b), -120.7ppm (c)

Figure 6.1. Preparation of $^{\text{F}}\text{PrMgCl}$, with ^{19}F chemical shift values of reactant and major byproducts.

Even though there are a lot of reported reactions that use perfluoroalkyl Grignard reagent at -20 °C or 0 °C, our VT NMR results shows that $^{\text{F}}\text{PrMgCl}$ or $^{\text{F}}\text{BuMgCl}$ will significantly decompose at -20 °C and slowly decompose at -78 °C in both THF and diethyl ether solutions. Higher concentration will speed up the decomposition. The successful applications reported at 0 °C are probably due to $^{\text{F}}\text{RMgX}$ reacting faster with reactant than self-decomposition. Therefore all NMR experiments mentioned below will use -78 °C as the temperature for both sample preparation and NMR analysis.

6.3.2 Perfluoropropyl Magnesium Chloride ($^{\text{F}}\text{PrMgCl}$) in Diethyl Ether Solution

A freshly made ether solution of $^{\text{F}}\text{PrMgCl}$ presents two sets of “ $^{\text{F}}\text{PrMg}$ ” peaks in ^{19}F NMR (**Figure 6.2** bottom), which are labeled as $^{\text{F}}\text{Pr-Mg}$ (1) and $^{\text{F}}\text{Pr-Mg}$ (2). After storage at $-78\text{ }^{\circ}\text{C}$ for 3.5 h, $^{\text{F}}\text{Pr-Mg}$ (1) can be barely detected, and $^{\text{F}}\text{Pr-Mg}$ (2) slightly increases. A new type of “ $^{\text{F}}\text{PrMg}$ ” species appear, labeled as $^{\text{F}}\text{Pr-Mg}$ (3) (**Figure 6.2** top). A full assignment is given in **Figure 6.3** & **6.4** and is supported by ^{19}F COSY spectra in **Figure 6.5**. Significant amount of perfluoro propene (C_3F_6) was observed after 3.5 h as the decomposed product of “ $^{\text{F}}\text{PrMg}$ ” complexes. There are several minor unassigned peaks in the ^{19}F spectra, which display numerous cross-peaks in the ^{19}F COSY spectra. These impurities are probably traces of perfluoro-*n*-hexane and polymer byproduct, whose formations involves a heptafluoropropyl radical intermediate.^{1b, 6}

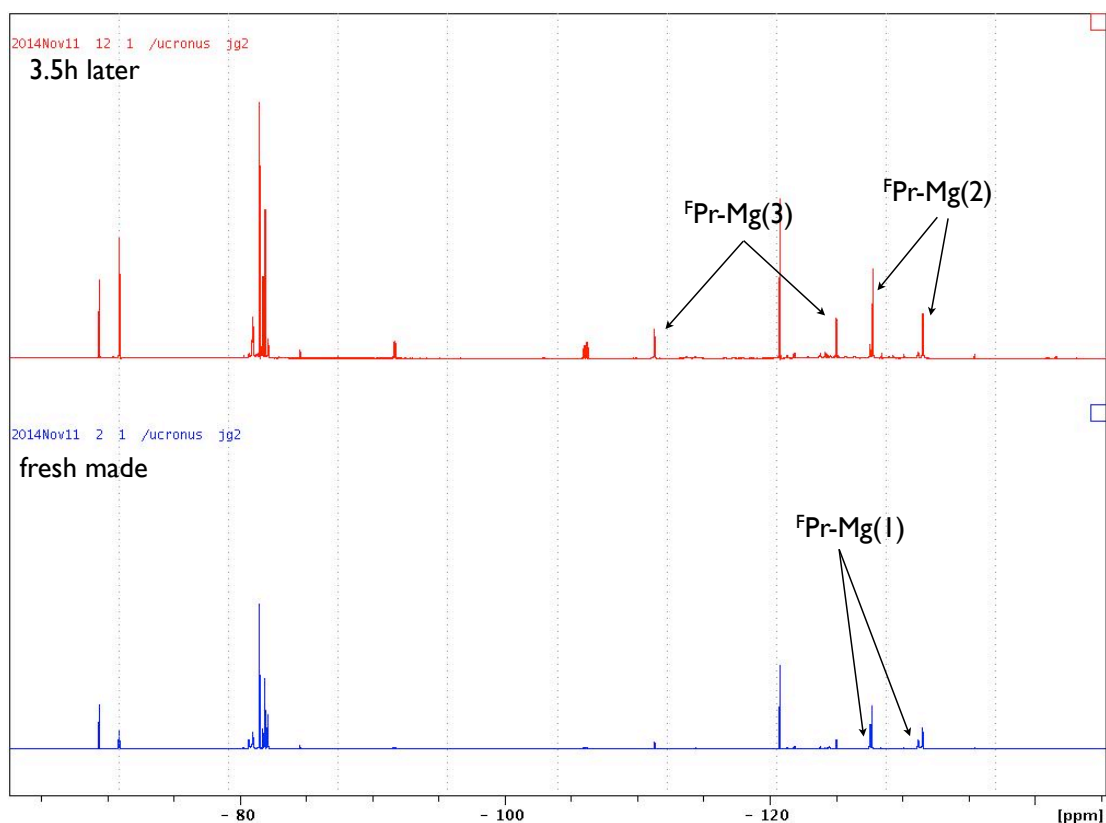


Figure 6.2. ^{19}F NMR, 0.4 M ether solution of $^{\text{F}}\text{PrMgCl}$ at $-78\text{ }^{\circ}\text{C}$.

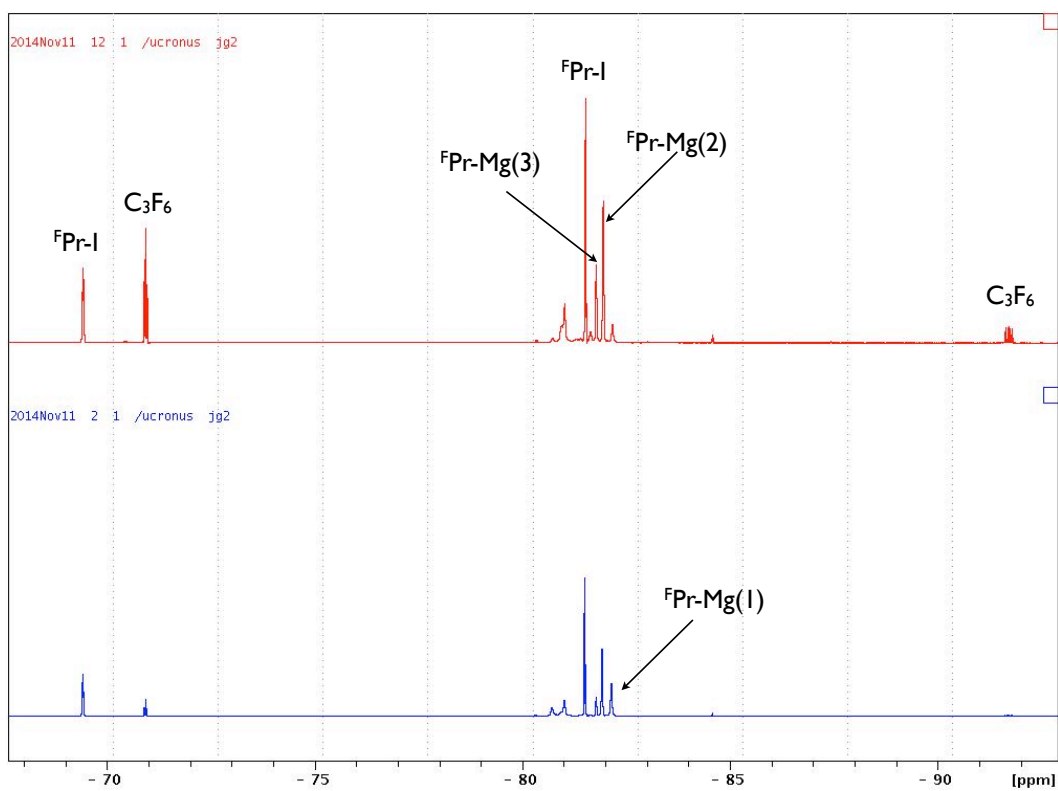


Figure 6.3. ^{19}F NMR (downfield), 0.4 M ether solution of $^{\text{F}}\text{PrMgCl}$ at $-78\text{ }^{\circ}\text{C}$.

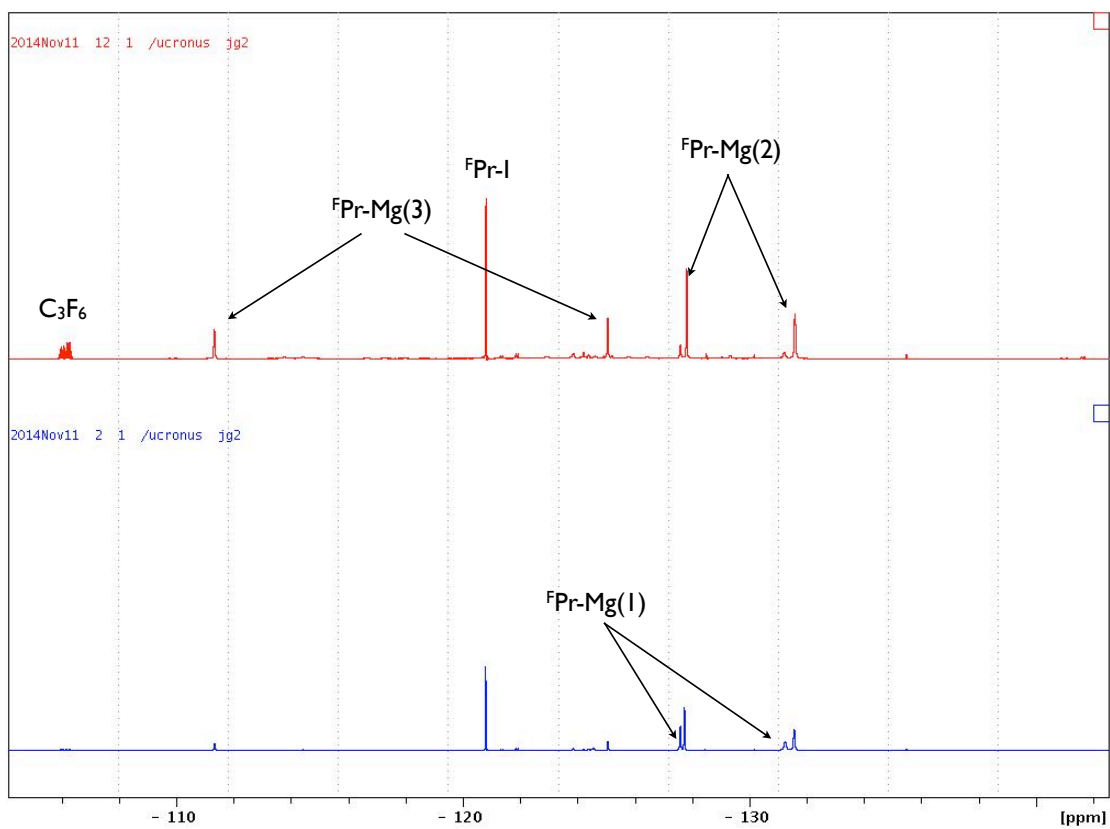


Figure 6.4. ^{19}F NMR (upfield), 0.4 M ether solution of $^{\text{F}}\text{PrMgCl}$ at $-78\text{ }^{\circ}\text{C}$.

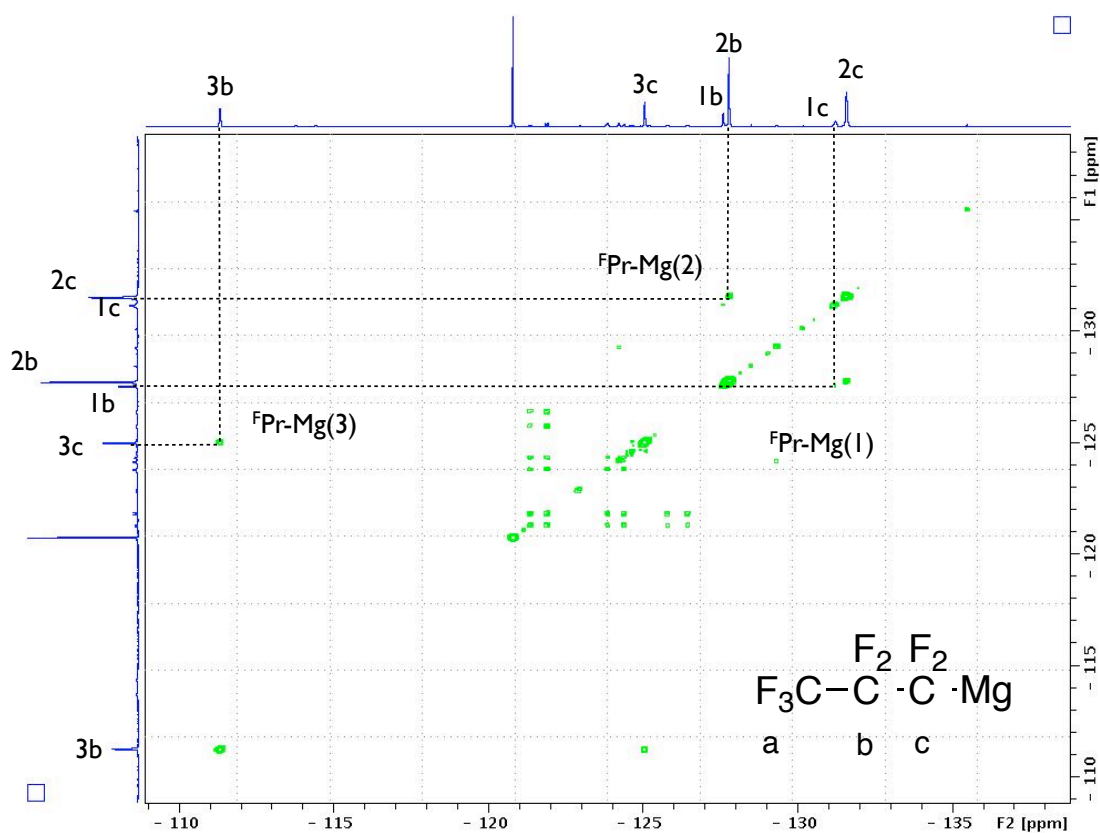


Figure 6.5. $\{^{19}\text{F}, ^{19}\text{F}\}$ COSY NMR, 0.4 M ether solution of $^{\text{F}}\text{PrMgCl}$ at $-78\text{ }^{\circ}\text{C}$.

If the sample concentration is lowered to 0.2 M, $^{\text{F}}\text{Pr-Mg}$ (1) is the dominant magnesium species in the solution at first, which suggest $^{\text{F}}\text{Pr-Mg}$ (1) is relatively more stable in diluted sample (**Figure 6.6**). However, 2 h later, $^{\text{F}}\text{Pr-Mg}$ (2) is still the dominant intermediate and $^{\text{F}}\text{Pr-Mg}$ (3) shows up.

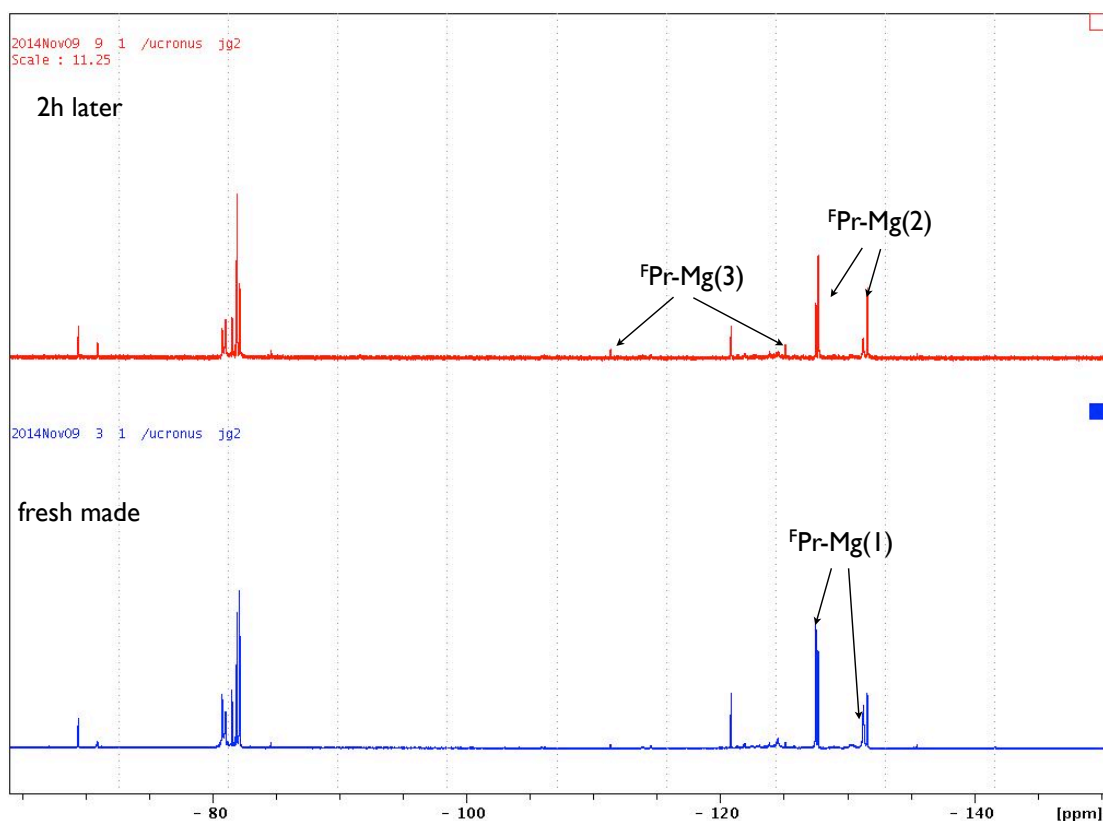


Figure 6.6. 0.2 M ether solution of $^{\text{F}}\text{PrMgCl}$ at $-78\text{ }^{\circ}\text{C}$.

6.3.2 Perfluoropropyl Magnesium Chloride ($^{\text{F}}\text{PrMgCl}$) in THF Solution

A much cleaner ^{19}F NMR spectrum was observed when THF was the solvent. As shown in **Figure 6.7**, $^{\text{F}}\text{Pr-Mg}(3)$ is the only detectable magnesium species. Heptafluoropropane shows up even in fresh-prepared sample, probably because THF is easier to be deprotonated by $^{\text{F}}\text{Pr}\cdot$ radical than diethyl ether. The ^{19}F COSY spectrum clearly illustrates the position of one CF_3 and two CF_2 peaks (**Figure 6.8**). Identical ^{19}F spectra will be obtained if using ether as solvent but a tiny amount of THF was included because commercial BuMgCl that we utilized was dissolved in THF.

It is worth noting that two CF_2 groups of $^{\text{F}}\text{Pr-Mg}(3)$ show significantly different chemical shifts comparing with correlated CF_2 groups of $^{\text{F}}\text{Pr-Mg}(1)$ and (2) .

Moreover, the formation of $^{\text{F}}\text{Pr-Mg}$ (3) is much slower in ether. We assume that $^{\text{F}}\text{Pr-Mg}$ (3) is “ $(^{\text{F}}\text{Pr})_2\text{Mg}$ ” type species and $^{\text{F}}\text{Pr-Mg}$ (1) and (2) are “ $^{\text{F}}\text{PrMgCl}$ ” type species, due to relatively slowly $^{\text{F}}\text{R}$ group shifting.

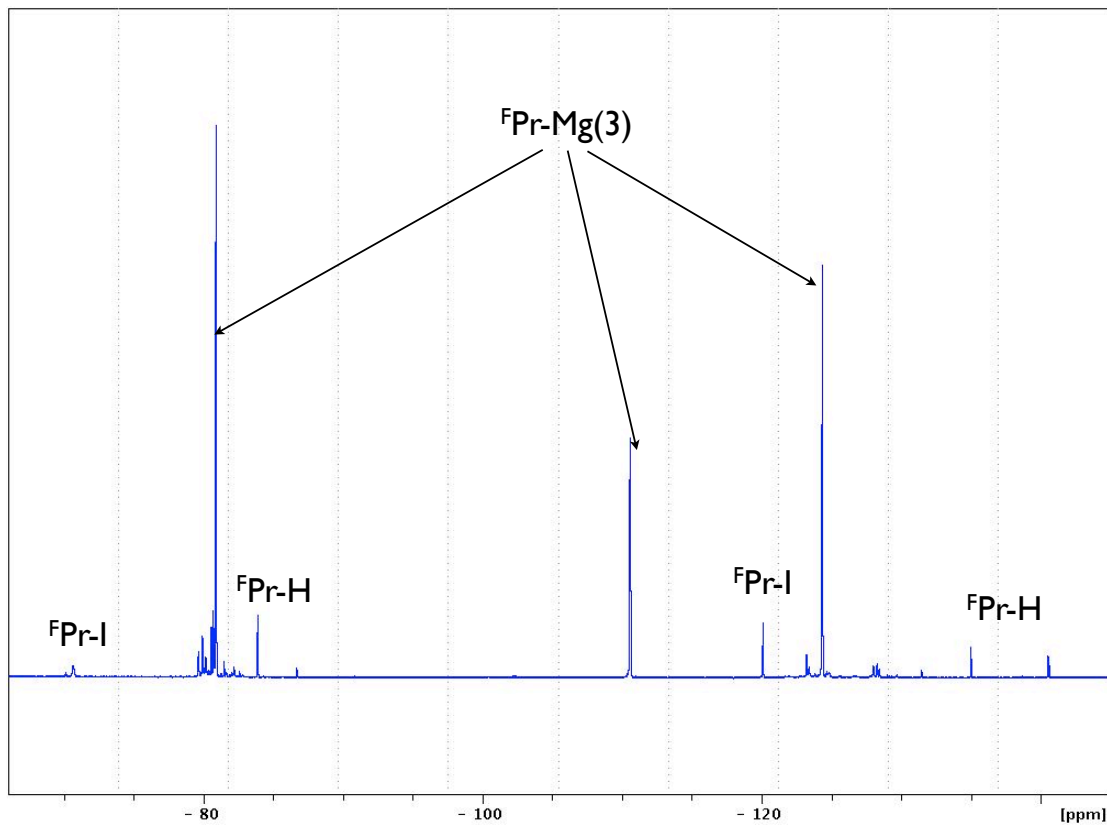


Figure 6.7. 0.4 M THF solution of $^{\text{F}}\text{PrMgCl}$ at $-78\text{ }^{\circ}\text{C}$.

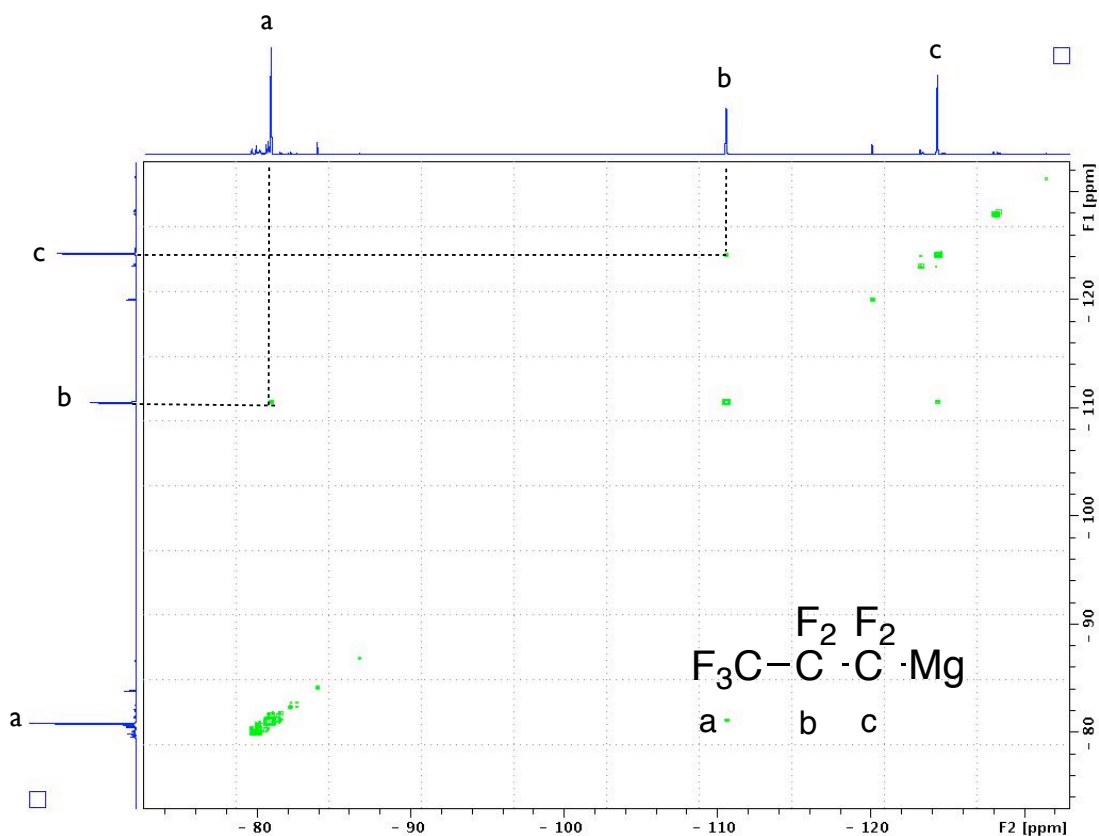


Figure 6.8. $\{^{19}\text{F}, ^{19}\text{F}\}$ COSY NMR, 0.4 M THF solution of $^{\text{F}}\text{PrMgCl}$ at $-78\text{ }^{\circ}\text{C}$.

6.3.3 Schlenk Equilibrium

^{19}F pulsed-gradient spin-echo (PGSE) experiment was applied to measure self-diffusion coefficients of various magnesium species in ether solution in order to ascertain aggregated information. As shown in **Figure 6.9**, $^{\text{F}}\text{Pr-Mg}$ (2) has similar size as $^{\text{F}}\text{Pr-Mg}$ (3) and is larger than $^{\text{F}}\text{Pr-Mg}$ (1). Moreover, exchange cross-peaks are observed between $^{\text{F}}\text{Pr-Mg}$ (1) and (2), and also between $^{\text{F}}\text{Pr-Mg}$ (2) and (3) in $\{^{19}\text{F}, ^{19}\text{F}\}$ NOESY experiment (**Figure 6.10**).

In **Scheme 6.1**, On the basis of all the information mentioned above, we depicted Schlenk equilibrium of “ $^{\text{F}}\text{PrMgCl}$ ” in ethereal solution. $^{\text{F}}\text{Pr-Mg}$ (1) is $^{\text{F}}\text{PrMgCl}$ monomer, generated immediately with the mixing of two reactants. Monomer is not a

stable aggregate and will self-aggregate to dimer, which is ${}^{\text{F}}\text{Pr-Mg (2)}$. THF enhances the ${}^{\text{F}}\text{PrMgCl}$ dimer transfer to ${}^{\text{F}}\text{Pr-Mg-}{}^{\text{F}}\text{Pr}$ compound and this suggests that ${}^{\text{F}}\text{Pr-Mg (3)}$ is more stable solvated by THF than by ether.

${}^{19}\text{F}$ _PGSE data:

Comp.	C_3F_6	$\text{C}_3\text{F}_7\text{H}$	$\text{C}_3\text{F}_7\text{I}$	${}^{\text{F}}\text{Pr-Mg(1)}$	${}^{\text{F}}\text{Pr-Mg(2)}$	${}^{\text{F}}\text{Pr-Mg(3)}$
$D \cdot 10^{-10}$ m^2/s	7.3	5.6	4.7	2.7	2.2	2.2

Complex Size: ${}^{\text{F}}\text{Pr-Mg(1)} < {}^{\text{F}}\text{Pr-Mg(2)} \approx {}^{\text{F}}\text{Pr-Mg(3)}$

Figure 6.9. ${}^{19}\text{F}$ PGSE data and results of 0.4 M ether solution of ${}^{\text{F}}\text{PrMgCl}$ at $-78\text{ }^\circ\text{C}$.

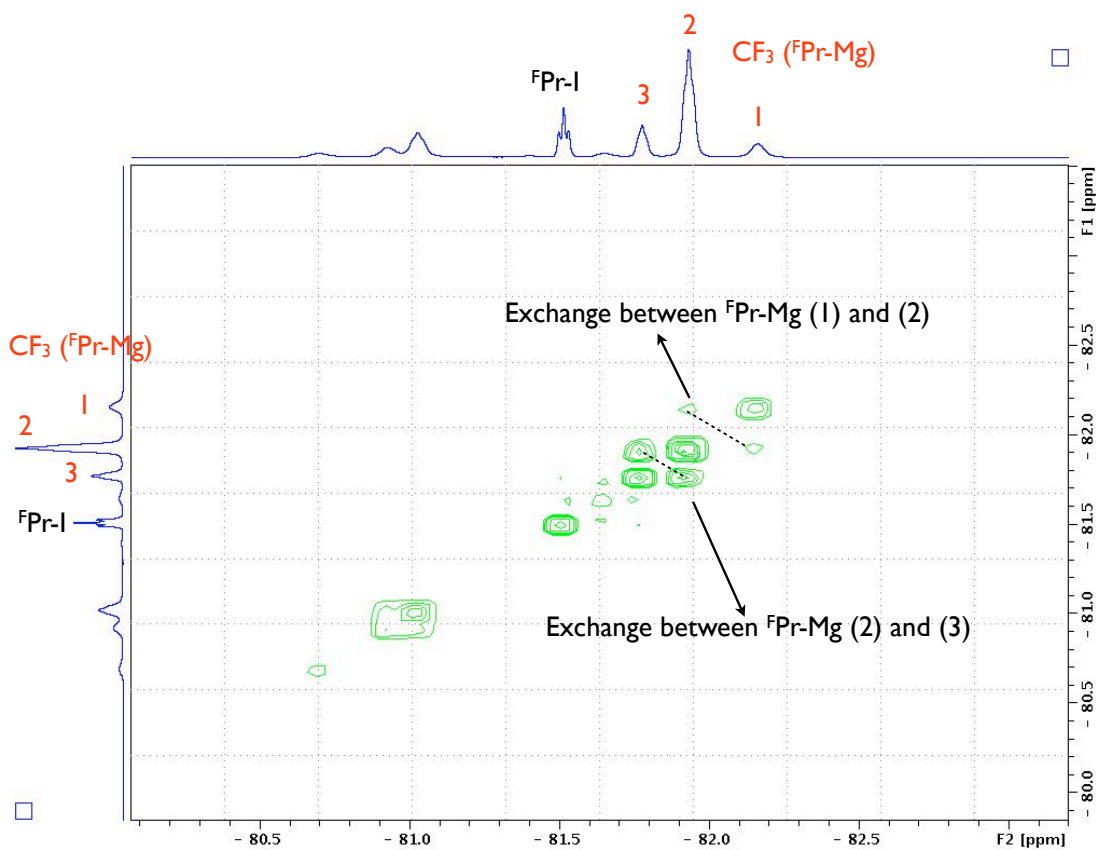
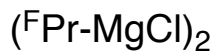


Figure 6.10. $\{^{19}\text{F}, ^{19}\text{F}\}$ NOESY of 0.4 M ether solution of $^{\text{F}}\text{PrMgCl}$ at $-78\text{ }^{\circ}\text{C}$.

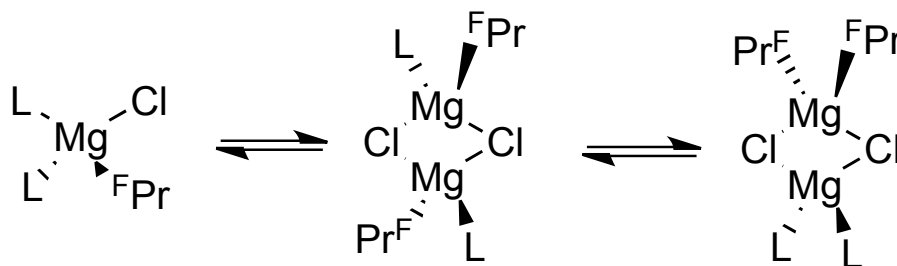
Scheme 6.1. Schlenk equilibrium observed in ethereal solutions.

“ $^{\text{F}}\text{Pr-MgCl}$ ” in diethyl ether:



Dominant species in THF

Possible solvation states:



6.4 Conclusion

Schlenk equilibrium has been observed in ether solution of C_3F_7MgCl and this equilibrium is favored on the “ ${}^F RMgX$ ” side. C_3F_7MgCl will slowly decompose even at $-78\text{ }^\circ\text{C}$ and generate byproduct perfluoropropene (C_3F_6). Increasing temperature or concentration speeds up decomposition. In THF, Schlenk equilibrium is strongly favored on the “ ${}^F RMg{}^F R$ ” side, with by product ${}^F RH$.

6.5 Experimental Section

Procedures for NMR Experiments. NMR samples were prepared in tubes sealed with rubber septa cap and parafilm. NMR tubes were evacuated *in vacuo*, flame-dried and filled with argon before use. ${}^{19}\text{F}$ chemical shifts were referenced to C_6F_6 at -164.9 ppm. All NMR experiments were acquired on a Bruker Avance III HD 600 MHz spectrometer equipped with a z-axis gradient BBFO smartprobe. The maximum spectral width (sw) is no more than 60 ppm for all 2D ${}^{19}\text{F}$ NMR experiments due to the requirement of uniform excitation over the entire bandwidth of observed resonances. For ${}^{19}\text{F}$ PGSE experiments, a GRASP II 10A z-axis gradient amplifier was employed, with maximum gradient strength of 0.5 T/m. A standard Bruker pulse program `dstebpgp3s` was selected, employing a double stimulated echo sequence, bipolar gradient pulses for diffusion, and 3 spoil gradients. Diffusion time was 100 ms, and the rectangular gradient pulse duration was 1000 μs . Individual rows of the quasi-2-D diffusion databases were phased and baseline corrected. Actual diffusion coefficients used for D-FW analysis were obtained using the T1/T2 analysis module in commercially available software.

General Procedures for preparing $^{\text{F}}$ RMgX NMR sample. To a 0.4M RMgX (1.0 mmol) solution in 2.5 ml ethereal solvent at $-78\text{ }^{\circ}\text{C}$ under Ar atmosphere was slowly added 1.0 mmol of $^{\text{F}}$ R-I. The reaction mixture was allowed to stir at $-78\text{ }^{\circ}\text{C}$ for 10 minutes.

6.6 References

-
- ¹ (a) R. N. Haszeldine, *Nature*, **1951**, *167*, 139-140. (b) R. N. Haszeldine, *J. Chem. Soc.*, **1952**, 3423-3428. (c) A. L. Henne, W. C. Francis, *J. Am. Chem. Soc.* **1951**, *73*, 3518-3518. (d) O. R. Pierce, M. Levine, *J. Am. Chem. Soc.* **1953**, *75*, 1254-1254. (e) A. L. Henne, W. C. Francis, *J. Am. Chem. Soc.* **1953**, *75*, 992-994.
- ² (a) O. R. Peirce, A. F. Meiners, E. T. McBee, *J. Am. Chem. Soc.*, **1953**, *75*, 2516-2516. (b) E. T. McBee, C. W. Roberts, A. F. Meiners, *J. Am. Chem. Soc.*, **1957**, *79*, 335-337. (c) A. F. Meiners, Ph. D. Thesis, Purdue University, Indiana, 1956.
- ³ (a) R. Sullivan, J. R. Lacher, J. D. Park, *J. Org. Chem.*, **1964**, *29*, 3664-3668. (b) D. D. Denson, C. F. Smith, C. Tamborski, *J. Fluorine Chem.*, **1973/74**, *3*, 247-258.
- ⁴ Evans, D. F.; Khan, M. S. *J. Chem. Soc.*, **2007**, 1643-1648.
- ⁵ (a) Mikami, K.; Murase, T.; Itoh, Y. *J. Am. Chem. Soc.*, **2007**, *129*, 11686-11687. (b) Xue, C.; He, G.; Fu, C.; Xue, L.; Lin, Z.; Ma, S. *Eur. J. Org. Chem.*, **2010**, 7012-7019. (c) Itoh, Y.; Murase, T.; Mikami, K. *J. Am. Chem. Soc.*, **2004**, *126*, 13174-13175.
- ⁶ (a) Ashby, E. C. *Acc. Chem. Res.* **1988**, *21*, 414-421. (b) Barr, D. A.; Francis, W. C.; Haszeldine, R. N. *Nature*, **1956**, *177*, 785-786.

Appendix A. CCDC numbers for all crystal structures

Crystal structures: CCDC 1050617-1050620

Appendix B. Supporting Information for Chapter 2

Table of Contents

Figure S2.1. ^1H NMR of 2,2,2- ^2H -4'-tert-butylacetophenone in CDCl_3 .

Figure S2.2. ^{13}C NMR of 2,2,2- ^2H -4'-tert-butylacetophenone in CDCl_3 .

Figure S2.3. ^1H NMR of (Z)-Heptadec-2-ene-1,1,1- ^2H in CDCl_3 .

Figure S2.4. ^{13}C NMR of (Z)-Heptadec-2-ene-1,1,1- ^2H in CDCl_3 .

Figure S2.5. ^1H NMR of 2-methyl-2-(methoxy- ^2H)-tricosane in CDCl_3 .

Figure S2.6. ^{13}C NMR of 2-methyl-2-(methoxy- ^2H)-tricosane in CDCl_3 .

Figure S2.7. ^1H NMR of cis-(methyl- ^2H)-oleate in CDCl_3 .

Figure S2.8. ^{13}C NMR of cis-(methyl- ^2H)-oleate in CDCl_3 .

Figure S2.9. ^2H DOSY NMR of LDA-*d* in general toluene with 1 eq of THF- d_8 .

Table S2.1. D-FW Analysis of ^2H DOSY Data of LDA-*d* in general toluene with 1 eq of THF- d_8

Figure S2.10. D-FW Analysis of ^2H DOSY Data of LDA-*d* in general toluene with 1 eq of THF- d_8

Figure S2.11. ^2H DOSY NMR of LDA-*d* in general toluene with 1 eq of THF- d_8 and 1 eq of general THF.

Table S2.2. D-FW Analysis of ^2H DOSY Data of LDA-*d* in general toluene with 1 eq of THF- d_8 and 1 eq of general THF

Figure S2.12. D-FW Analysis of ^2H DOSY Data of LDA-*d* in general toluene with 1 eq of THF- d_8 and 1 eq of general THF

Figure S2.13. ^2H DOSY NMR of LDA-*d* in general toluene with 1 eq of THF- d_8 and 9 eq of general THF.

Table S2.3. D-FW analysis of ^2H DOSY NMR data of LDA-*d* in general toluene with 1 eq of THF-*d*₈ and 9 eq of general THF

Figure S2.14. D-FW analysis of ^2H DOSY NMR data of LDA-*d* in general toluene with 1 eq of THF-*d*₈ and 9 eq of general THF

Figure S2.15. ^2H DOSY NMR of LDA-*d* in general toluene with 20 eq of general THF.

Table S2.4. D-FW analysis of ^2H DOSY NMR data of LDA-*d* in general toluene with 20 eq of general THF

Figure S2.16. D-FW analysis of ^2H DOSY NMR data of LDA-*d* in general toluene with 20 eq of general THF

Figure S2.17. ^2H DOSY NMR of 0.4 M acetanilide in general acetone with 10 μl D₂O (2.5 eq).

Table S2.5. D-FW analysis of ^2H DOSY NMR data of 0.4 M acetanilide in general acetone with 10 μl D₂O (2.5 eq).

Figure S2.18. D-FW analysis of ^2H DOSY NMR data of 0.4 M acetanilide in general acetone with 10 μl D₂O (2.5 eq).

Figure S2.19. ^1H DOSY NMR of 0.4 M acetanilide in acetone-*d*₆ with 10 μl D₂O (2.5 eq).

Table S2.5. D-FW analysis of ^1H DOSY NMR data of 0.4 M acetanilide in acetone-*d*₆ with 10 μl D₂O (2.5 eq).

Figure S2.20. D-FW analysis of ^1H DOSY NMR data of 0.4 M acetanilide in acetone-*d*₆ with 10 μl D₂O (2.5 eq).

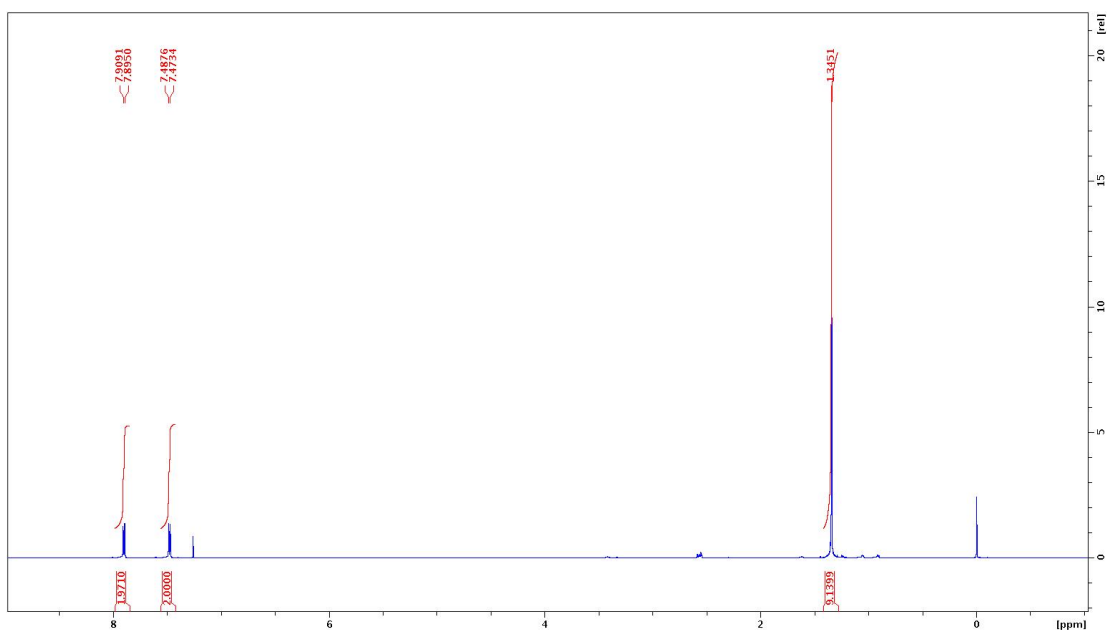


Figure S2.1. ^1H NMR of 2,2,2- ^2H -4'-tert-butylacetophenone in CDCl_3 .

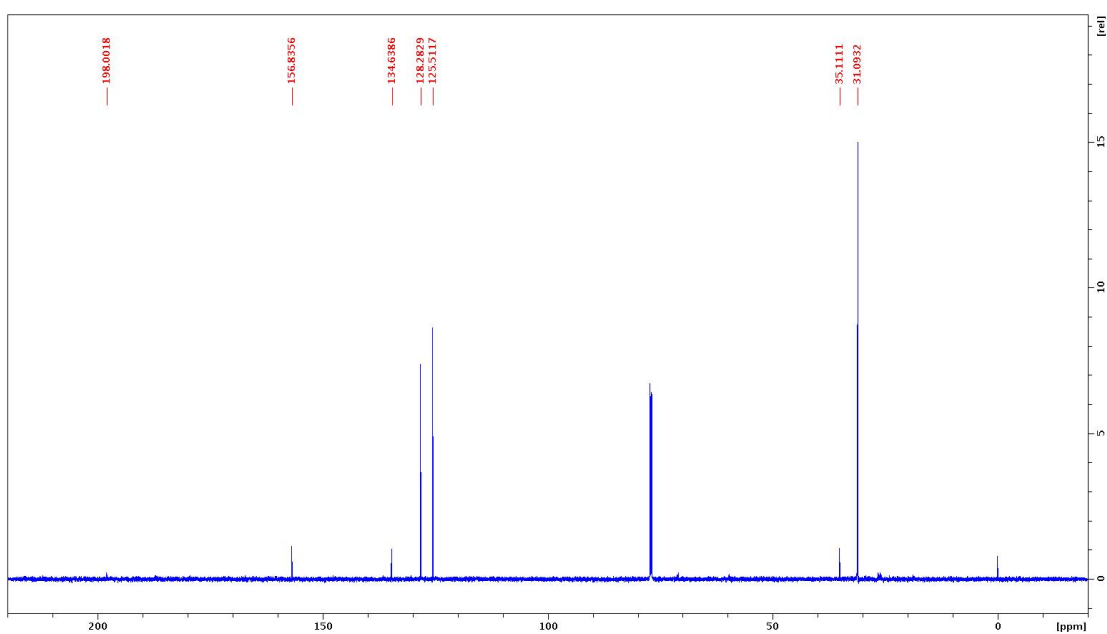


Figure S2.2. ^{13}C NMR of 2,2,2- ^2H -4'-tert-butylacetophenone in CDCl_3 .

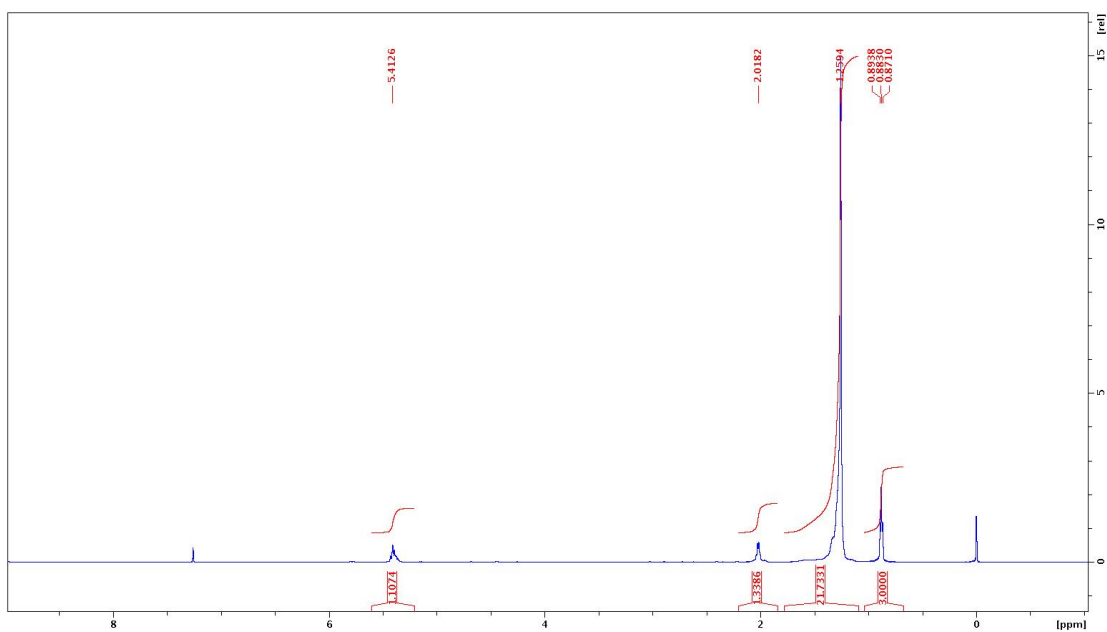


Figure S2.3. ^1H NMR of (Z)-Heptadec-2-ene-1,1,1- ^2H in CDCl_3 .

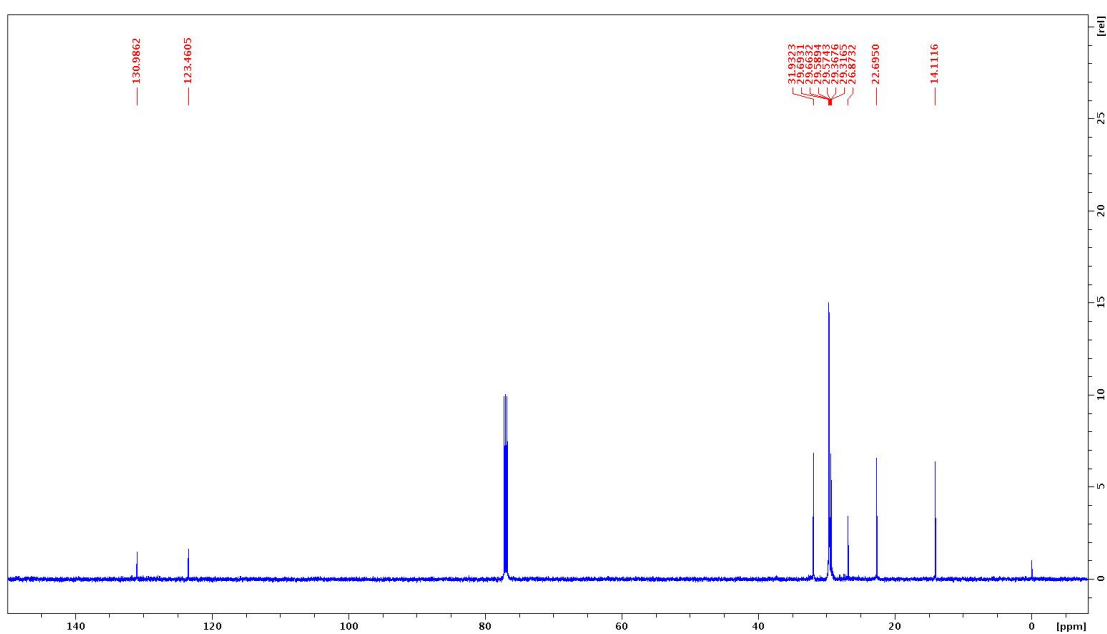


Figure S2.4. ^{13}C NMR of (Z)-Heptadec-2-ene-1,1,1- ^2H in CDCl_3 .

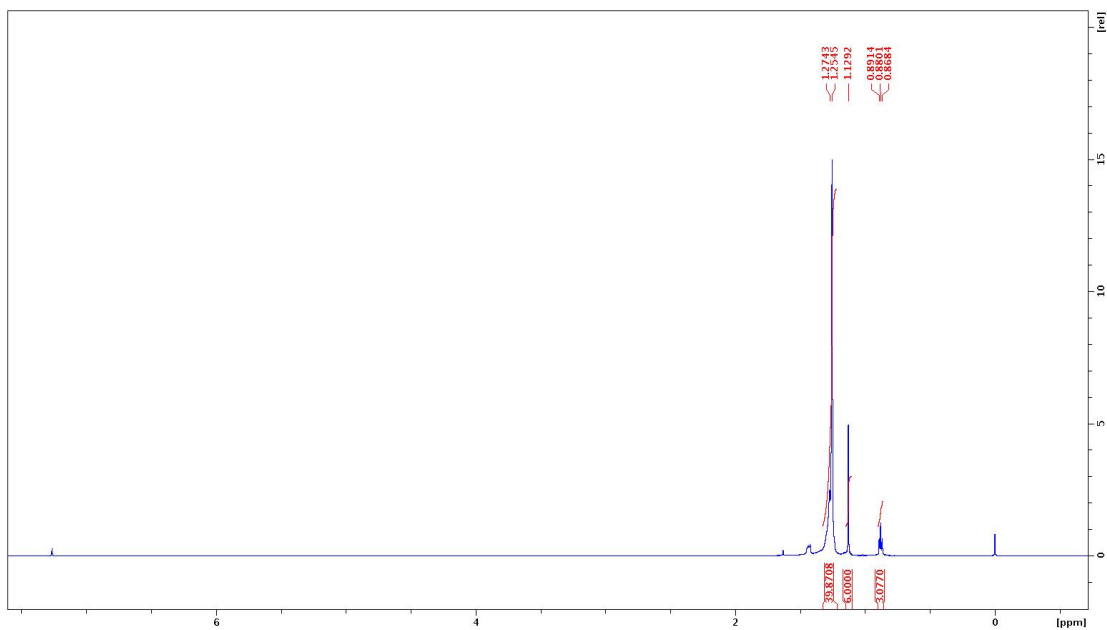


Figure S2.5. ^1H NMR of 2-methyl-2-(methoxy- ^2H)-tricosane in CDCl_3 .

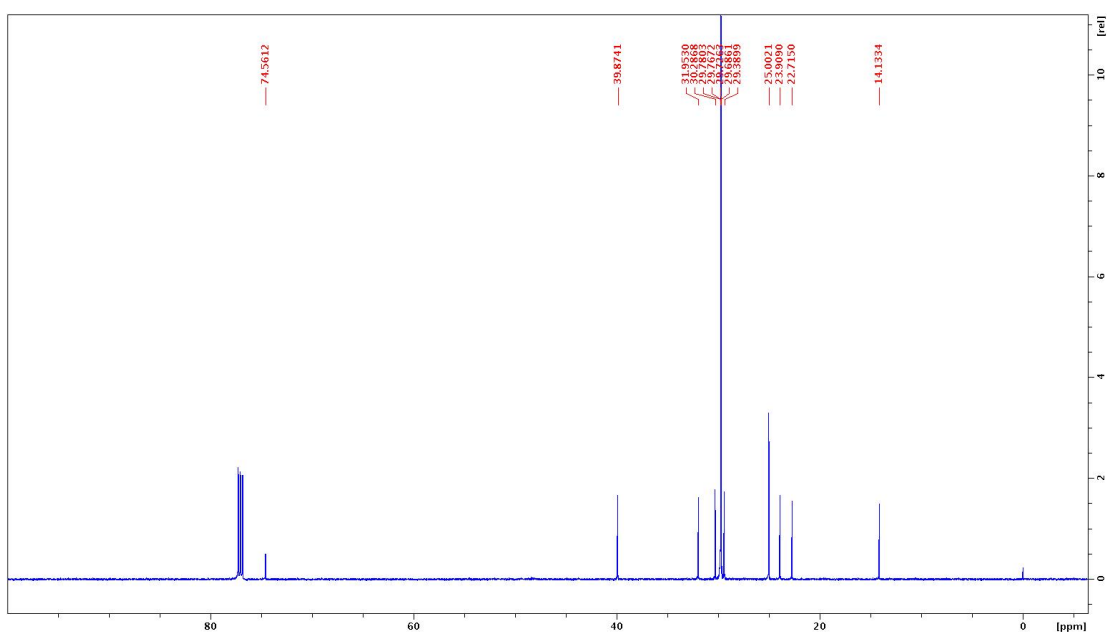


Figure S2.6. ^{13}C NMR of 2-methyl-2-(methoxy- ^2H)-tricosane in CDCl_3 .

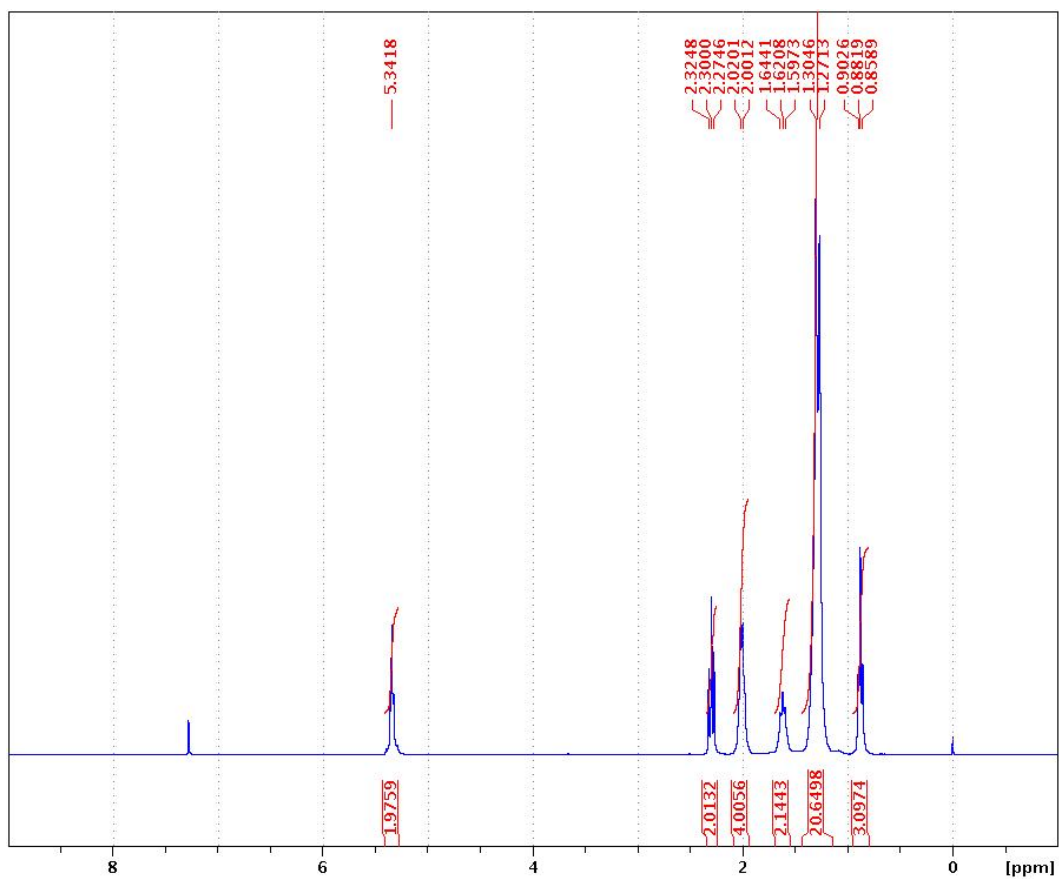


Figure S2.7. ^1H NMR of cis-(methyl- ^2H)-oleate in CDCl_3 .

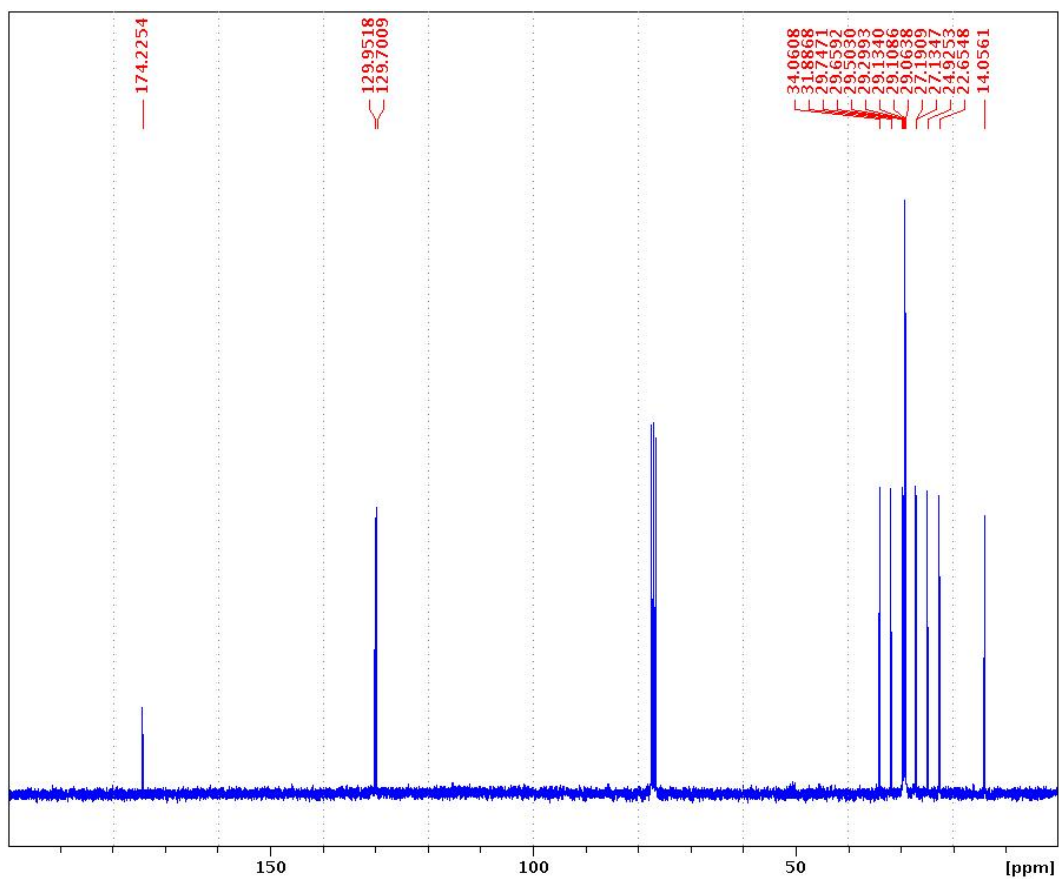


Figure S2.8. ^{13}C NMR of cis-(methyl- ^2H)-oleate in CDCl_3 .

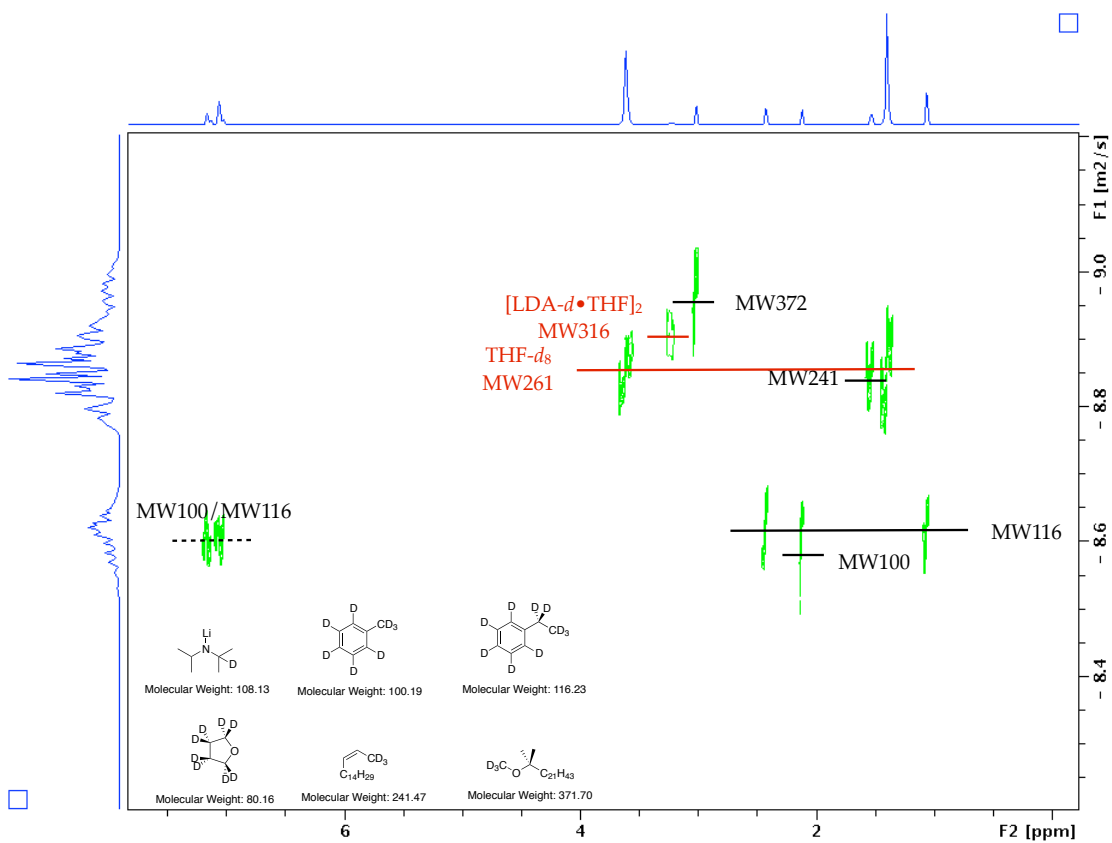


Figure S2.9. 2H DOSY NMR of LDA- d in general toluene with 1 eq of THF- d_8 .

Table S2.1. D-FW Analysis of ^2H DOSY Data of LDA-*d* in general toluene with 1 eq of THF- d_8

Entry	Compound	FW	D	Predicted FW	%
		g/mol	m^2/s	g/mol	Error
1	toluene- d_8	100	$2.55\text{E-}9$	101	1
2	ethylbenzene- d_{10}	116	$2.35\text{E-}9$	114	-2
3	(Z)-2-heptadecene- d_3	241	$1.43\text{E-}9$	242	0
4	ether- d_3	372	$1.08\text{E-}9$	370	0
5	THF- d_8	80.1 (free) 360	$1.36\text{E-}9$	261	
6	LDA- <i>d</i> (di-solvated dimer)	(di-solvated dimer)	$1.20\text{E-}9$	316	

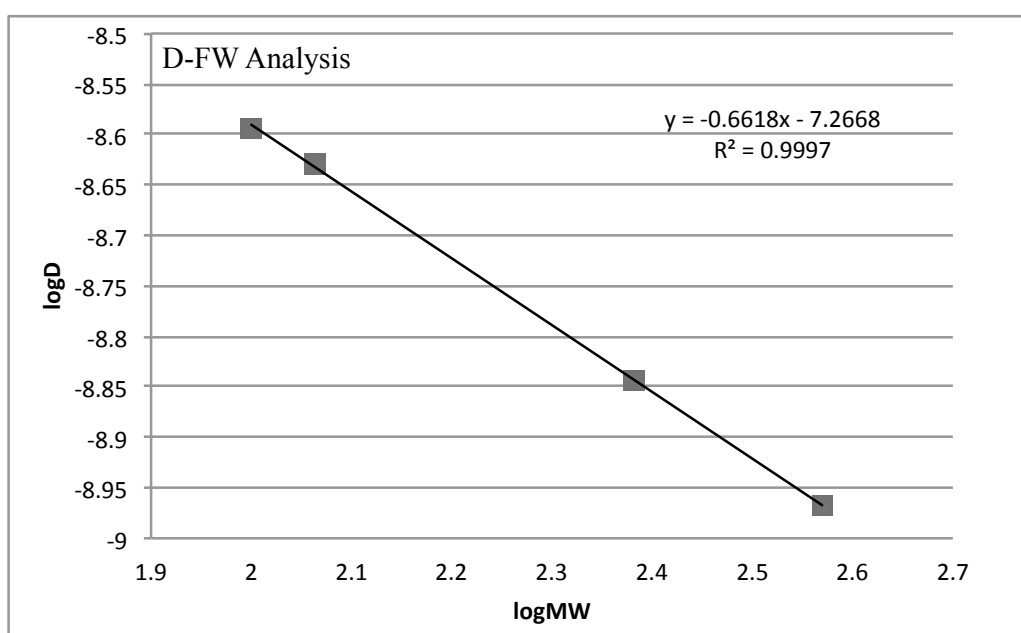


Figure S2.10. D-FW Analysis of ^2H DOSY Data of LDA-*d* in general toluene with 1 eq of THF- d_8

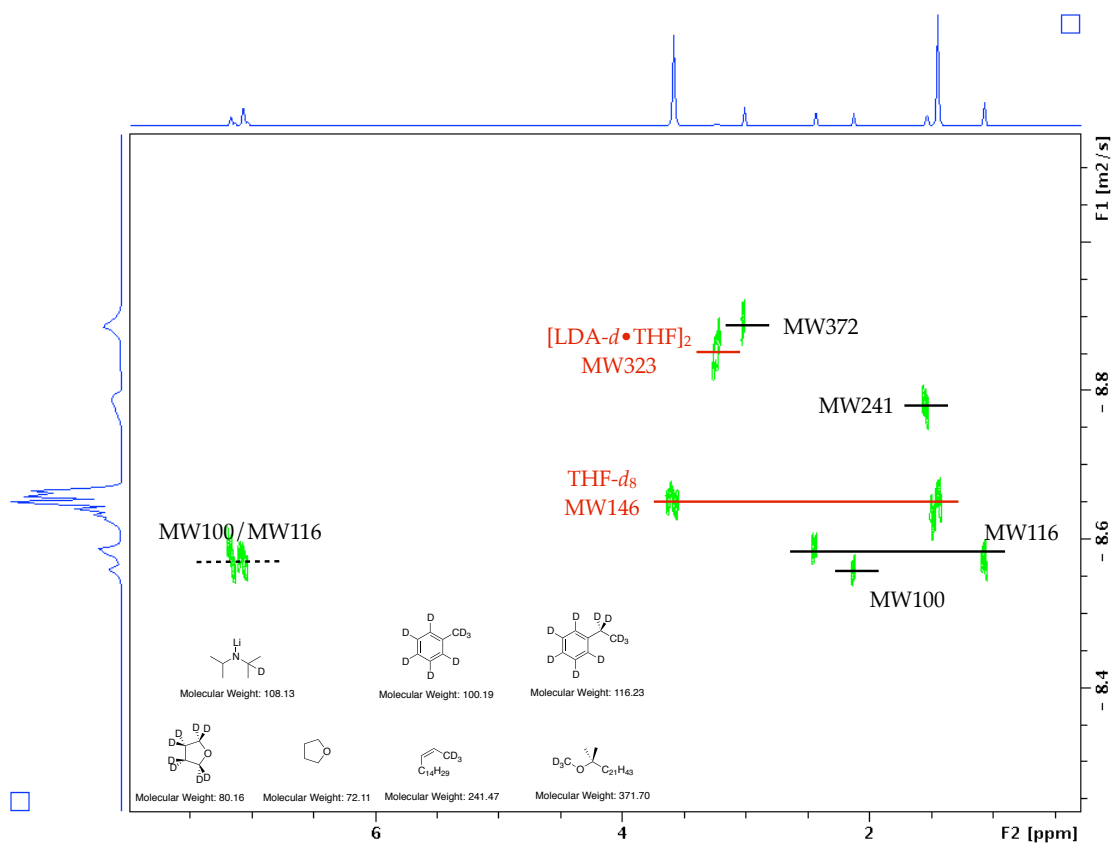


Figure S2.11. ^2H DOSY NMR of LDA- d in general toluene with 1 eq of THF- d_8 and 1 eq of general THF.

Table S2.2. D-FW Analysis of ^2H DOSY Data of LDA-*d* in general toluene with 1 eq of THF-*d*₈ and 1 eq of general THF

Entry	Compound	FW	D	Predicted FW	% Error
		g/mol	m ² /s	g/mol	
1	toluene- <i>d</i> ₈	100	2.82E-9	100	0
2	ethylbenzene- <i>d</i> ₁₀	116	2.60E-9	115	-1
3	(Z)-2-heptadecene- <i>d</i> ₃	241	1.66E-9	243	1
4	ether- <i>d</i> ₃	372	1.29E-9	369	-1
5	THF- <i>d</i> ₈	80.1 (free) 360	2.25E-9	146	
6	LDA- <i>d</i>	(di-solvated dimer)	1.40E-9	323	

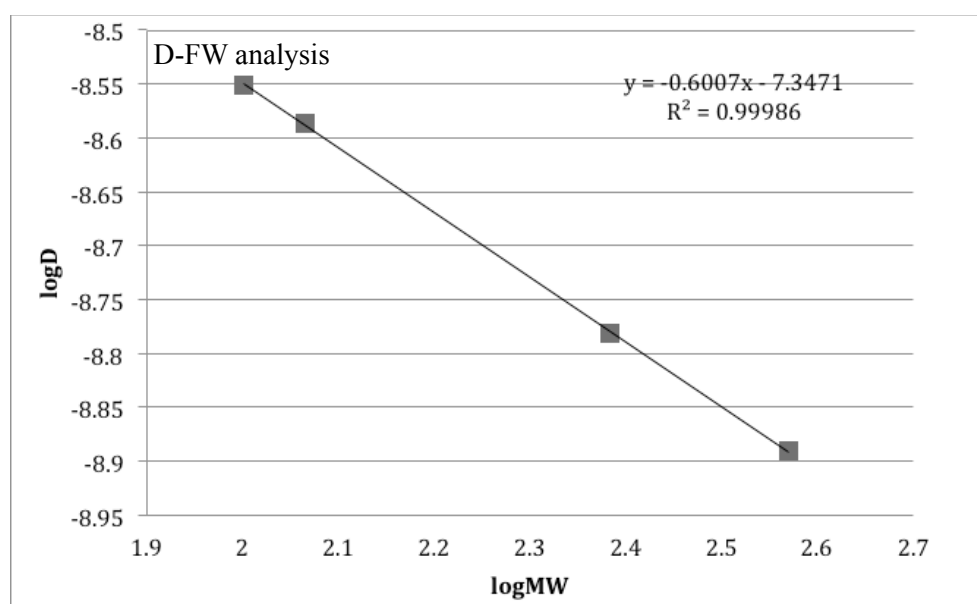


Figure S2.12. D-FW Analysis of ^2H DOSY Data of LDA-*d* in general toluene with 1 eq of THF-*d*₈ and 1 eq of general THF

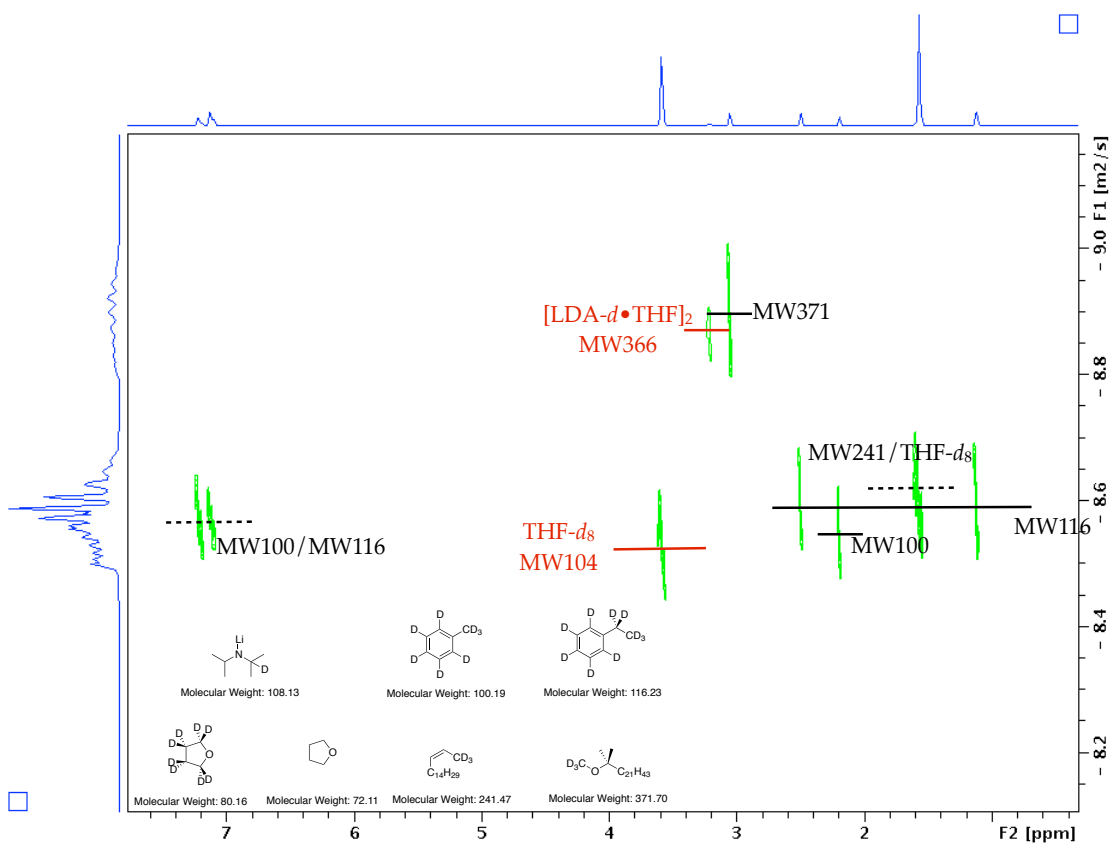


Figure S2.13. ^2H DOSY NMR of LDA-*d* in general toluene with 1 eq of THF-*d*₈ and 9 eq of general THF.

Table S2.3. D-FW analysis of ^2H DOSY NMR data of LDA-*d* in general toluene with 1 eq of THF- d_8 and 9 eq of general THF

Entry	Compound	FW	D	Predicted	
		g/mol	m^2/s	FW g/mol	% Error
1	toluene- d_8	100	2.96E-9	99	-1
2	ethylbenzene- d_{10}	116	2.67E-9	117	1
3	(Z)-2-heptadecene- d_3	241	overlap with THF- d_8	--	--
4	ether- d_3	372	1.30E-9	371	0
5	THF- d_8	80.1 (free) 360	2.85E-9	104	
6	LDA- <i>d</i>	(di-solvated dimer)	1.31E-9	366	2

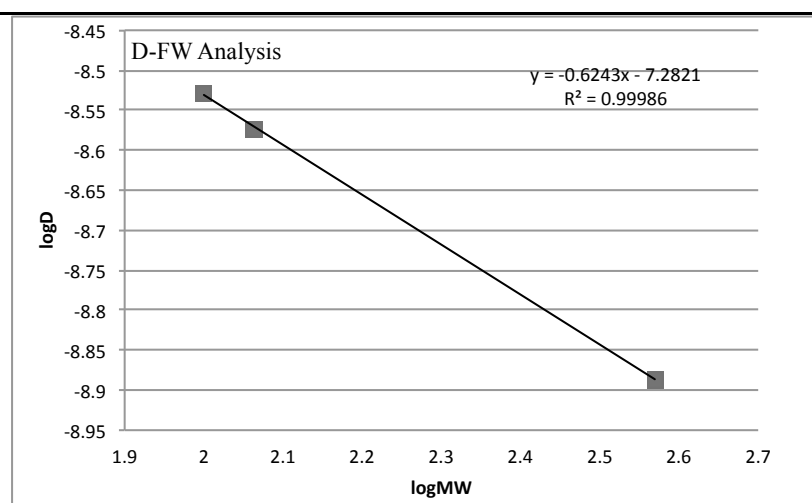


Figure S2.14. D-FW analysis of ^2H DOSY NMR data of LDA-*d* in general toluene with 1 eq of THF- d_8 and 9 eq of general THF

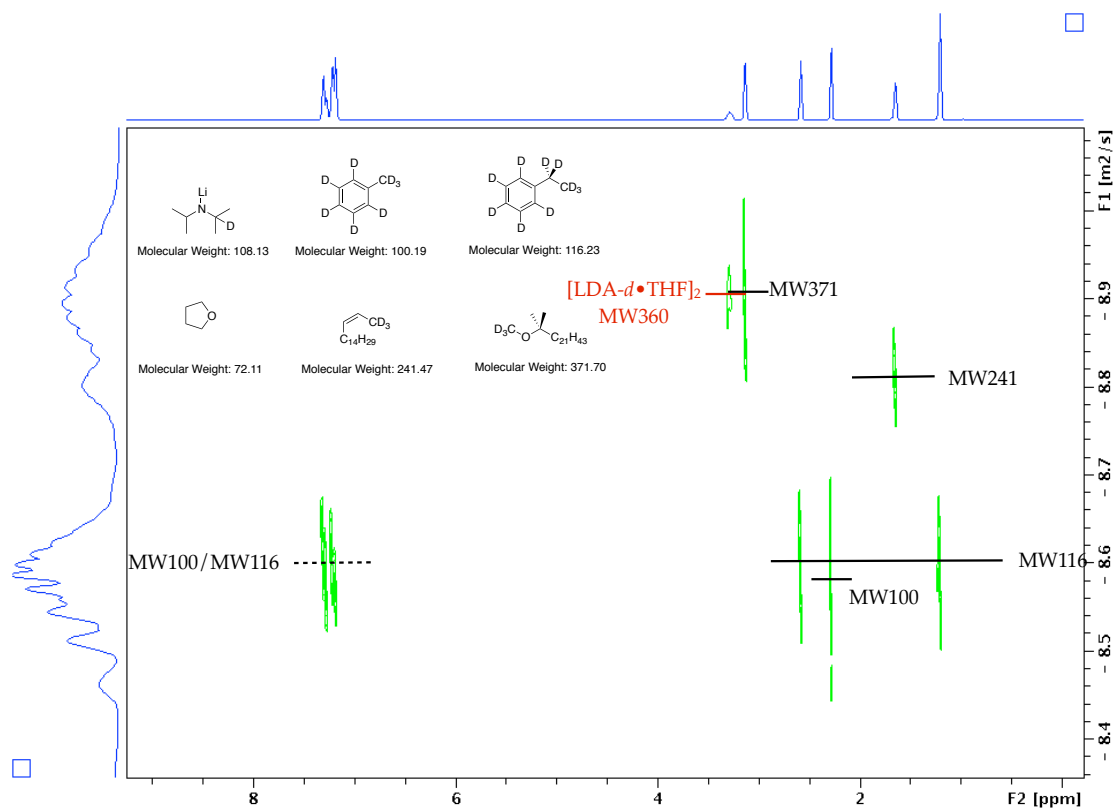


Figure S2.15. ^2H DOSY NMR of LDA-*d* in general toluene with 20 eq of general THF.

Table S2.4. D-FW analysis of ^2H DOSY NMR data of LDA-*d* in general toluene with 20 eq of general THF

Entry	Compound	FW g/mol	D m^2/s	Predicted FW g/mol	% Error
1	toluene- d_8	100	$2.75\text{E-}9$	101	1
2	ethylbenzene- d_{10}	116	$2.56\text{E-}9$	114	-2
3	(Z)-2-heptadecene- d_3	241	$1.65\text{E-}9$	243	1
4	ether- d_3	372	$1.29\text{E-}9$	371	0
5	LDA- <i>d</i> (di-solvated dimer)	360	$1.31\text{E-}9$	360	0

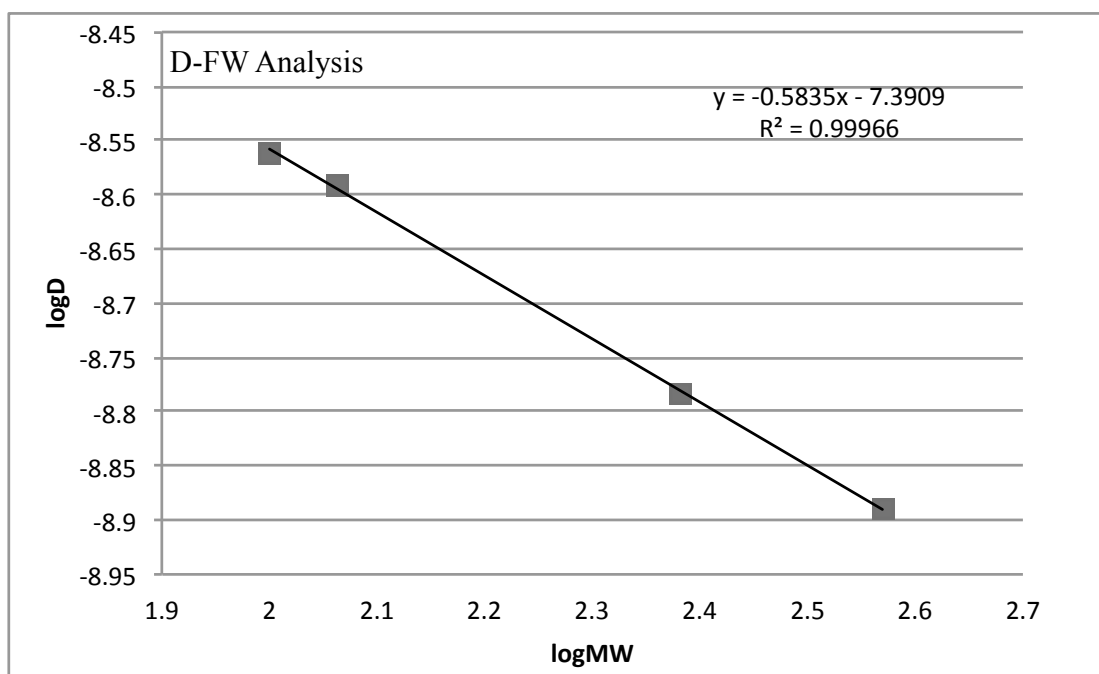


Figure S2.16. D-FW analysis of ^2H DOSY NMR data of LDA-*d* in general toluene with 20 eq of general THF

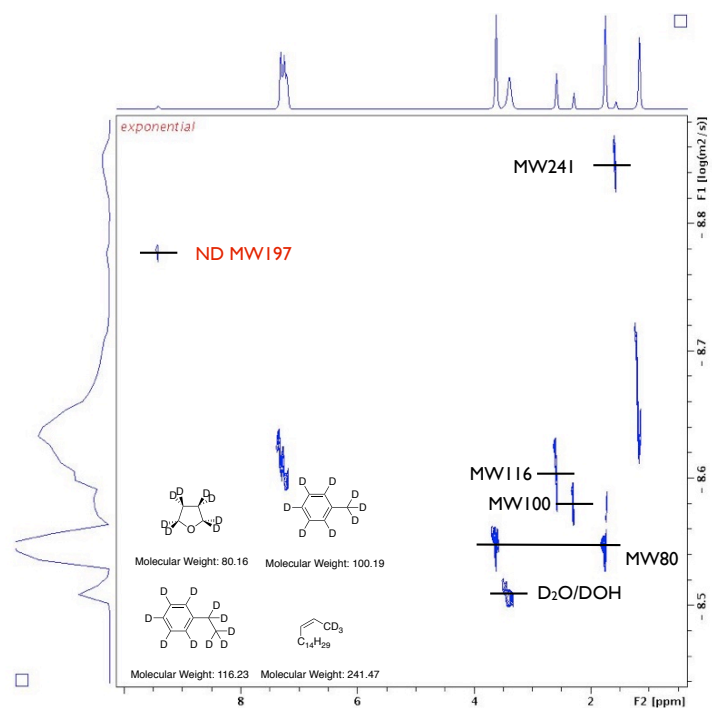


Figure S2.17. ^2H DOSY NMR of 0.4 M acetanilide in general acetone with 10 μl D_2O (2.5 eq).

Table S2.5. D-FW analysis of ^2H DOSY NMR data of 0.4 M acetanilide in general acetone with 10 μl D_2O (2.5 eq).

Entry	Compound	FW	D	Predicted FW	% Error
		g/mol	m^2/s	g/mol	
1	THF- d_8	80	$1.26\text{E-}9$	82	2
2	Tol- d_8	100	$1.14\text{E-}9$	96	-4
3	ethylbenzene- d_{10}	116	$1.01\text{E-}9$	117	1
4	(Z)-2-heptadecene- d_3	241	$0.64\text{E-}9$	242	0
5	ND		$0.75\text{E-}9$	188	
6	$\text{D}_2\text{O}/\text{DOH}$		$1.31\text{E-}9$	72	

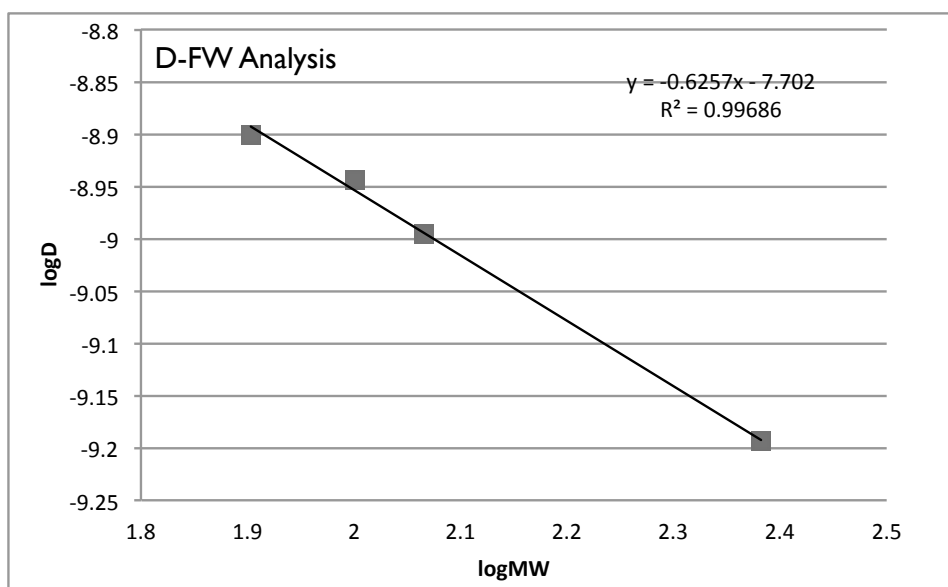


Figure S2.18. D-FW analysis of ^2H DOSY NMR data of 0.4 M acetanilide in general acetone with 10 μl D_2O (2.5 eq).

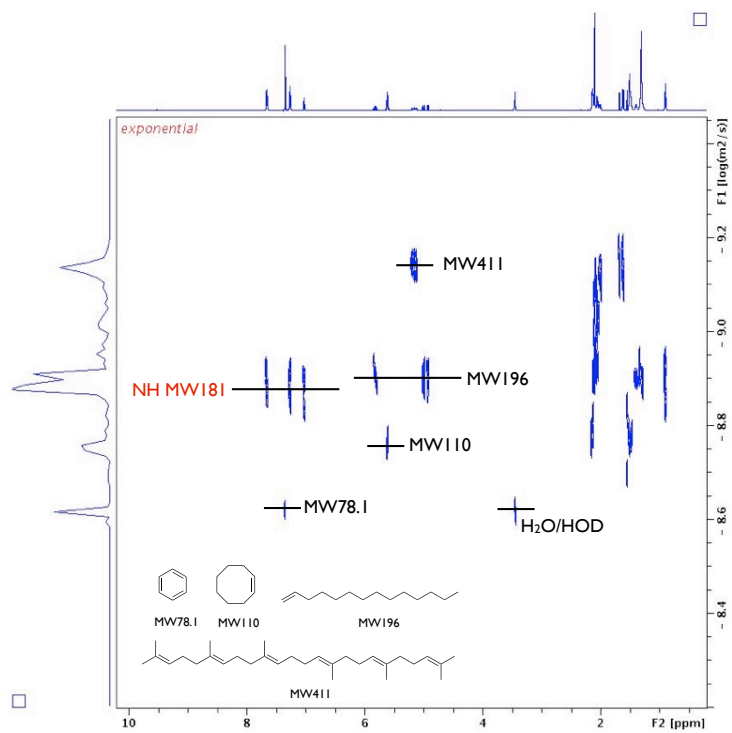


Figure S2.19. ¹H DOSY NMR of 0.4 M acetanilide in acetone-*d*₆ with 10 μl D₂O (2.5 eq).

Table S2.5. D-FW analysis of ^1H DOSY NMR data of 0.4 M acetanilide in acetone- d_6 with 10 μl D_2O (2.5 eq).

Entry	Compound	FW	D	Predicted FW	% Error
		g/mol	m^2/s	g/mol	
1	BEN	78.1	2.36E-9	76.8	2
2	COD	110	1.76E-9	115	-5
3	TDE	196	1.24E-9	188	4
4	SQU	411	0.70E-9	417	-1
5	NH		1.28E-9	180	
6	$\text{H}_2\text{O}/\text{HOD}$		2.39E-9	75	

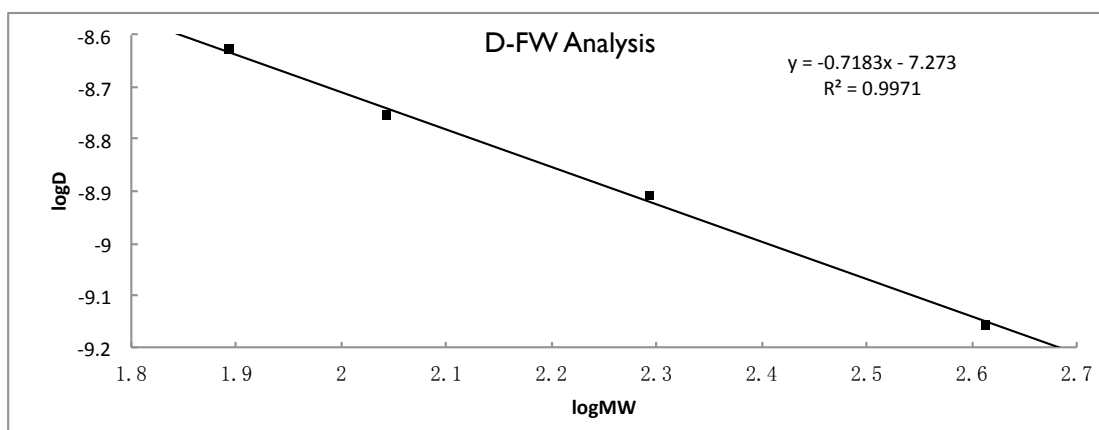


Figure S2.20. D-FW analysis of ^1H DOSY NMR data of 0.4 M acetanilide in acetone- d_6 with 10 μl D_2O (2.5 eq).

Appendix C. Supporting Information for Chapter 3

Table of Contents

Figure S3.1. ^6Li NMR of T_3 crystal dissolved in toluene- d_8 at $-20\text{ }^\circ\text{C}$.

Figure S3.2. ^{31}P NMR of T_3 crystal dissolved in toluene- d_8 at $-20\text{ }^\circ\text{C}$.

Figure S3.3. $\{^1\text{H}, ^{13}\text{C}\}$ HSQC of T_3 crystal dissolved in toluene- d_8 at $-20\text{ }^\circ\text{C}$.

Figure S3.4. $\{^1\text{H}, ^{13}\text{C}\}$ HMBC of T_3 crystal dissolved in toluene- d_8 at $-20\text{ }^\circ\text{C}$.

Table S3.1. D-FW Analysis of ^1H DOSY Data of T_3 crystal dissolved in toluene- d_8 at $-20\text{ }^\circ\text{C}$

Figure S3.5. Calibration curve of D-FW Analysis of Table S1.

Figure S3.6. ^{13}C NMR of T_3 and **pseudo- T_4** in toluene- d_8 at $-40\text{ }^\circ\text{C}$.

Figure S3.7. ^1H NMR of $[(\text{LiOPin})_5 \cdot \text{LDA} \cdot 2\text{HMPA} \cdot \text{Li}_2\text{O}]$ crystal dissolved in toluene- d_8 at $-20\text{ }^\circ\text{C}$.

Figure S3.8. ^{13}C NMR of $[(\text{LiOPin})_5 \cdot \text{LDA} \cdot 2\text{HMPA} \cdot \text{Li}_2\text{O}]$ crystal dissolved in toluene- d_8 at $-20\text{ }^\circ\text{C}$.

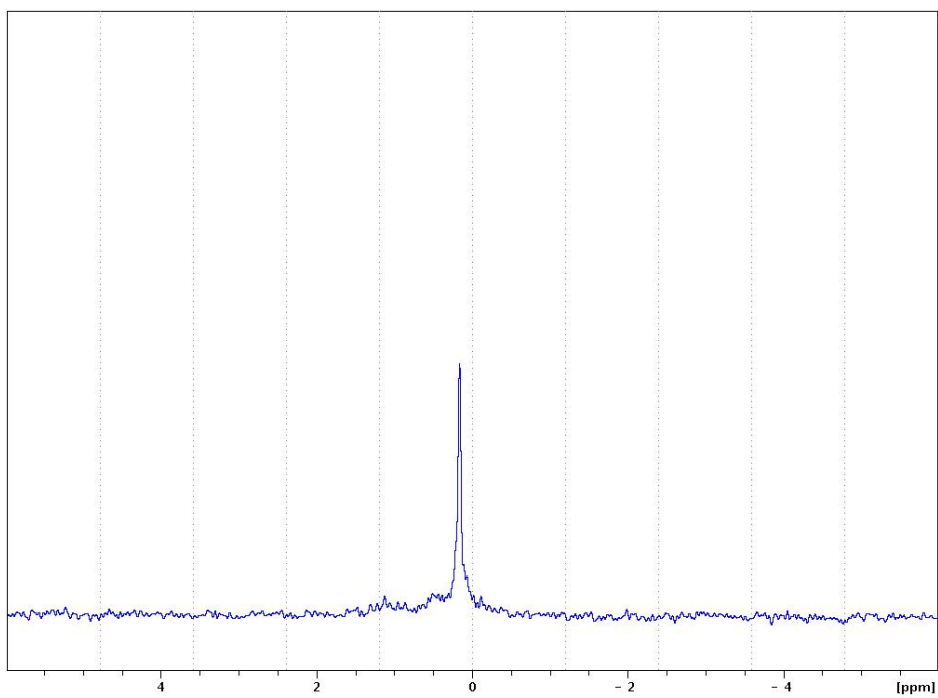


Figure S3.1. ^6Li NMR of T_3 crystal dissolved in toluene- d_8 at $-20\text{ }^\circ\text{C}$.

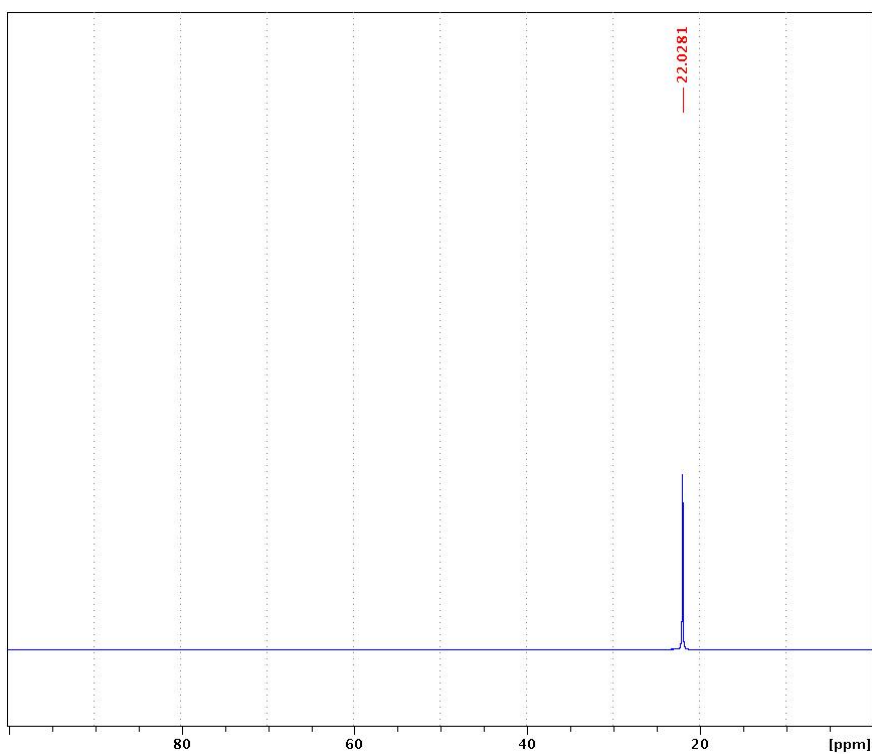


Figure S3.2. ^{31}P NMR of T_3 crystal dissolved in toluene- d_8 at $-20\text{ }^\circ\text{C}$.

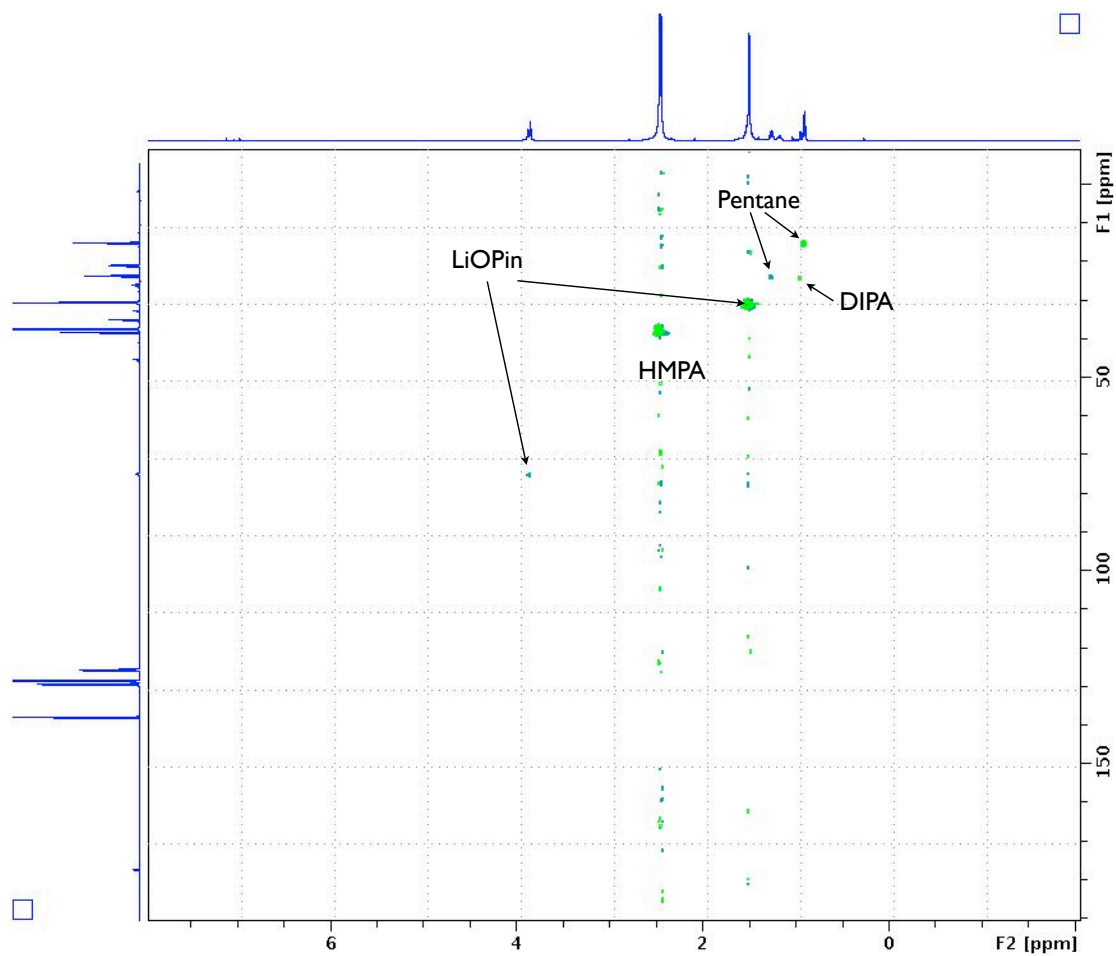


Figure S3.3. $\{^1\text{H}, ^{13}\text{C}\}$ HSQC of T_3 crystal dissolved in toluene- d_8 at $-20\text{ }^\circ\text{C}$.

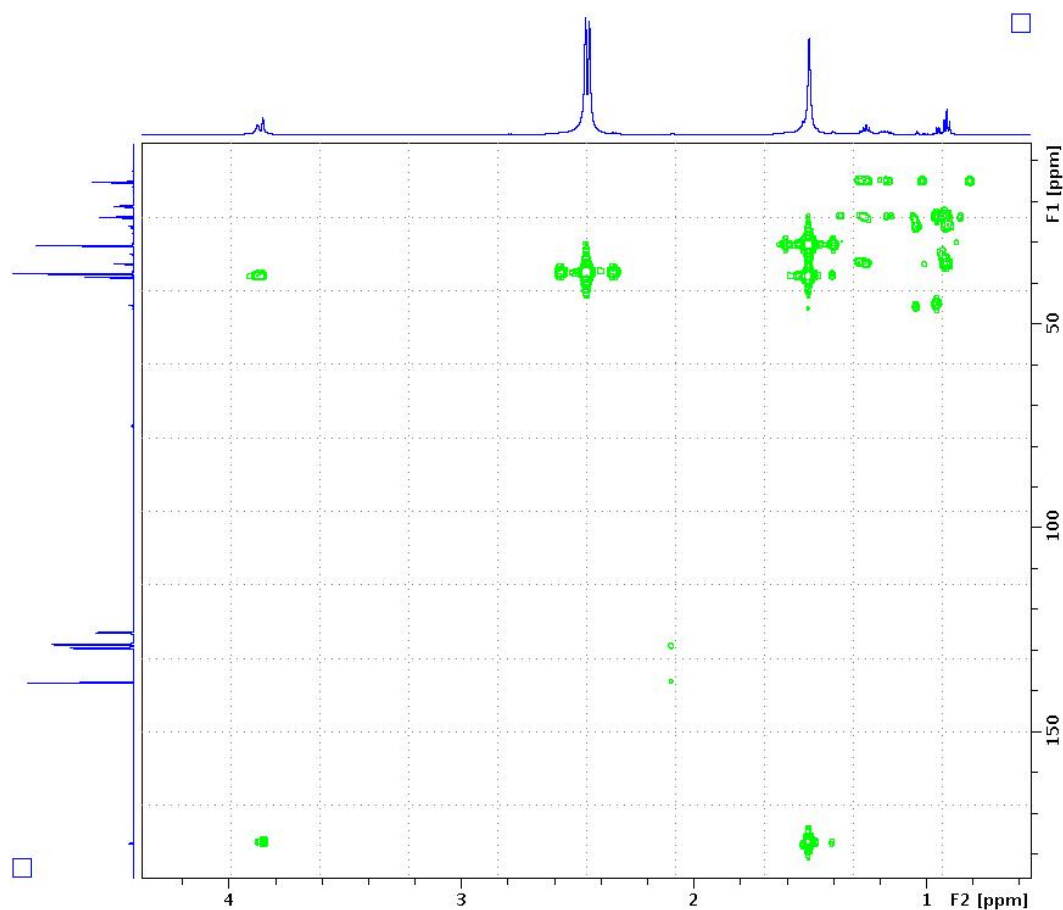


Figure S3.4. $\{^1\text{H}, ^{13}\text{C}\}$ HMBC of T_3 crystal dissolved in toluene- d_8 at $-20\text{ }^\circ\text{C}$.

Table S3.1. D-FW Analysis of ^1H DOSY Data of T_3 crystal dissolved in toluene- d_8 at $-20\text{ }^\circ\text{C}$

Entry	Compound	FW g/mol	D m^2/s	Predicted	
				FW g/mol	% Error
1	BEN	78.1	$7.353\text{E}-10$	80	2
2	COD	110	$6.319\text{E}-10$	103	-6
3	TDE	196	$4.185\text{E}-10$	210	7
4	SQU	410	$2.873\text{E}-10$	401	-2
5	T_3	961	$2.117\text{E}-10$	678	
6	HMPA	179	$3.261\text{E}-10$	322	

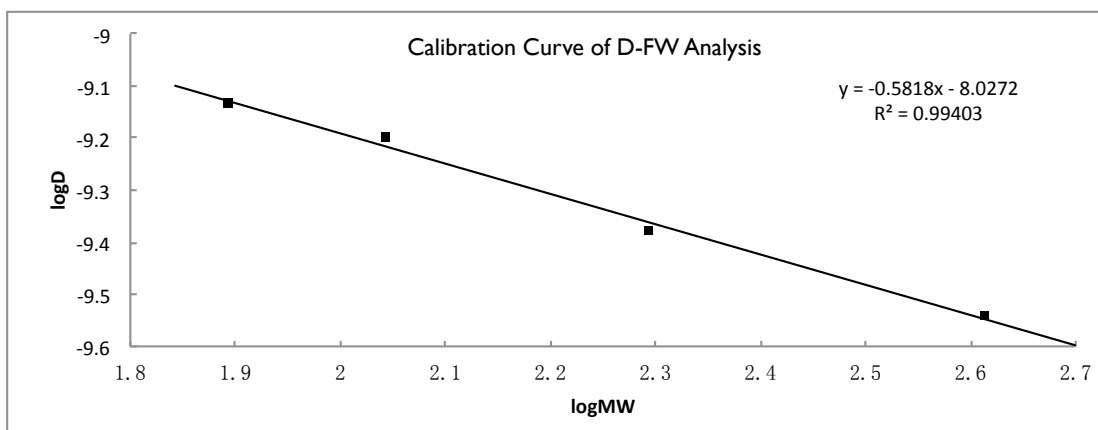


Figure S3.5. Calibration curve of D-FW Analysis of **Table S3.1**.

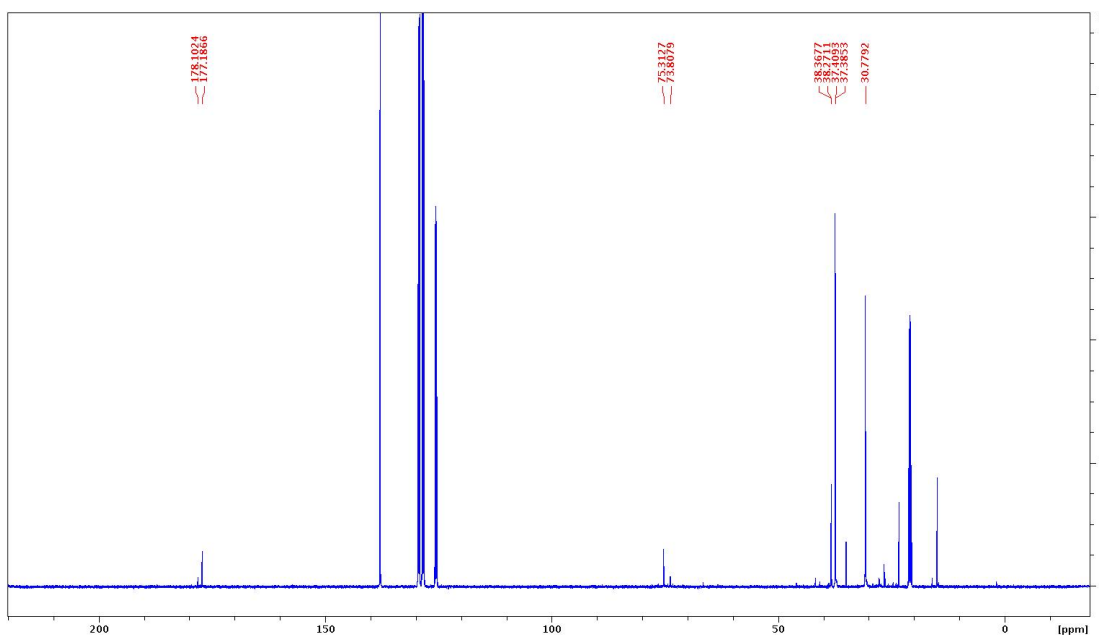


Figure S3.6. ¹³C NMR of **T₃** and **pseudo-T₄** in toluene-*d*₈ at -40 °C. Dissolving **pseudo-T₄** crystal in toluene, NMR presents the mixture of **T₃** and **pseudo-T₄**, due to the extremely low yield of **pseudo-T₄**.

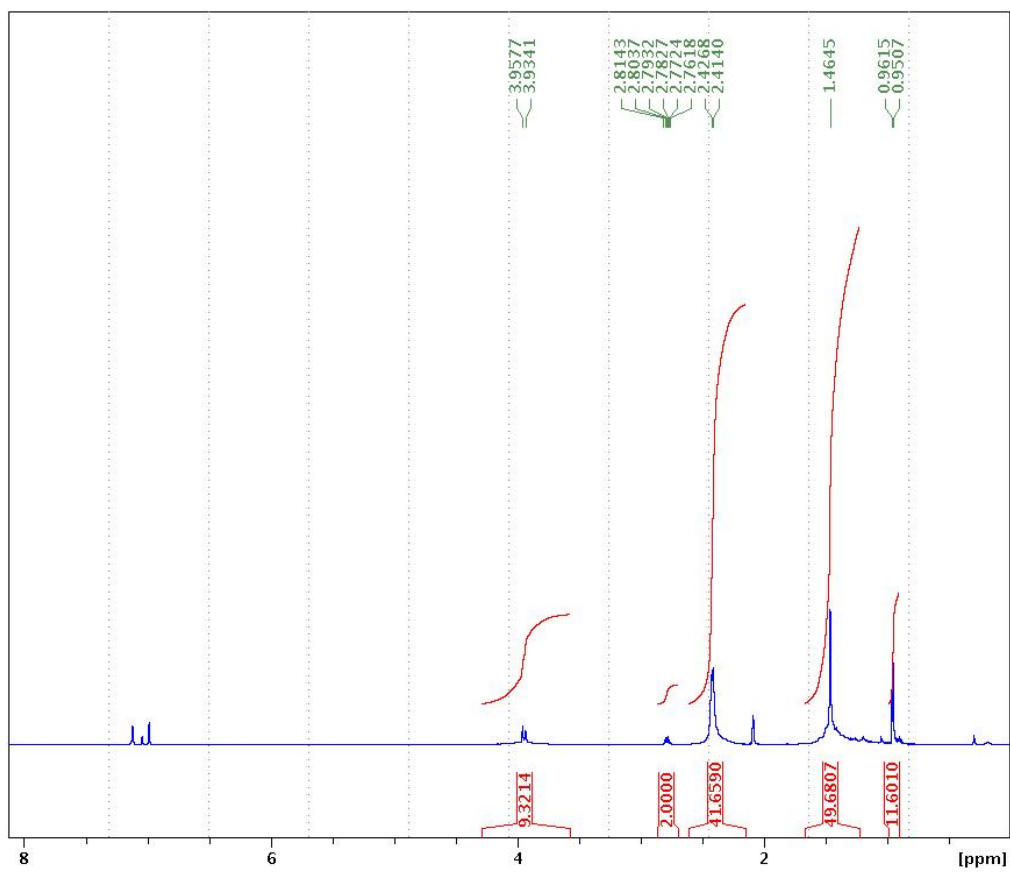


Figure S3.7. ^1H NMR of $[(\text{LiOPin})_5 \cdot \text{LDA} \cdot 2\text{HMPA} \cdot \text{Li}_2\text{O}]$ crystal dissolved in toluene- d_8 at $-20\text{ }^\circ\text{C}$.

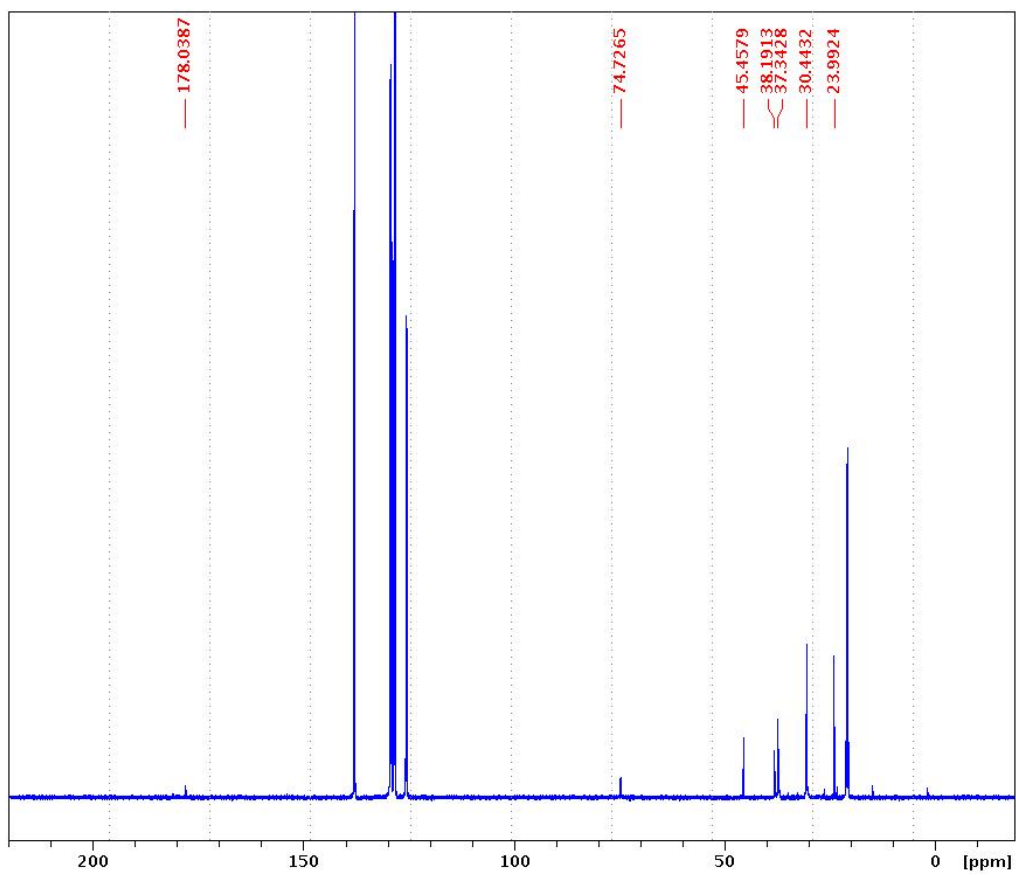


Figure S3.8. ^{13}C NMR of $[(\text{LiOPin})_5 \cdot \text{LDA} \cdot 2\text{HMPA} \cdot \text{Li}_2\text{O}]$ crystal dissolved in toluene- d_8 at $-20\text{ }^\circ\text{C}$.

Appendix C. Supporting Information for Chapter 4

Table of Contents

Figure S4.1. $\{^1\text{H}, ^{13}\text{C}\}$ HMBC of LiOPin hexamer crystal in Tol- d_8 at $-20\text{ }^\circ\text{C}$.

Figure S4.2. $\{^1\text{H}, ^{13}\text{C}\}$ HSQC of LiOPin hexamer crystal in Tol- d_8 at $-20\text{ }^\circ\text{C}$.

Figure S4.3. $\{^1\text{H}, ^1\text{H}\}$ NOESY of LiOPin hexamer crystal in Tol- d_8 at $-30\text{ }^\circ\text{C}$.

Figure S4.4. ^6Li NMR of LiOPin hexamer crystal in Tol- d_8 at $-30\text{ }^\circ\text{C}$.

Figure S4.5. $\{^1\text{H}, ^6\text{Li}\}$ HMBC of LiOPin hexamer crystal in Tol- d_8 at $-30\text{ }^\circ\text{C}$.

Figure S4.6. Overlay of ^1H NMR spectra of adding pinacolone to the solution.

Figure S4.7. D-FW analysis of ^1H DOSY data of LiOPin hexamer crystal dissolved in cyclohexane- d_{12} at $23\text{ }^\circ\text{C}$.

Table S4.1. D-FW analysis of ^1H DOSY data of LiOPin hexamer crystal dissolved in cyclohexane- d_{12} at $23\text{ }^\circ\text{C}$.

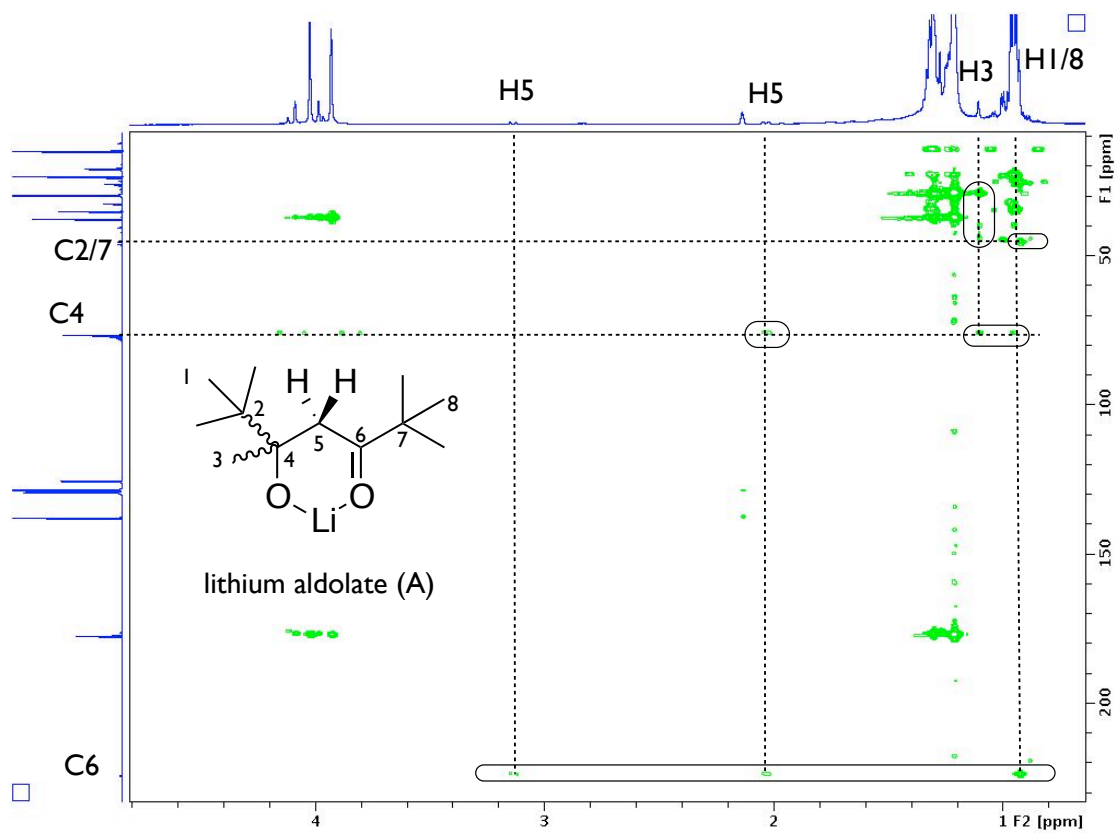


Figure S4.1. $\{^1\text{H}, ^{13}\text{C}\}$ HMBC of LiOPin hexamer crystal in $\text{Tol-}d_8$ at -20°C .

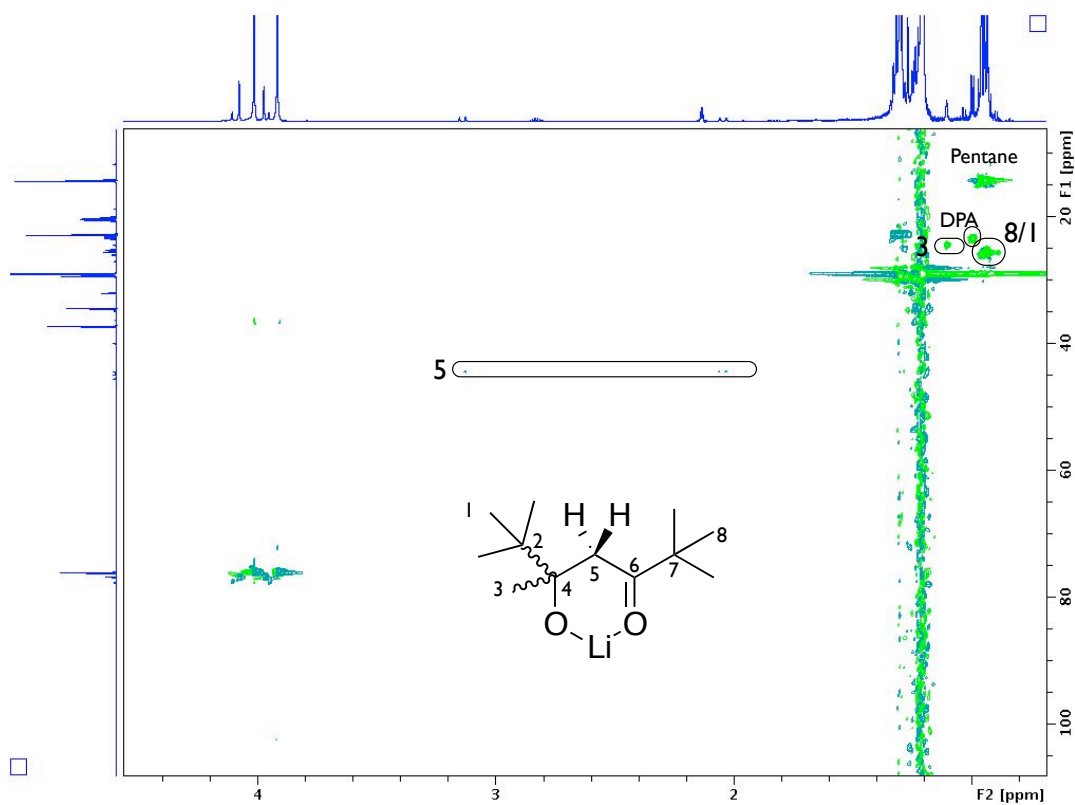


Figure S4.2. $\{^1\text{H}, ^{13}\text{C}\}$ HSQC of LiOPin hexamer crystal in $\text{Tol-}d_8$ at $-20\text{ }^\circ\text{C}$.

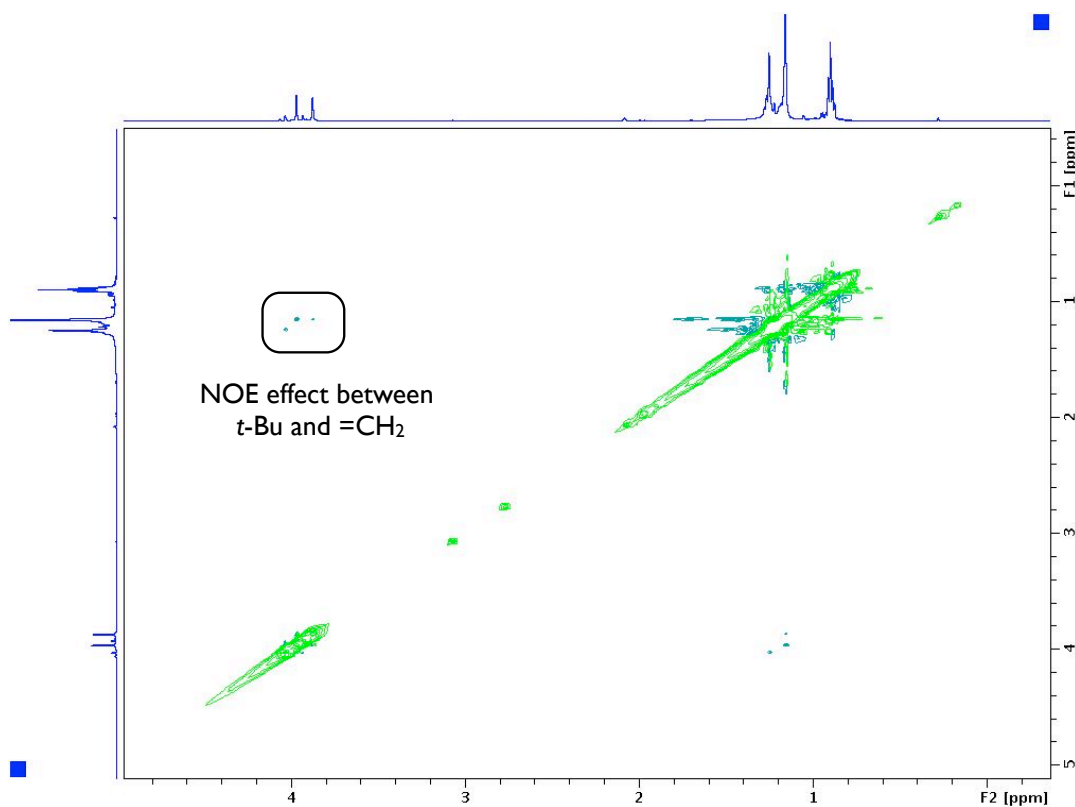


Figure S4.3. $\{^1\text{H}, ^1\text{H}\}$ NOESY of LiOPin hexamer crystal in $\text{Tol-}d_8$ at $-30\text{ }^\circ\text{C}$.

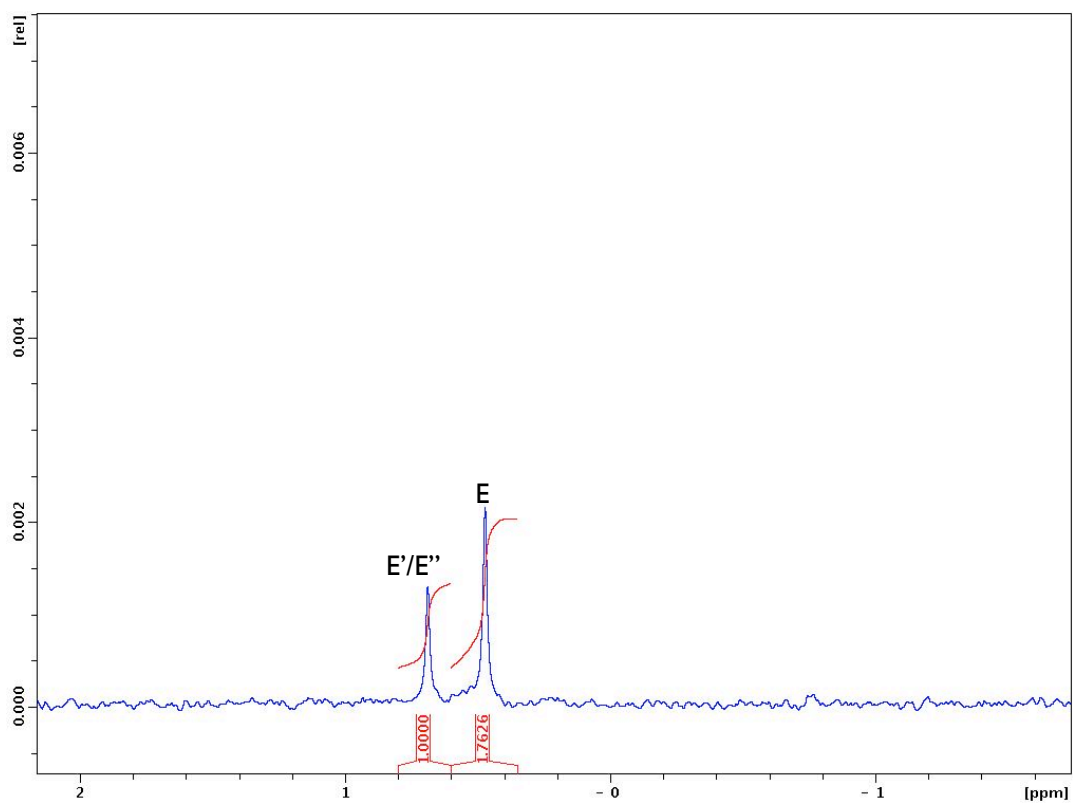


Figure S4.4. ^6Li NMR of LiOPin hexamer crystal in $\text{Tol-}d_8$ at $-30\text{ }^\circ\text{C}$.

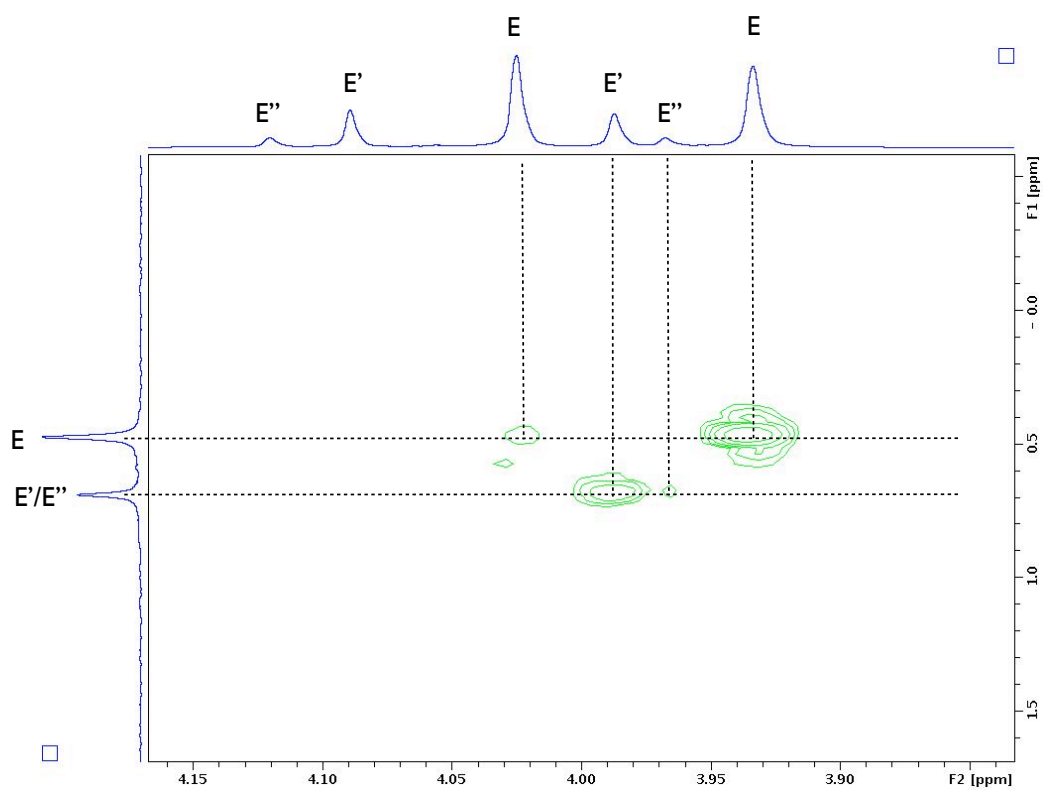


Figure S4.5. $\{^1\text{H}, ^6\text{Li}\}$ HMBC of LiOPin hexamer crystal in $\text{Tol-}d_8$ at $-30\text{ }^\circ\text{C}$.

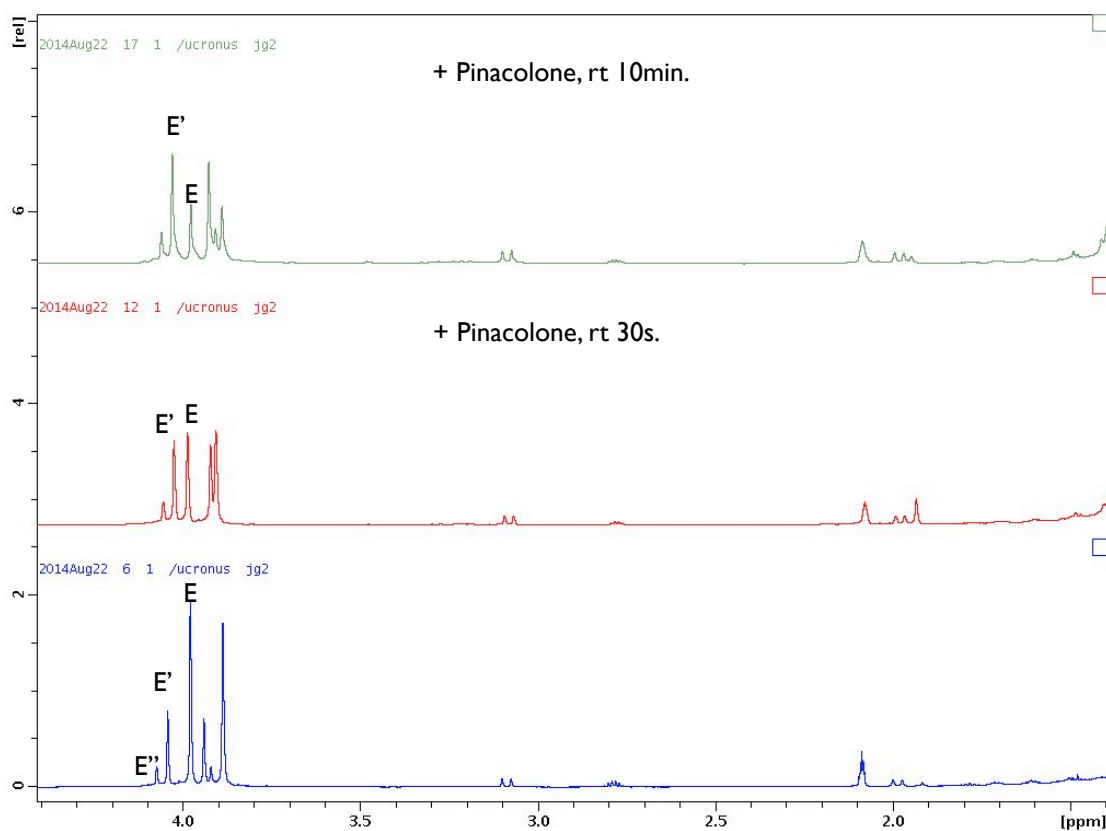


Figure S4.6. Overlay of ^1H NMR spectra of adding pinacolone to the solution. E' increases comparing with E. LiOPin hexamer crystal dissolved in Tol- d_8 at $-30\text{ }^\circ\text{C}$.

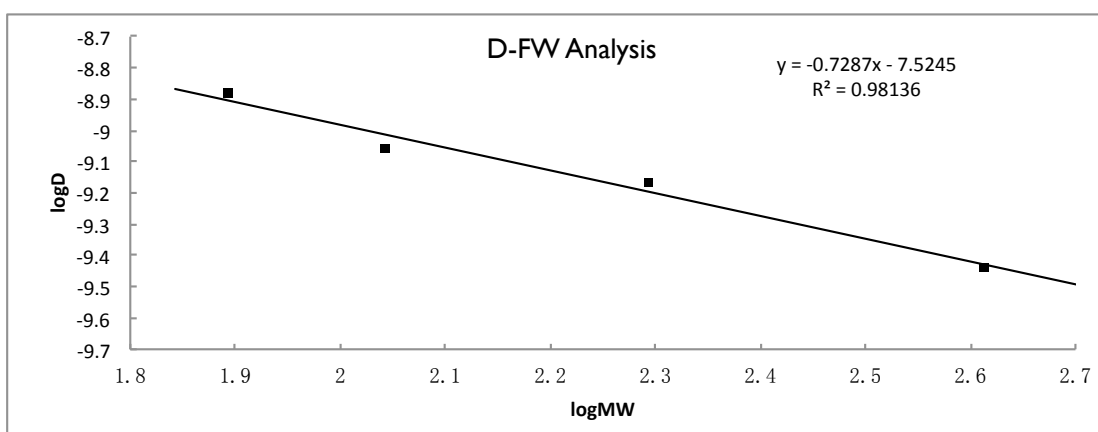


Figure S4.7. D-FW analysis of ^1H DOSY data of LiOPin hexamer crystal dissolved in cyclohexane- d_{12} at $23\text{ }^\circ\text{C}$.

Table S4.1. D-FW analysis of ^1H DOSY data of LiOPin hexamer crystal dissolved in cyclohexane- d_{12} at 23 °C.

Entry	Compound	FW	D	Predicted FW	% Error
		g/mol	m^2/s	g/mol	
1	BEN	78.1	1.307E-9	73	-6
2	COD	110	8.825E-10	126	14
3	TDE	196	6.810E-10	179	-9
4	SQU	411	3.660E-10	420	2
5	E		3.019E-10	548	--

